METABOLIC ENGINEERING APPLICATIONS OF *IN VIVO* ^{31}P AND ^{13}C NMR STUDIES OF *SACCHAROMYCES CEREVISIAE*

by

Jacqueline Vanni Shanks

In Partial Fulfillment of the Requirements

for the Degree of

Doctor of Philosophy

Department of Chemical Engineering

California Institute of Technology

Pasadena, California USA

1989

(Submitted June 27, 1988)

To Brent.

ACKNOWLEDGEMENTS

I wish to thank Professor James Bailey for his support of this research, for becoming my advisor after my second year at Caltech, and for the "Ho–Ho's" at the Athenaeum after group meetings. Thanks are given to James Yesinowski, Hellmut Eckert, Paula Watnick, and Tracy Handel for their assistance in my training in NMR. I appreciated the fruitful NMR discussions with Jorge Galazzo.

I very much appreciate the wisdom and encouragement given to me by some of the very special women at Caltech: the Original Female Mafia (Carol Jones, Julia Lester, and Malina Hills), Janet Howell, Jeannette Butler, Paula Watnick, Kathy Kanes, Betty Hannoun, Nancy DaSilva, Eliane Meilhoc, Anne McQueen, Rita Mendelson, April Olson, Alicia Loffler, and many others.

Thanks to my mom for deciding that seven were not enough. She has proved that patience and endurance are rewarded. I acknowledge the influence of my father, long ago deceased, who instilled in me the willingness to overcome obstacles. I am grateful for the support of my sisters and brothers: Joan, John, Jerry, Jean, Janette, Joyce, Julie, and Jenny. I thank Howard and Laura for their faith in me.

Much love and thanks are given to my husband Brent. We have shared many joys and sorrows during the process of graduate school and have accomplished this goal for both of us together.

Finally, thank you, God.

ABSTRACT

Noninvasive, multicomponent measurements are required for characterization of the results from metabolically manipulated organisms. The consequences of genetic manipulation by mutation and by introduction of recombinant plasmids to *Saccharomyces cerevisiae* is explored by ^{31}P and ^{13}C nuclear magnetic resonance (NMR) spectroscopy.

The *in vivo* NMR measurements should be quantified and detailed as much as possible. With this intent, analysis techniques of the *in vivo* ^{31}P NMR spectrum are developed. A systematic procedure is formulated for estimating the relative intracellular concentrations of the sugar phosphates in *S. cerevisiae* based upon the ^{31}P NMR spectrum. In addition, *in vivo* correlations of inorganic phosphate chemical shift with the chemical shifts of 3–phosphoglycerate, β–fructose 1,6–diphosphate, fructose 6–phosphate, and glucose 6–phosphate are determined. Elucidation of the cytoplasmic and vacuolar components of inorganic phosphate in the ^{31}P NMR spectrum of *S. cerevisiae* is another method of analysis that was developed. Concentrations and pH values for these components may be determined from this method. An *in vivo* correlation relating the inorganic phosphate chemical shift of the vacuole with the chemical shift of the resonance for pyrophosphate and the terminal phosphate of polyphosphate (PP_1) is established. Extension of these strategies to other cellular systems should be straightforward.

Transient measurements provided by ^{31}P NMR are applied to *reg1* mutant and standard strains. The *reg1* mutation will allow the expression of a cloned gene on a plasmid under the control of a *GAL* promoter in the presence of glucose. Despite similar values of ATP and cytoplasmic pH, the transient profiles of glucose 6–phosphate, fructose 6–phosphate, fructose 1,6–diphosphate, and 3–phosphoglycerate were very different for the two strains during anaerobic catabolism of glucose. The glucose uptake step or hexokinase step appears to be altered in the *reg1* strain. The *reg1* strain also catabolized galactose faster than the standard

strain. These results concur with the hypothesis that the *reg1* product operates early in the regulatory circuitry for glucose repression.

^{31}P and ^{13}C NMR measurements are used to analyze the performance of recombinant strains in which the glucose phosphorylation step had been altered. The strain with hexokinase PI had higher rates of glucose consumption and ethanol production in comparison to healthy diploid strains in the literature. The hexokinase PII strain that had the highest *in vitro* enzyme activity for glucose phosphorylation did not have the highest glucose consumption rate or ethanol production. The differences observed in *in vivo* utilization of the glucose phosphorylation capacity among the strains are insensitive to cytoplasmic pH and levels of cytoplasmic inorganic phosphate, sugar phosphates, and total ATP. Regulation of hexokinase PII by magnesium–free ATP appears to account for the differences observed with respect to the strain containing this enzyme.

TABLE OF CONTENTS

CHAPTER 1

INTRODUCTION

Metabolic engineering is the process of manipulating one or more steps in the metabolic pathway of an organism in order to produce or enhance production of desired biochemicals. These manipulations are performed via genetic and/or environmental alterations. Alterations by recombinant DNA methods include insertion of foreign genes to create new steps, amplification of existing enzymes, and control of expression of enzyme activity. Deletion of pathway steps can be performed by mutagenesis. Environmental manipulations such as immobilization can alter the activity or regulation of certain steps.[1]

Examples of metabolic engineering via insertion of foreign genes are the production of indigo in *Escherichia coli*[2] and 2–keto–L–gulonate in *Erwinia herbicola*.[3] Enhancement of ethanol production has been reported for immobilized cells of *Saccharomyces cerevisiae*; the glucose uptake step or the hexokinase reaction has been suggested to be altered by immobilization.[4,5]

One of the dangers in the future of metabolic engineering is the current trial and error procedure of making an organism with enhanced capabilities.[1] Trial and error methods will almost certainly lead to suboptimal solutions. Criteria or selection rules are needed for the choice of manipulations to be performed. In the case of production of 2–keto–L–gulonate in *Erwinia herbicola*, the knowledge of regulatory aspects of the involved enzymes was stressed for the successful application in the future of the implemented modifications.[3] A basic premise of increasing enzyme amount or activity (as measured by *in vitro* methods) as much as possible in the newly created step may not lead to a better solution; this is evident if regulatory aspects of the enzyme are important to *in vivo* activity.

A multifaceted approach towards optimization of an organism for purposes of metabolic engineering includes the use of metabolic–pathway–synthesis models, metabolic–pathway–kinetic models, cellular growth models, and noninvasive, experimental techniques for obtaining multicomponent measurements.[1] These noninvasive, experimental techniques preferably should provide transient as well as

steady–state measurements of intracellular concentrations of direct physiological and biochemical interest, of pH values in the cytoplasm, and of cell mass synthesis and degradation. Fluorescence measurements[6,7,8] and radioactive tracers[9] are examples of two noninvasive measurements that provide estimates of biomass concentration, NADH and NADPH levels, and rates of cellular synthesis and degradation.

In vivo nuclear magnetic resonance (NMR) spectroscopy has become a popular method of studying bioenergetics and metabolism in diverse living systems, from microbial cells to humans.[10–12] A primary goal of this thesis is to relate the use of NMR spectroscopy as a noninvasive measurement in metabolic engineering applications.

The principle of the noninvasive NMR technique is briefly described in the next few paragraphs. Certain atomic nuclei, such as ^{1}H, ^{13}C, and ^{31}P, possess a property known as spin and thus have a magnetic dipole moment. In *in vivo* NMR experiments, two magnetic fields are applied to the cellular sample in the spectrometer. First, application of a strong static field (the magnet) causes the nuclear dipoles to orient themselves so that the dipole of each nucleus is aligned with the field or against it. A net magnetization results in the direction of the applied static field, since more nuclei are aligned with the field than against it (nuclei store less energy in this configuration). The nuclei precess at their own characteristic Larmor frequency in the static field. For example, ^{31}P nuclei have a Larmor frequency of 202.46 MHz in an 11.7 Tesla field.

Then a second field, a radio frequency (rf) field is applied in the Fourier–Transform (FT) NMR experiment in short powerful pulses, typically the duration on the order of 30 μs. The bandwidth (spread in frequency) of these pulses is sufficient to cause all of the nuclei of a given isotope to resonate. Different isotopes have very different Larmor frequencies, so in a given frequency setting in a NMR experiment, only resonances from a single isotope can be detected. The exception

is with double–tuned frequency probes. The NMR measurement is based upon slight differences in the environment of the nuclei in different compounds. For example, in the ^{31}P NMR experiment, the β phosphate in ATP is in a different chemical environment than that of the α phosphate in ATP. Consequently, the α and β phosphates of ATP resonate at slightly different frequencies or at different chemical shifts (dimensionless frequencies). After application of the short rf pulse, the spins of the nuclei freely relax back to their original magnetic state according to their frequencies.

The signal resulting from a radio frequency pulse is called a free–induction decay (FID): the induced signal decays according to the free precession of the nuclei in the static field. A series of rf pulses are applied in a FT NMR experiment, so a series of FID's are collected and summed to give enough signal. Then, the Fourier transform of this decay gives the conventional NMR frequency–domain spectrum. The experiment just described is a one–dimensional NMR experiment and is the type of experiment used in this thesis.

Intially, the ^{31}P nucleus is the most suitable nucleus for observation in living cells because it is a natural isotope, the spectra observed are simpler than proton or ^{13}C, and the spectra exhibit a wide range of chemical shifts for biological phosphates.[13] Some of the phosphate compounds detectable are: intracellular inorganic phosphate, extracellular inorganic phosphate, sugar phosphates, ATP, NAD^+/NADH, and polyphosphate. Intracellular pH can be determined from the intracellular inorganic phosphate resonance.

^{13}C NMR studies require feeding the cells with ^{13}C enriched compounds because of the low sensitivity of the ^{13}C nucleus. Labelled amino acids, substrate, and fermentation end products can be observed in the ^{13}C NMR spectrum.[13] Concentrations may be determined from the spectrum since the area of a resonance is proportional to the number of nuclei that contribute to the signal. Spectral accumulation times are on the order of minutes for *in vivo* studies of microbial

cells. Consequently, transient NMR experiments can be performed in which the concentration profiles with time can be followed after a metabolic stimulus.

Shulman and coworkers (originally at Bell Laboratories) initiated studies of ^{31}P NMR on microbial cells. Feasibility studies were conducted on *Saccharomyces cerevisiae* and *Escherichia coli*.[14,15] Since then, ^{31}P NMR studies on microbial cells have centered on bioenergetics, carbohydrate metabolism, phosphate transport, and the role of polyphosphate. Many of these studies have tended to focus on a particular application and not to coordinate all the information possible from the spectra.

Quantitative analysis of the contributions of the metabolites in ^{31}P NMR spectra has not been developed to its full extent. In particular, the sugar phosphate region, which for glucose metabolism consists mainly of overlapping resonances of glucose 6–phosphate, fructose 1,6–diphosphate, fructose 6–phosphate, and 3 phosphoglycerate, has been resolved previously into its individual components by *in vitro* NMR spectroscopy of cell extracts.[16] Simultaneous determination of individual sugar phosphate levels with bioenergetics and phosphate metabolism data is desirable for obtaining a more complete intracellular picture of the cell *in vivo*. A systematic procedure has been formulated for estimating the relative concentrations of sugar phosphates from ^{31}P NMR spectra of *Saccharomyces cerevisiae*. This procedure is explained in Chapter 2.

Concentrations of inorganic phosphate can be monitored in compartments within the cells that have different pH values. In yeast, signals for inorganic phosphate in the cytoplasm, the vacuoles, and extracellular medium have been observed in ^{31}P NMR spectra.[11,17] Protocols established for the analysis of the phosphomonoester region in the ^{31}P NMR spectrum will allow faster and more detailed data interpretation. In Chapter 3, a method is presented for elucidation of the cytoplasmic and vacuolar components in this region for *S. cerevisiae*.

The eucaryote *Saccharomyces cerevisiae* (Bakers Yeast) is the organism chosen for illustration of *in vivo* NMR to study metabolic engineering applications. Yeast have been used successfully for many years in the fermentation industry. Molecular techniques for cloning and manipulating yeast genes and transforming yeast cells have been developed.[18,19] *S. cerevisiae* is one of the best characterized eucaryotic cells in terms of physiology and molecular biology. *S. cerevisiae* is a GRAS (generally recognized as safe) organism, can be cultivated to high cell densities, and relative to mammalian cells, can be grown in relatively inexpensive medium. In addition, the studies by Shulman and coworkers provide a foundation for NMR spectroscopy applied to this organism.[11]

An application of NMR spectroscopy to a genetically manipulated strain of *S. cerevisiae* is given in Chapter 4. Promoters from the *GAL* operon have been applied in cloning and expression vehicles for *S. cerevisiae*.[20] To achieve induction by galactose in glucose–containing media, a host strain must be chosen that will not exhibit catabolic repression by glucose. A host strain that has the *reg1* mutation can express a cloned gene from a *GAL* promoter when galactose is added to a glucose–containing medium. The mechanism by which the *reg1* mutation inhibits catabolic repression has not been determined.[21]

The *reg1* mutation illustrates an unknown change in the metabolic pathway of an organism in order to affect a useful change for metabolic engineering. The *reg1* mutant strain is studied here by transient *in vivo* ^{31}P NMR experiments in order to gain insight into the influence of the *reg1* mutation on glucose catabolism. The NMR experiments are performed for cells that had been previously grown on glucose and then fed glucose under anaerobic conditions in the NMR. Also, experiments are performed for cells using galactose for growth and galactose for the NMR experiment. Finally, similar NMR experiments are performed for a standard strain of *S. cerevisiae* for comparison. The simultaneous changes in levels of polyphosphate, extracellular inorganic phosphate, intracellular inorganic phos-

phate, the individual sugar phosphates, and ATP and changes in the cytoplasmic and extracellular pH values are monitored as the cells catabolize the carbon source.

A second application of *in vivo* NMR to metabolic engineering is given in Chapter 5. Recombinant *S. cerevisiae* strains in which the enzyme activities for glucose phosphorylation have been altered are used in this study. The step in which glucose is phosphorylated by MgATP has been suggested as being a major control point in glycolysis in *S. cerevisiae*.[11,22] In the wild–type strain, three enzymes that phosphorylate glucose are present: hexokinase PI and PII and glucokinase.[23,24] A linear relationship between *in vitro* glucose–phosphorylating enzyme activity and *in vivo* glucose consumption had been reported for *S. cerevisiae* strains containing different enzymes for the first step in glycolysis - a strain with all three kinases; a mutant strain with hexokinase PI as the kinase; and a mutant strain with only hexokinase PII as its kinase.[25] Increasing *in vitro* activity was correlated with increasing *in vivo* rates of glucose consumption.[25] The three strains studied in Chapter 5 have a single kinase for glucose phosphorylation: hexokinase PI, hexkinase PII, and glucokinase, respectively. In addition, the strain containing hexokinase PII has an *in vitro* enzyme activity for glucose phosphorylation 3–10 times greater than the other two strains.

Glucose consumption, ethanol and glycerol production, and polysaccharide formation are determined by ^{13}C NMR measurements of these strains. Intracellular metabolic state variables (as in Chapter 4) are determined by ^{31}P NMR spectroscopy. The consequences of the manipulated changes as observed from the NMR measurements are discussed in relation to the general maxim of increasing *in vitro* enzyme activity for enhanced production.

REFERENCES

1. J.E. Bailey, D.D. Axe, J.L. Galazzo, K.F. Reardon, A. Seressiotis and J.V. Shanks, *Biochem. Engr. V* (Ann. N.Y. Acad. Sci.), **506**, 1 (1987).

2. B.D. Ensley, B.J. Ratzkin, T.D. Osslund, M.J. Simon, L.P. Wackett, and D.T. Gibson, *Science*, **222**, 167 (1983).

3. S. Anderson, C.B. Marks, R. Lazarus, J. Miller, K. Stafford, J. Seymour, D. Light, W. Rastetter, and D.E. Stell, *Science*, **230**, 144 (1985).

4. P.M. Doran and J.E. Bailey, *Biotechol. Bioeng.*, **28**, 73 (1986).

5. J.L. Galazzo and J.E. Bailey, "Fermentation Pathway Kinetics and Metabolic Flux Control in Suspended and Immobilized *Saccharomyces cerevisiae*," manuscript in preparation.

6. D.W. Zabriskie and A.E. Humphrey, *Appl. Environ.*, **35**, 337 (1978).

7. T. Scheper and K. Schugerl, *Appl. Microbiol. Biotechnol.*, **23**, 440 (1986).

8. K.F. Reardon, T. Scheper, and J.E. Bailey, *Biotechnol. Prog.*, **3**, 153 (1987).

9. S.F. Karel, C.A. Briasco, and C.R. Robertson, *Biochem. Engr. V* (Ann. N.Y. Acad. Sci.), **506**, 84 (1987).

10. R.B. Moon and J.H. Richards, *J. Biol. Chem.*, **248**, 7276 (1973).

11. S.L. Burk and R.G. Shulman, *Ann. Rev. Microbiol.*, **41**, 595 (1987).

12. M.J. Avison, H.P. Hetherington, and R.G Shulman, *Ann. Rev. Biophys. Chem.*, **15**, 377 (1986).

13. D.G. Gadian, *Nuclear Magnetic Resonance and Its Application to Living Systems*, (Oxford University Press, Oxford, 1982).

14. J.M. Salhany, T. Yamane, R.G. Shulman, and S. Ogawa, *Proc. Natl. Acad. Sci.*, **72**, 4966 (1975).

15. G. Navon, R.G. Shulman, T. Yamane, T.R. Eccleshall, K. -B. Lam, J.J. Baronofsky, and J. Marmur, *Biochemistry*, **18**, 21 (1979).

16. J.A. den Hollander, K. Ugurbil, and R.G. Shulman, *Biochemistry*, **25**, 212 (1986).

17. K. Nicolay, W.A. Scheffers, P.M. Bruinenberg, and R. Kaptein, *Arch. Microbiol.*, **134**, 270 (1983).

18. D. Botstein and R.W. Davis, "Principles and Practice of Recombinant DNA Research with Yeast," in *The Molecular Biology of the Yeast Saccharomyces, Metabolism and Gene Expression*, p.607, (Cold Spring Harbor, New York, 1982).

19. K. Struhl, *Nature*, **305**, 391 (1983).

20. L. Guarante, R.R. Yocum, and P. Gifford, *Proc. Natl. Acad. Sci.*, **79**, 7410 (1982).

21. M. Carlson, *J. Bacteriol.*, **169**, 4873 (1987).

22. A. Boiteux and B. Hess, *Phil. Trans. R. Soc. Lond. B*, **293**, 5 (1981).

23. S.P. Colowick, "The Hexokinases" in *The Enzymes*, (P.D. Boyer, ed.), Vol. 9, Part B, 3^{rd} ed., p. 1, (Academic Press, New York, 1973).

24. P.K. Maitra, *J. Biol. Chem.*, **245**, 2423 (1970).

25. Z. Lobo and P.K. Maitra, *Arch. Bioc. Biop.*, **182**, 639 (1977).

26. R.B. Walsh, G. Kawasaki, and D.G. Fraenkel, *J. Bacteriol.*, **154**, 1002 (1983).

CHAPTER 2

ESTIMATION OF INTRACELLULAR SUGAR PHOSPHATE CONCENTRATIONS IN *SACCHAROMYCES CEREVISIAE* USING ^{31}P NUCLEAR MAGNETIC RESONANCE SPECTROSCOPY

ABSTRACT

A systematic procedure has been formulated for estimating the relative intracellular concentrations of sugar phosphates in *Saccharomyces cerevisiae* based upon phosphorus-31 nuclear magnetic resonance (NMR) measurements. The sugar phosphate region of the ^{31}P NMR spectrum is first decomposed by computer analysis, and the decomposition consistency and identification of individual sugar phosphate resonances are established based on *in vitro* chemical shift calibrations determined in separate experiments. Numerous evaluations of intracellular *S. cerevisiae* compositions for different strains and different cell environments provide the basis for *in vivo* correlations of inorganic phosphate chemical shift with the chemical shifts of 3-phosphoglycerate, β-fructose 1,6-diphosphate, fructose 6-phosphate, and glucose 6-phosphate. Relative intracellular sugar phosphate concentrations are obtained by correcting peak areas for partial saturation during transient *in vivo* experiments. *In vivo* concentrations estimated by this method agree well with estimates for similar systems based on other techniques. This approach does not require costly labelled compounds, and has the advantage that other important metabolic state variables such as internal and external pH and intracellular levels of phosphate, ATP, ADP, NAD(H), and polyphosphate may be determined from the same ^{31}P spectrum. Extension of this strategy to other cellular systems should be straightforward.

INTRODUCTION

The microbial cell can be viewed as a reactor with complex reaction pathways and controls. With high resolution nuclear magnetic resonance spectroscopy (NMR), it is feasible to view these pathways in concert noninvasively in the living cell. Of the atomic nuclei that possess intrinsic magnetism, ^{31}P is more commonly used for *in vivo* studies than other nuclei such as ^{1}H, ^{13}C, and ^{15}N : it is a natural isotope, the spectra are simpler, and the spectra exhibit a wide range of biological phosphates. Since the pioneering study of the determination of intracellular pH in red blood cells by Moon and Richards in 1973,[1] ^{31}P NMR has been a noninvasive probe into the areas of bioenergetics, carbohydrate metabolism, and phosphate metabolism for cells, organelles, and tissues.[2,3,4,5] Intracellular pH, extracellular pH, and concentration measurements have been obtained from the ^{31}P spectra. Some of the biological phosphates detected in these spectra are the sugar phosphates, intracellular phosphate, extracellular phosphate, phosphoenolpyruvate, UDPG, NTP, NAD(H), and polyphosphate.

Quantitative analysis of the contributions of metabolites in ^{31}P NMR spectra has not been developed to its full extent. In particular, the sugar phosphate peak, which for glucose metabolism consists mainly of overlapping peaks of glucose 6-phosphate, fructose 6-phosphate, fructose 1,6-diphosphate, and 3-phosphoglycerate, has been resolved previously into its individual components by *in vitro* NMR spectroscopy, using cell extracts.[6] ^{13}C NMR can provide information on these EMP pathway intermediates *in vivo*;[7] however, the bioenergetic and phosphate metabolism information of the cells is not present in ^{13}C spectra. Simultaneous determination of sugar phosphate levels with bioenergetics and phosphate metabolism data is desirable for obtaining a more complete intracellular picture of the cell *in vivo*. These sugar phosphate levels should be obtained not only for a single metabolic state of the cells as provided by cell extracts, but for a broad range of conditions such as those encountered in transient experiments

in which the cell response is monitored after the application of a stimulus such as a carbon source, an ATPase inhibitor, or an electron donor.

Estimation of intracellular sugar phosphate concentrations from ^{31}P NMR spectra requires a means of identifying the individual sugar phosphate contributions in the *in vivo* spectrum, and then determining the relative peak areas of the individual sugar phosphates in order to evaluate relative concentrations. With this objective in mind, a method was developed for dissecting the sugar phosphate region of ^{31}P spectra into the individual sugar phosphate contributions. In formulating this method, *Saccharomyces cerevisiae* subject to glucose as the metabolic stimulus was used as a model system. The method is based on the pH dependencies of the chemical shifts of the sugar phosphates and intracellular phosphate for resonance identification, on consistency of the pool of sugar phosphates identified with cell extract data, and on the constraints that the estimated NMR parameters should be internally consistent and physically reasonable.

MATERIALS AND METHODS

Yeast Strains

Saccharomyces cerevisiae ATCC 18790 and *S. cerevisiae* D603 [8] were the yeast strains used in this study. *S. cerevisiae* 18790 is a standard diploid strain. *S. cerevisiae* D603 is the homozygous diploid version of YM603 (*ade* 2-101, *ura* 3-52, *his* 3, *met*, *lys* 2-801, *reg* 1-501). The *reg* mutation inhibits catabolic repression by glucose.

Culture and NMR Preparation

The strains were grown aerobically in a rotary shaker at 30°C in 1 L flasks containing 400 mL of the following medium: 1% Difco Bacto-Yeast Extract, 2% Difco Bacto-Peptone, and 2% glucose, adjusted to pH 4.5 with citrate buffer (50 mM final buffer concentration). The flasks were inoculated to a final volume

percent of 1% with early stationary phase cell cultures grown in the same medium. Midexponential phase cells (0.5 g cell dry weight (CDW)/L; 15% of stationary cell density) were chilled in an ice bath to 5°C under continuous shaking, then harvested by low–speed centrifugation. The cells were then washed twice in an ice-cold sterile buffered salt solution: 0.85 g/L KH_2PO_4, 0.15 g/L K_2HPO_4, 0.5 g/L $MgSO_4$, and 0.1 g/L NaCl in 50 mM 2-(N-morphilino)ethanesulfonic acid (MES) buffer, pH adjusted to 6 with NaOH.

The cells were resuspended in wash medium supplemented with an additional 15 mM P_i (7.5 mM KH_2PO_4: 7.5 mM K_2HPO_4)[9] at a 1:1 ratio of cell pellet volume to resuspension volume. Cell suspensions (2 mL) were placed in 10 mm o.d. NMR sample tubes, tightly capped, and kept on ice until used, always less than 4 hrs. before an experiment. A "dummy" sample for each experiment was prepared in an identical fashion, except that each "dummy" sample contained 20 v/v % D_2O (final sample volume 2.1 mL).

In Vitro pH—Chemical Shift Relationships

The solution used to approximate the intracellular milieu of *S. cerevisiae* was similar to that used by den Hollander *et al.* [9] (30 mM NH_4Cl, 200 mM KCl, 20 mM $MgCl_2 \cdot 6H_2O$, 10mM KH_2PO_4, approximate ionic strength of 300 mM), except that 5 mM of two or three of the following sugar phosphates were added for each experiment: galactose 1-phosphate, α-glucose 1-phosphate, β-glucose 1-phosphate, glucose 6-phosphate, fructose 6-phosphate, and fructose 1,6-diphosphate. (Galactose 1-phosphate and glucose 1-phosphate are not expected in glucose metabolism but were included for reference in future work.) The combinations of the sugar phosphates examined were: glucose 6-phosphate, fructose 6-phosphate, and α-glucose 1-phosphate; fructose 1,6-diphosphate and galactose 1-phosphate; β-glucose 1-phosphate and fructose 6-phosphate; and glucose 6-phosphate and fructose 1,6-diphosphate. The pH of the solutions was adjusted at

20°C with 0.5 N KOH or 1 N HCl, and measured within ±0.01 pH by a Brinkmann 632 pH meter. 2 mL NMR samples were then prepared. "Dummy" samples were also prepared with 20 v/v % D_2O. The chemical shifts of the compounds in the four different titration experiments were reproducible within ± 0.02 ppm.

^{31}P NMR Spectroscopy

^{31}P NMR spectra were obtained in the Fourier-transform mode at 202.46 MHz on a Bruker WM-500 NMR spectrometer at 20°C. The "dummy" sample was used for shimming, and for cellular "dummy" samples, 0.1 mL of 1 M phosphate buffer then was added, and the 90° pulse width was determined. Free induction decays (FID's) were accumulated in consecutive 2 min. blocks (240 scans, 8K files) using 70° pulses, 0.5 s acquisition time, and a spectral width of 8000 Hz. Samples were run unlocked (magnet drift < 1 Hz (^{31}P) per hour); sample spinning and ^{1}H decoupling were not employed. The broadband probe matching was optimized for aqueous 0.15 M NaCl solutions.

For the cellular samples, an initial spectrum was taken, then 75 μL of a 40 wt % glucose solution was added, and a sequence of spectra were collected during subsequent 2 min. intervals. At the end of each experiment, a known amount of phosphate buffer was added to the sample for calibration purposes, and then another spectrum was taken. The final spectrum was collected after adding 200 μL of a 25 mg/mL aqueous solution of glycerol phosphorylcholine (P-L Biochemicals) for a chemical shift reference: it resonates 0.49 ppm downfield from 85% phosphoric acid, which is assigned to zero ppm. Cell density (CDW/L) was determined for each sample at the end of the experiment.

Calibration experiments for estimation of intracellular concentrations were performed by alternating fully relaxed spectra with partially saturated spectra. Fully relaxed spectra were obtained with a 2.5 s repetition time (0.5 s acquisition time, 2.0 s relaxation delay), 240 scans and 70° pulse; the partially saturated spec-

tra were obtained with 0.5 s repetition time (0.5 s acquisition time), 240 scans and 70° pulse. Phosphate and GPC were added at the end of the calibration experiments also. For estimation of intracellular concentrations, 1.67 g wet weight/mL intracellular volume and 0.2 g dry weight/g wet weight were assumed.[10]

Data Processing

The 8K FID files taken by the Bruker Aspect-2000 computer were transferred to a VAX(11/780) computer for analysis, using the LAB ONE (TM) NMR1 Spectroscopic Data Analysis Software System.[11] All subsequent processing was performed by the software system on the VAX computer. The FID's were multiplied by an exponential apodization function corresponding to a line broadening of 20 Hz, Fourier transformed, phased, and baseline flattened (4^{th} degree polynomial).

FEATURES OF ^{31}P NMR SPECTRA FOR *S. cerevisiae*

A 202.46 MHz ^{31}P NMR spectrum of *S. cerevisiae* D603 during the steady-state period after glucose feeding is shown in Figure 1. ^{31}P metabolites are distinguished in the NMR spectrum by their chemical shift position (a dimensionless frequency), which is a function of the different electronic environments of phosphorus in these various compounds. The peaks are assigned from previous work in the literature.[9,12,13] Starting from the low field (at the left) in Figure 1, the assignments are as follows. The resonances from 4.5 ppm to 3 ppm are in the sugar phosphate (SP) region. Cytoplasmic inorganic phosphate (P_i^{cyt}) at 1.62 ppm and extracellular inorganic phosphate (P_i^{ex}) at 0.68 ppm are the next clearly observable resonances. The left shoulder on the extracellular inorganic phosphate peak could be due to the phosphate in the vacuole.[14] The resonance at -1.34 ppm is from phosphate in phosphomannan (PM).[13] The nucleotide resonances at -5.39 ppm, -10.05 ppm, and -18.90 ppm were assigned to ATP_γ + ADP_β, ATP_α + ADP_α, and ATP_β, respectively, since other nucleotides were not observed for

S. cerevisiae experiments under similar conditions.[9] The ADP resonances are included for completeness even though they probably contribute less than 10% of the overall signal.[9] PP_1 (-6.62 ppm) is the sum of several phosphate resonances from pyrophosphate and the terminal phosphates of polyphosphate. PP_2 (-18.00 ppm) and PP_3 (-20.17 ppm) are penultimate phosphates from polyphosphate chains, and PP_4 (-22.37 ppm) is the inner phosphate from longer polyphosphate. NAD(H), at -10.66 ppm, includes both NAD^+ and NADH, but in perchloric cell extracts of *S. cerevisiae*, this peak was predominantly NAD^+.[12] Finally, UDPG and similar compounds resonate in the region of -12 ppm.

The low field (6 ppm to 0 ppm) regions for some different example spectra are shown in Figure 2. The figure illustrates how the features in the SP to P_i region change with changing cell state or cell type. Spectra (A) and (B) were taken approximately 8 min. after glucose addition for strains D603 and 18790, respectively. These two spectra have approximately the same chemical shifts for cytoplasmic inorganic phosphate, 2.17 ppm for (A) and 2.15 ppm for (B). The sugar phosphates are also in the cytoplasm, which means that these sugar phosphates have the same chemical environment as does P_i^{cyt}. The chemical shift positions of the sugar phosphate regions are similar for these spectra, but the intensities at the same chemical shift positions differ; the low field compounds in the sugar phosphate regions are more prominent in strain D603 (A) than in strain 18790 (B). This is an example of how different cell types in similar environments can yield different spectra. Spectra (B) and (C) are both for strain 18790 but are at different time points in metabolizing an added pulse of glucose. Here the sugar phosphate resonances and the cytoplasmic inorganic phosphate resonance shift upfield, reflecting changing intracellular conditions. More information on these and other different features besides the ones noted here can be obtained by careful analysis of the spectra. The identities and levels of the sugar phosphates for *S. cerevisiae* 18790 undergoing glycolysis will be estimated later in this paper.

The methodology for this analysis will now be described.

In Vitro pH—CHEMICAL SHIFT RELATIONSHIPS FOR SUGAR PHOSPHATES AND INORGANIC PHOSPHATE

Intracellular pH can be determined *in vivo* by measuring the chemical shift of the intracellular inorganic phosphate peak in the *in vivo* NMR spectrum, and then interpolating the corresponding pH from a previously established *in vitro* relationship between pH and P_i chemical shift.[1,2,3] The mechanics of the pH determination is based on the fact that inorganic phosphate exists in the region of physiological pH in the ionic forms $H_2PO_4^-$ and HPO_4^{-2}. In solution, these two species exchange rapidly so that a single resonance is observed, the chemical shift of which is determined by the relative amount of the two species, which in turn is strongly influenced by pH. A similar concept applies to the sugar phosphates, the chemical shifts of which also vary with pH. Ideally, the pH dependence of the chemical shifts of the sugar phosphates should be determined with a solution that mimics the intracellular ionic strength, free Mg^{2+} level, concentrations of proteins, organic acids, *etc.*, since these factors influence the pK_a and binding of P_i. If the medium ionic strength is known only within the most usual physiological units (within 0.1—0.2 M ions), then the corresponding uncertainty in pH corresponding to a given chemical shift is of the order 0.2—0.5 pH units.[2]

Chemical shifts for sugar phosphates and inorganic phosphate in solutions at different pH values were determined from experiments in which the solutions' compositions were based on the approximate composition inside the cell (approximately 300 mM ionic strength) as cited in den Hollander *et al.*[9] From previous cell extract ^{31}P NMR data in the literature for *S. cerevisiae*,[9,12] the major contributors to the sugar phosphate region of the ^{31}P spectrum during glucose metabolism were identified. These sugar phosphates were investigated *in vitro* in detail. In addition, ^{31}P NMR data by Gadian *et al.*[4] for sugar phosphate

solutions at approximately 120 mM ionic strength provided a comparison for the present experiments at 300 mM ionic strength.

From the *in vivo* spectra in Figure 2 and the *in vitro* spectra in Figure 3, the concept of pH determination is illustrated. In the *in vitro* spectrum all resonances shift upfield (*i.e.*, toward smaller values of chemical shift) with a decrease in pH of 6.66 to 5.66. In the *in vivo* spectra (B) and (C) in Figure 2, the upfield shifts of the sugar phosphate region and cytoplasmic inorganic phosphate reflect a decrease in cytoplasmic pH. In Figure 4, the pH dependencies of the *in vitro* P_i chemical shift at 300 mM ionic strength and 120 mM ionic strength are depicted. These curves provide bounds for the estimation of cytoplasmic pH's based on the data in Figure 2. The cytoplasmic pH's for (A), (B), and (C) in Figure 2 are estimated from Figure 4 to be 6.75, 6.73, and 6.30 at 300 mM ionic strength and 6.91, 6.89, and 6.45 at 120 mM ionic strength.

As noted earlier and illustrated in the data in Figures 2 and 3, the sugar phosphate resonances also shift downfield (*i.e.*, to larger ppm values) as pH increases. Therefore, in principle, the sugar phosphate chemical shifts could be used to estimate intracellular pH. This is less convenient, however, than using the P_i chemical shift, because the P_i peak is relatively distinct. The SP region of *in vivo* ^{31}P spectra is a broad region, the position and shape of which is a function of the intracellular composition.

Joint dependence of the P_i and sugar phosphates' chemical shifts on pH suggests another strategy for utilizing these data. That is, the chemical shift of each sugar phosphate should correlate with the chemical shift of inorganic phosphate in the same solution. Then, using such a correlation, the P_i chemical shift can be used to estimate the expected chemical shift for each sugar phosphate *in vivo*.

Figures 5 and 6 present correlations between P_i and SP chemical shifts de-

termined from *in vitro* ^{31}P spectra. These correlations were generated by varying the pH to effect consistent, simultaneous shifts in the resonances of P_i and of sugar phosphates. Because these correlations may depend on ionic strength, and because previously published data provide these correlations *in vitro* at 120 mM ionic strength (Figure 5),[4] the data shown in Figure 6 were measured at 300 mM ionic strength. Combined with the previously reported data at an ionic strength of 120 mM, these data bracket the range of expected *in vivo* chemical shifts for each sugar phosphate at a corresponding inorganic phosphate chemical shift. These estimates of *in vivo* sugar phosphate chemical shifts are next applied in concert with the deconvolution analysis of the sugar phosphate region of the ^{31}P NMR spectrum in order to check the deconvolution analysis and to assign the contributions to the overall SP region to particular sugar phosphate compounds.

DECONVOLUTION OF THE SUGAR PHOSPHATE RESONANCES IN THE *In Vivo* ^{31}P NMR SPECTRUM

The SP region of an *in vivo* ^{31}P spectrum is, as shown in Figure 2, a broad feature which, upon careful examination, can be seen to contain multiple modes, shoulders, and other evidences that several individual resonances here overlap and sum together to give the overall SP signal. Unfortunately, the sharp peaks for individual sugar phosphates in *in vitro* spectra, such as those in Figure 3, are sufficiently broadened in the spatially heterogenous *in vivo* samples that they clearly cannot be identified by visual inspection. The different metabolite sugar phosphates, which have relatively narrowly separated chemical shifts under a variety of solution environments (see Figures 5 and 6), combine to produce the SP region resonance seen in the *in vivo* spectra. However, using spectral analysis methods, such as those encoded in the NMR1 software, it is possible to fit the overall sugar phosphate region of the spectrum as a linear combination of separate resonances, each of which has a reasonable single-component lineshape.

Final acceptance of such a decomposition analysis of the sugar phosphate region in a ^{31}P spectrum depends on satisfaction of several criteria: plausible assignment of the chemical shift based on the *in vitro* correlations described above, correct phasing, excellent fit of the sum of the decomposition results to the experimental spectrum, physically reasonable linewidths, and smooth transition of the integrated area of a compound in comparison to the previous and subsequent spectra in a transient experiment. The flowsheet for the deconvolution process is outlined in Figure 7.

The spectrum (processed FID) at the stage as described in Material and Methods is the starting point for the process. After Fourier transformation of an FID, a phase correction is applied to the spectrum for obtaining absorption lineshapes for all peaks. Phase correction is inherent because of the nature of the detection scheme.[15] Therefore, an absolute value of the zeroth and first order phase corrections is not known *a priori*. Consequently, phase corrections are essentially adjustable parameters. Proper phasing is important because a slight change of a few degrees will alter the relative areas in the deconvoluted region in a spectrum but will not change the chemical shift values significantly (*e.g.*, only by approximately 0.02 ppm for the more intense peaks in the sugar phosphate region). Fortunately, phase corrections should be similar for all spectra within a given experiment, so that only fine tuning will be necessary from one spectrum to the next.

Peak installation and initial parameter estimation are provided automatically by the Peak Analysis algorithm in the NMR1 software. The user reviews peaks installed and manually installs/deletes peaks in the sugar phosphate region by visually detecting the shoulders and clearly distinguished peaks in the spectrum. Deconvolution of the spectrum is accomplished using the curve fitting routine in the NMR1 software. A three parameter (chemical shift, linewidth, and intensity) Lorentzian was chosen as the theoretical functional form for indi-

vidual sugar phosphate resonances. Trial calculations with the other empirical lineshapes (Gaussian, ill-phased Lorenzian, and others) did not significantly improve the overall spectrum fit and, more importantly, did not give reasonable linewidths and intensities. Linewidth is the peak width at half height; intensity refers to peak height. The minimization algorithm employed for convergence is a modified Levenberg-Marquardt. Minimizing a correlation number is the objective function of the fitting procedure. A perfect fit gives a correlation number of zero.

The fit of the modeled and experimental spectrum are judged after convergence is obtained in deconvolution. (Here, the "model spectrum" refers to the spectrum calculated by summing the individual contributions, weighted by their estimated intensities, as determined by the NMR1 deconvolution calculations.) The model and experimental curves should fit not only in the central part of the deconvoluted region but also in the left and right wings. If this is not accomplished, the user must loop back, as indicated in the flowsheet. Phasing parameters can be modified, and peaks can be installed or deleted. For judgment in fit, minimization of the correlation number is employed for the choice between rival models for a given experimental spectrum. A change in the phasing or in any other input to the fitting calculation should not give a better fit for the "final" spectrum; if so, the optimum fit has not been reached.

If the fit is acceptable, the chemical shifts of the estimated individual component contributions to the spectrum can be compared to the expected values for metabolites. From the chemical shift position of the cytoplasmic inorganic phosphate position in the spectrum, the chemical shifts of each sugar phosphate metabolite is determined from the correlation curves at 120 mM ionic strength and at 300 mM ionic strength (Figures 5 and 6). These two correlations define a range of expected chemical shift values for each of the sugar phosphate metabolites; then these estimates are compared with the NMR1 analysis results for the identification of the sugar phosphate resonances identified in the decomposition

calculations.

For resonance assignment purposes, assumptions were made for the chemical shift positions of F6P and G6P. F6P, when present, was assumed to overlap with β-FDP 6-P. Consolidation of these peaks into one is a reasonable assumption, as seen from the chemical shift positions in Figures 5 and 6. The calibration curve for F6P at 300 mM ionic strength overlaps the titration curve for β-FDP 6-P. In the 120 mM ionic strength data, the maximum deviation of the chemical shift for F6P is 0.08 ppm downfield from the chemical shift of β-FDP 6-P. Also, the α and β anomers of glucose 6-phosphate (G6P) were accepted as one peak in the fitted spectra. For G6P in solution, the intensity ratio of the peak for the α anomer to the peak of the β anomer is 2/3.[4] Also, the chemical shifts of the α and β forms are a maximum of 0.08 ppm apart, as shown in Figures 5 and 6.

If the chemical shift positions of the peaks evaluated from the deconvolution calculations fall within the range of chemical shifts predicted for some compounds based on the correlations in Figures 5 and 6, then the next criterion, reasonable linewidths and intensities, must be consistent with the assignments so established. Linewidths assist in a decision to accept a particular model spectrum. For example, if β-FDP is present and not F6P, then the linewidths of the 1-P and 6-P peaks should be equal ($\pm$3 Hz), and also the intensities should be equal. This condition is illustrated in Figure 3. If F6P overlaps with the β-FDP 6-P position, then the linewidth and intensity should be greater in the 6-P position than in the 1-P position. In solution, the α-FDP contribution is approximately one seventh the intensity of a β-FDP peak at pH 6.15.[16] Spectra of the sugar phosphates in solution provide useful rough estimates of the chemical shifts, relative linewidths, and relative intensities expected for *in vivo* spectra.

A common type of *in vivo* NMR experiment in this laboratory involves adding a pulse of glucose to resting cells in buffer, and subsequently acquiring a sequence of spectra as time progresses. Relative levels of the metabolites over the time

course of such a transient experiment provide an additional piece of information for acceptance of a deconvoluted spectrum. The transitions of each metabolite from one point in time to the next should be physically reasonable, that is, suitably continuous. Soon after the input of a metabolic stimulus such as a glucose pulse, rapidly fluctuating levels may occur in the intracellular pH and other metabolite levels; when the quasi-steady state conditions are reached later, transitions should be smoother. For example, for *Saccharomyces cerevisiae* 18790, the cytoplasmic pH decreases from an initial value of 6.7 to 6.45 two minutes after glucose addition, then rises to a maximum value of 7.08 at 7 minutes, before decaying slowly for a total of 0.3 pH units in the time period from 11 to 23 minutes. The concentration continuity criterion is used the least of all criteria because of its subjectiveness.

Since a deconvoluted spectrum may give reasonable chemical shift positions but unreasonable linewidths or levels, the deconvolution process must be reiterated until all criteria have been satisfied.

Examples of deconvoluted sugar phosphate regions for two different *S. cerevisiae* strains are given in Figure 8. The graphical signal to noise (2.5 times the peak height divided by the trough to crest height of the noise) of the sugar phosphate region for both spectra is approximately 25. The experimental and the model spectra fit closely in the left and right wings and in the middle for the wild-type (18790) and mutant (D603) yeast spectra. In Figure 8(A), FDP is the major compound present in the sugar phosphate region; the linewidths of the 1-P and 6-P positions of the β form are on the order of 95 Hz (after apodization; *i.e.*, with 20 Hz line broadening applied in data processing). The sugar phosphate region for strain D603 [Figure 8(B)] at 30 minutes after glucose addition contained the following resonances: G6P, FDP, F6P, 3-PGA, and 2 unknown resonances. The linewidths of α-FDP, G6P, β-FDP 1-P, β-FDP 6-P plus F6P, and 3-PGA were 51 Hz, 51 Hz, 62 Hz, 73 Hz,and 68 Hz, respectively.

RESONANCE ASSIGNMENT USING *In Vivo* CHEMICAL SHIFT COORDINATES

Even though the sugar phosphate levels are very different in *S. cerevisiae* strains 18790 and D603, the chemical shift positions of the metabolites were consistent, as shown in Figures 9 and 10. After passing all of the acceptance criteria in the sugar phosphate deconvolution procedure, the chemical shifts of the metabolites for both strains were plotted versus the chemical shift position of the cytoplasmic inorganic phosphate peak. It is important to note that each spectrum was analyzed independently by the deconvolution method, and deconvolution results from different spectra were not compared to each other to aid in resonance identification. The range of chemical shifts for both strains arose because of changes in intracellular pH during the transient experiments.

Different symbols are used in Figures 9 and 10 to indicate chemical shift values obtained from 18790 spectra and those derived from analysis of D603 spectra. It is very interesting that although the sugar phosphate contents of these two strains are significantly different, the chemical shift coordinates of each sugar phosphate cluster along a fairly continuous pattern common to both strains. This strongly suggests that the cytoplasmic solution environment, insofar as this affects the phosphorus chemical shift, is essentially identical in both strains. Furthermore, since these data are derived from measurements taken during transient experiments with changing conditions outside (*e.g.*, extracellular glucose concentration) and inside (*e.g.*, intracellular pH) the cells, these experimentally defined *in vivo* correlations between the chemical shifts of P_i and various sugar phosphates appear to be quite general. They are valid for two different strains under a wide variety of environmental conditions.

The *in vivo* chemical shift data points are very similar to the chemical shift coordinates based on the *in vitro* correlations discussed earlier. The *in vitro* correlation curves at 300 mM ionic strength either underestimate (α-FDP, G6P, β-

FDP 6-P) or fit (β-FDP 6-P, F6P) the *in vivo* chemical shift values (Figure 9). The chemical shift correlations based on *in vitro* measurements at 120 mM ionic strength either overestimate (3PGA, few of G6P points) or fit (all β-FDP curves, most of G6P points) the *in vivo* chemical shift values (Figure 10). An *in vitro* correlation curve at 300mM ionic strength for 3-PGA was not performed; the *in vitro* correlation curve for α-FDP at 120 mM ionic strength is not available.

The scatter in the data for G6P can be explained by the assumptions made earlier. The combination of two peaks (α and β anomers) with slightly different intensities into one peak may not consistently give the same chemical shift position, especially if the intensities of the peaks are weak. It is also possible that other compounds contribute to the scatter. The data for G6P are shown again in Figure 11(A) with these considerations in mind. Blackened squares in Figure 11(A) are from the spectra in which the G6P peak has an intensity lower than the α-FDP peak intensity. These weak intensity cases all correspond to quasi-steady state conditions and strain 18790, situations for which a G6P contribution is barely detectable. Therefore, these points are more uncertain than the others that correspond to more significant intracellular levels of G6P.

α-Glycerophosphate (α-GP) was considered as an alternative assignment for this resonance since in a similar experiment by den Hollander *et al.*,[6] a standard strain of *S. cerevisiae* contained α-GP; using cell extracts, α-GP was determined to be one-fifth the concentration of G6P at steady state. As shown in Figure 11(A), the α-GP *in vitro* correlation curve consistently underestimates the deconvoluted chemical shift values; the *in vitro* correlation curves for G6P much better approximate the relationship indicated by the data. From these observations, the assignment of the deconvolution chemical shift values to G6P is valid.

The deconvoluted values for the chemical shift of 3-phosphoglycerate (3PGA) also form a correlation. Although the data do not correspond exactly to the 120 mM ionic strength *in vitro* correlation for 3PGA, assignment of these resonances

to other sugar phosphates (glucose 1-phosphate, 2-phosphoglycerate) is not appropriate, since their chemical shift correlations (at 120 mM) consistently fall below the *in vitro* values [Figure 11(B)]. This assignment is also supported by previous observations that 3PGA is the major sugar phosphate detected in ^{31}P NMR spectra of extracts of resting yeast cells.[9,12] The cluster of data at the low end of P_i chemical shifts is from spectra of resting D603 cells after glucose exhaustion; also, data points at 1.73 and 1.87 ppm are from resting yeast cells (*S. cerevisiae* D603 and *S. cerevisiae* 18790, respectively) before glucose addition. 3PGA is the only sugar phosphate evident in the ^{31}P NMR spectrum for these cases [dark points in Figure 11(B)]. The chemical shifts for these experimental conditions were determined directly from the original spectra; no deconvolution analysis was required. These chemical shifts for 3PGA during resting conditions are consistent with the chemical shifts deduced from the deconvoluted spectra [open points in Figure 11(B)]. Therefore, the assignment of these deconvolution values to 3PGA is reasonable.

CORRECTING FOR UNSATURATED CONDITIONS TO OBTAIN RELATIVE CONCENTRATIONS

The relative concentrations of compounds within a sample can be determined from the relative areas of their resonances, provided that the appropriate controls are performed. The areas of the resonances for these compounds are proportional to the number of nuclei that contribute toward them, subject to the condition that effects of finite pulse width and other spectrometer nonidealities (such as nonoptimal receiver filter settings) are corrected or assumed negligible.[3] However, for FT NMR of *in vivo* systems, a large number of scans are needed to achieve the required sensitivity; this requires short pulse intervals, which in turn causes the resonances to be partially saturated. Therefore, spectra that occur under saturated conditions must be compared to spectra taken under unsaturated conditions (achieved by adding a relaxation delay so that the nuclei relax back to

their original state before a subsequent pulse is applied). Then a saturation factor is determined for each compound, which may then be used to correct peak areas measured under saturated conditions. Specifically, the saturation factor is defined as the peak area under saturated conditions divided by the peak area under unsaturated conditions. Relative concentrations can be determined in this way within ± 10%.[3,9] Absolute concentrations are determined after calibrating a known amount of phosphorus to spectral peak area and estimating the intracellular volume of the cells that contribute to the signal.[3]

The calibration procedure used for this study was adapted from den Hollander *et al.*[9] Since the sugar phosphate region is lumped together in that work, saturation factors for the individual sugar phosphates were considered here. However, difference in the values for the saturation factors were not expected to vary more than the errors for concentration estimation. The amount of saturation for a compound depends on the relationship between the pulse interval and the T_1 value (spin lattice relaxation time) for its resonance. The T_1's of the individual sugar phosphate components should be similar, since the compounds are similar.

Saturation and unsaturated spectra were compared before glucose addition, and after glucose exhaustion. Under these conditions 3PGA is the only glucose metabolite present in the sugar phosphate region. The saturation factors calculated for the before and final periods were 0.64 and 0.58, respectively. From a suspended cell experiment in which 300 mM glucose was added to strain 18790,[17] saturated and unsaturated spectra were compared for the quasi-steady state conditions achieved 20 minutes after glucose addition. Sugar phosphates other than 3PGA are present in this case (see Figure 8). The saturation factor for the quasi-steady state sugar phosphate region was 0.64. Consequently, a single saturation factor of 0.62 was used to estimate the unsaturated resonance intensities for all of the sugar phosphate compounds.

ESTIMATED INTRACELLULAR SUGAR PHOSPHATE CONCENTRATIONS

The time courses of the intracellular concentrations for the sugar phosphates as determined by the deconvolution method are given in Figure 12 for *S. cerevisiae* 18790. The deconvolution procedure was employed for all spectra with one exception: the F6P and 3PGA levels of the fourth spectrum (approximately seven minutes after glucose addition) could not be resolved into separate components at the P_i^{cyt} chemical shift of 2.40 ppm. The sum of these concentrations is 14.5 mM at this point.

Glucose-repressed cells were resuspended in a buffer free of amino acids and glucose. The first time point was obtained before the addition of glucose; this time point reflects the original steady-state values for resting yeast cells. After 40 seconds, 75 mM glucose was added to the cell suspension. A subsequent time interval of approximately 9.5 minutes is required for transition of intracellular sugar phosphate levels to quasi-steady state fermentation. This steady-state period lasted approximately 13 minutes; FDP is the major sugar phosphate detectable during this time. After approximately 25 minutes, glucose was exhausted, and all sugar phosphate levels except 3PGA returned to their original low values. Metabolite levels after glucose exhaustion are identical to those before glucose addition.

The oscillatory behavior observed in Figure 12 for the sugar phosphates has been previously reported in the literature. The trajectory for β-FDP in Figure 12 was previously observed for *S. cerevisiae* BC-9A under similar conditions based upon *in vivo* ^{13}C NMR measurements.[7] In addition, for *S. cerevisiae* NCYC 239 under similar conditions in an *in vivo* ^{31}P NMR experiment,[9] the total sugar phosphate concentrations, expressed as mM intracellular sugar phosphate, followed a time course similar to that of the sum of the sugar phosphate concentrations determined in this work.

For *S. cerevisiae* 18790, the total sugar phosphate concentrations (as mM phosphate) before glucose addition (4.64 mM), for steady-state fermentation (20 mM), and after glucose exhaustion (4.4 mM) compare well with the just mentioned ^{31}P NMR experiment for anaerobic *S. cerevisiae* NCYC 239 (2.3 mM, 23 mM, 2.6 mM).[9] Interestingly, these values are similar to those for an *in vivo* ^{31}P NMR study of *Candida utilis* (5 mM, 20 mM, 10 mM).[18]

The concentrations of the sugar phosphate metabolites for quasi-steady state anaerobic fermentation of *S. cerevisiae* NCYC 239 were determined by ^{31}P NMR of cell extracts.[6] The concentrations so determined were: G6P = 1.6 mM; α-GP = 0.3 mM; 3PGA = 0.4 mM; FDP = 10.1 mM; and F6P could not be determined. The average of the sugar phosphate values for the 7 time points between 10 and 23 minutes in this research were: G6P = 0.4 mM; α-GP = not detected; 3PGA = 0.2 mM; β-FDP = 9.0 mM; α-FDP = 0.7 mM; and F6P could not be detected. The values based on *in vitro* measurements of extracts and the present *in vivo* method compare well, more so for the FDP concentrations than for the concentrations around 1 mM or lower. The error in concentrations from the *in vitro* method would be expected to be lower than for the *in vivo* method because of the enhanced resolution of cell extract spectra compared to spectra of whole cells. On the other hand, it is impossible to rule out some degree of alteration of metabolite levels resulting from extraction of a cytoplasmic fraction. Also, use of different strains in different experiments may contribute to some disparity in results. In view of all of these factors, estimates of the concentrations of sugar phosphates based on the present approach exhibit satisfactory consistency with previous determinations by other methods.

To the author's knowledge, concentrations of G6P, FDP, F6P, and 3PGA during the transient interval following glucose addition have not been determined previously *in vivo* for *S. cerevisiae*—or for any other strain.

DISCUSSION

The analysis described above also assists in reducing the uncertainty of intracellular pH measurements. The pK_a's of P_i and of the P_i groups in the sugar phosphates, and therefore, the ^{31}P NMR *in vitro* correlation curves, depend upon the ionic strength and composition of the phosphate solution being measured. The solution pH estimates from the *in vitro* pH—P_i chemical shift correlations at 300 mM and 120 mM ionic strength differ at most by 0.2 pH units, with the lower value estimated by the 300 mM data. Since for G6P and FDP (all resonances) the *in vivo* chemical shift correlations are bounded by the *in vitro* chemical shift correlations, the absolute intracellular pH is known within 0.2 pH units. However, noting that the *in vivo* chemical shift correlations agree more closely with the corresponding correlations determined *in vitro* at 120 mM, it can be concluded that the 120 mM solution more closely models the intracellular ionic environment in yeast. Therefore, the absolute pH inside the cells is determined more accurately from the *in vitro* pH—P_i chemical shift curve for 120 mM ionic strength; the error in the determination of pH is accordingly expected to be less than 0.2 pH units.

Since the 300 mM ionic strength solutions were formulated based on data in the literature on the particular ions present inside the cells and their intracellular concentrations, the previous statement would seem contradictory. However, the binding of ions to proteins or other molecules, and in addition, the formation of neutral ion pairs (including ions not present in the titration solution) inside the cell make the use of *in vitro* solutions for analysis ambiguous. On the basis of the comparison between *in vivo* and *in vitro* correlations, the data from this study indicate that the use of the data from the *in vitro* solutions at 120 mM ionic strength provide better estimates on the value of pH inside the cell. Hence, an ionic solution formulated by adding known amounts of ions inside the cell may not mimic the intracellular environment as much as initially expected.

The method developed in this paper also allows intracellular pH estimation

from *in vivo* ^{31}P NMR spectra in which P_i^{cyt} resonance is not detected. The chemical shift values of sugar phosphates can be identified by consistency with the *in vivo* correlations, the P_i chemical shift extracted, and finally the cytoplasmic pH estimated from the *in vitro* correlation curve. FDP is a good compound to use for this purpose because it contributes three different resonances to the spectrum, the chemical shifts of which should be consistent with the three corresponding *in vivo* correlations.

Because of the consistency of the correlations developed between the chemical shifts of the sugar phosphates and of cytoplasmic inorganic phosphate, future analysis of the sugar phosphate region is simplified, since these correlations can be used instead of the *in vitro* correlations for resonance identification. Although certainly these correlations can be used for *S. cerevisiae* utilizing glucose, these correlations may be applied to other systems if the assumption that the intracellular ionic strength and composition of other cells are similar to *S. cerevisiae* is valid. In any event, the groundwork has been developed, and the same methodology can be extended for other cells and other types of metabolism.

CONCLUSIONS

A method has been established for analysis of the sugar phosphate region of *in vivo* ^{31}P NMR spectra for *S. cerevisiae*. This method identifies resonances and estimates the relative intracellular concentrations of several sugar phosphate metabolites. Concentrations of sugar phosphates estimated from this method for *S. cerevisiae* 18790 compared well with literature values. The transient metabolite concentration profiles provided by the method are new information not previously observed.

In vivo correlations were established relating the intracellular inorganic phosphate chemical shift with the chemical shifts of the α and β anomers of fructose 1,6-diphosphate, fructose 6-phosphate, glucose 6-phosphate, and 3-phosphoglycerate.

In addition, the absolute intracellular pH values may be determined within 0.2 pH units from the *in vivo* ^{31}P spectrum. The methodology applied is general and hence can be extended to other biological systems.

The information provided by the analysis of the sugar phosphate resonances can be utilized with the wealth of other information provided by the same ^{31}P NMR spectra. Intracellular concentrations of sugar phosphates, inorganic phosphate, ATP, NAD^+, and polyphosphate can be determined simultaneously for analysis of metabolic flows in steady-state and transient conditions *in vivo*. Intracellular and extracellular pH measurements and estimates of ATP levels provide basic information on the energetics of the cell. The ability to coordinate measurements of metabolic flows with this information on the energy status of the cell *in vivo* is an extremely important step in understanding cellular metabolic kinetics and regulation. Application of this methodology for detailed experimental investigations of genetically engineered cells is now in progress.

Acknowledgement:

This research was supported by the Energy Conversion and Utilization Technology (ECUT) program of the U.S. Department of Energy. The nuclear magnetic resonance experiments reported here were made possible by the facilities of the Southern California Regional NMR Center (NSF Grant No. CHE-84-40137) and software for NMR spectral analysis was provided by the NIH Resource Laboratory at Syracuse University (Grant No. RR-01317). The authors are indebted to the following persons at the NMR center for their assistance in the use of NMR: Dr. James Yesinowski, Dr. Hellmut Eckert, Paula Watnick and Tracy Handel. The authors acknowledge the contribution of Yvette Madrid, a SURF student, in preparing some of the NMR samples.

REFERENCES

1. R.B. Moon and J.H. Richards, *J. Biol. Chem.*, **248**, 7276 (1973).

2. J.K.M. Roberts and O. Jardetsky, *Biochem. Biophys. Acta*, **639**, 53 (1981).

3. D.G. Gadian, *Nuclear Magnetic Resonance and Its Applications to Living Systems*, (Oxford University Press, Oxford, 1982).

4. D.G. Gadian, G.K. Radda, R.E. Richards, P.J. Seeley, "^{31}P NMR in Living Tissue: The Road from a Promising to an Important Tool in Biology," *Biological Applications of Magnetic Resonance*, (Academic Press, New York, 1979).

5. R.G. Shulman, *Sci. Amer.*, **248**, 86 (1983).

6. J.A. den Hollander, K. Ugurbil, and R.G. Shulman, *Biochemistry*, **25**, 212 (1986).

7. J.A. den Hollander, T.R. Brown, K. Ugurbil, and R.G. Shulman, *Proc. Natl. Acad. Sci.*, **76**, 6096 (1979).

8. F. Srienc, J.L. Campbell, and J.E. Bailey,*Cytometry*, **7**, 132 (1986).

9. J.A.den Hollander, K.Ugurbil, T.R.Brown, and R.G.Shulman, *Biochemistry*, **20**, 5871 (1981).

10. J.M. Gancedo and C. Gancedo, *Biochimie*, **55**, 205 (1973).

11. LABONE(TM) NMR1 Spectroscopic Data Analysis Software System, Revision 2.70, (Syracuse University, New Methods Research Inc., 1985).

12. G. Navon, R.G. Shulman, T. Yamane, T.R. Eccleshall, K.B. Lam, J.J. Baronofsky, and J.Marmur, *Biochemistry*, **18**, 4487 (1979).

13. R.A. Gage, W. Van Wijngaarden, A.P.R. Theuvenet, G.W.F.H. Borst-Pauwels, and C.A.G. Haasnoot, *Biochim. Biophys. Acta.*, **804**, 341 (1984).

14. K. Nicolay, W.A. Scheffers, P.M. Bruinenberg, R. Kaptein, *Arch. Microbiol.*, **133**, 83 (1982).

15. M.L. Martin, J.J. Delpuech, and G.J. Martin, *Practical NMR Spectroscopy*, (Heydon and Sons,LTD,Great Britain 1980)

16. G.R. Gray, *Biochemistry*, **10**, 4705 (1971).

17. J.L. Galazzo, J.V. Shanks and J.E. Bailey, *Biotechnology Techniques*, **1**, 1 (1987).

18. K. Nicolay, W.A. Scheffers, P.M. Bruinenberg, and R. Kaptein, *Arch. Microbiol.*, **134**, 270 (1983).

FIGURE CAPTIONS

Figure 1: ^{31}P NMR Spectrum at 202.46 MHz of *S.cerevisiae* D603. The spectrum was taken 20 minutes after addition of 75 mM glucose to a 50% w/w suspension of yeast cells in buffer. Accumulation time was 2 minutes. Abbreviations: SP : sugar phosphate; P_i^{cyt} : cytoplasmic inorganic phosphate; P_i^{ex} : extracellular inorganic phosphate; PM : phosphomannan; ATP : adenosine triphosphate; ADP : adenosine diphosphate; PP_1 : pyrophosphate and terminal phosphates of polyphosphate; NAD(H) : nicotinamide adenine dinucleotide; UDPG : uridinediphosphoglucose; PP_2 and PP_3 : penultimate phosphates of polyphosphate; and PP_4 : middle phosphates of polyphosphate.

Figure 2: Example of changing cell state and cell type in ^{31}P NMR spectra of yeast. (A) *S. cerevisiae* D603, 8 minutes after addition of glucose; P_i^{cyt} at 2.17 ppm. (B) *S. cerevisiae* 18790, 8 minutes after addition of glucose; P_i^{cyt} at 2.15 ppm. (C) *S. cerevisiae* 18790, 20 minutes after addition of glucose; P_i^{cyt} at 1.56 ppm. (A) to (B) is an example of changing cell type at the same cell state. (B) to (C) is an example of changing cell state for the same cell type. Abbreviations: P_i^{vac} : vacuolar inorganic phosphate; others as in Figure 1.

Figure 3: ^{31}P NMR spectra of *in vitro* solutions at 300 mM ionic strength. (A) pH 6.66. (B) pH 5.63. Abbreviations: α-FDP : α-fructose 1,6-diphosphate; β-FDP : β-fructose 1,6-diphosphate; 1-P : 1 phosphate of β-FDP; 6-P : 6 phosphate of β-FDP; GAL 1-P : galactose 1-phosphate; P_i : inorganic phosphate.

Figure 4: P_i chemical shift as a function of solution pH. Symbols: (○) 300 mM ionic strength; (●) 120 mM ionic strength.[4] 300 mM ionic strength data are from four experiments, as stated in Material and Methods.

Figure 5: *In vitro* correlations between inorganic phosphate chemical shift and chemical shifts for sugar phosphate compounds at 120 mM ionic strength.[4] Symbols: (□) β-glucose 6-phosphate : β-G6P; (■) α-glucose 6-phosphate : α-G6P; (★) α-glycerophosphate : α-GP; (△) β-FDP 1-P; (✣) β-FDP 6-P; (+) fructose 6-phosphate : F6P; (○) 3-phosphoglycerate : 3PGA; (∗) glucose 1-phosphate : G1P; (●) 2-phosphoglycerate.

Figure 6: *In vitro* correlations between inorganic phosphate chemical shift and chemical shifts for sugar phosphate compounds at 300 mM ionic strength. Symbols: (◇) α-FDP; (×) GAL 1-P; (∗) β-G1P; (⊕) α-G1P; others as in Figure 5.

Figure 7: Flowsheet for deconvolution and analysis of the sugar phosphate region of *in vivo* ^{31}P NMR spectra.

Figure 8: Deconvoluted ^{31}P NMR spectra in the sugar phosphate region for yeast. (A) *S. cerevisiae* 18790, 20 minutes after addition of glucose. (B) *S. cerevisiae* D603, 30 minutes after addition of glucose. Dotted lines - data; solid lines - model. (a) α-FDP; (b) unknown; (c) G6P; (d) β-FDP 1-P; (e) β-FDP 6-P + F6P; (f) 3PGA; (g) unknown.

Figure 9: Comparison of *in vivo* and *in vitro* chemical shift correlations for the sugar phosphates. *In vivo* chemical shift values are based on deconvolution analysis of ^{31}P NMR spectra measured during transient response experiments with *S. cerevisiae*. 18790 (open symbols) and D603 (solid symbols). Solid lines denote *in vitro* correlations at 300 mM ionic strength. Symbols: (□) G6P; (✣) β-FDP 6-P + F6P; others as in Figures 5 and 6.

Figure 10: Comparison of *in vivo* and *in vitro* chemical shift correlations for the sugar phosphates, as in Figure 9, except that the solid lines now denote *in vitro* correlations at 120 mM ionic strength.[4]

Figure 11: Expansion of Figure 10. (A) Chemical shift data for G6P, including the *in vitro* correlations for α-GP at 120 mM ionic strength[4] (dashed line) and for α-G6P and β-G6P (solid lines) at 120 mM ionic strength. Points represent values estimated from deconvolution of *in vivo* spectra. Darkened symbols indicate values for peaks with intensities less than the intensity of α-FDP. (B) Chemical shift data for 3PGA, including the *in vitro* correlation curves of 2-phosphoglycerate (broken dashed line), G1P (dashed line), and 3PGA (solid line) at 120 mM ionic strength.[4] Darkened symbols are for chemical shifts from spectra in which 3PGA was the only resonance in the sugar phosphate region.

Figure 12: Intracellular sugar phosphate concentrations obtained from the deconvolution analysis process for *S.cerevisiae* 18790. Glucose added at 0+ seconds; glucose exhausted after 30 minutes. (△) β-FDP; others as in Figures 5 and 9.

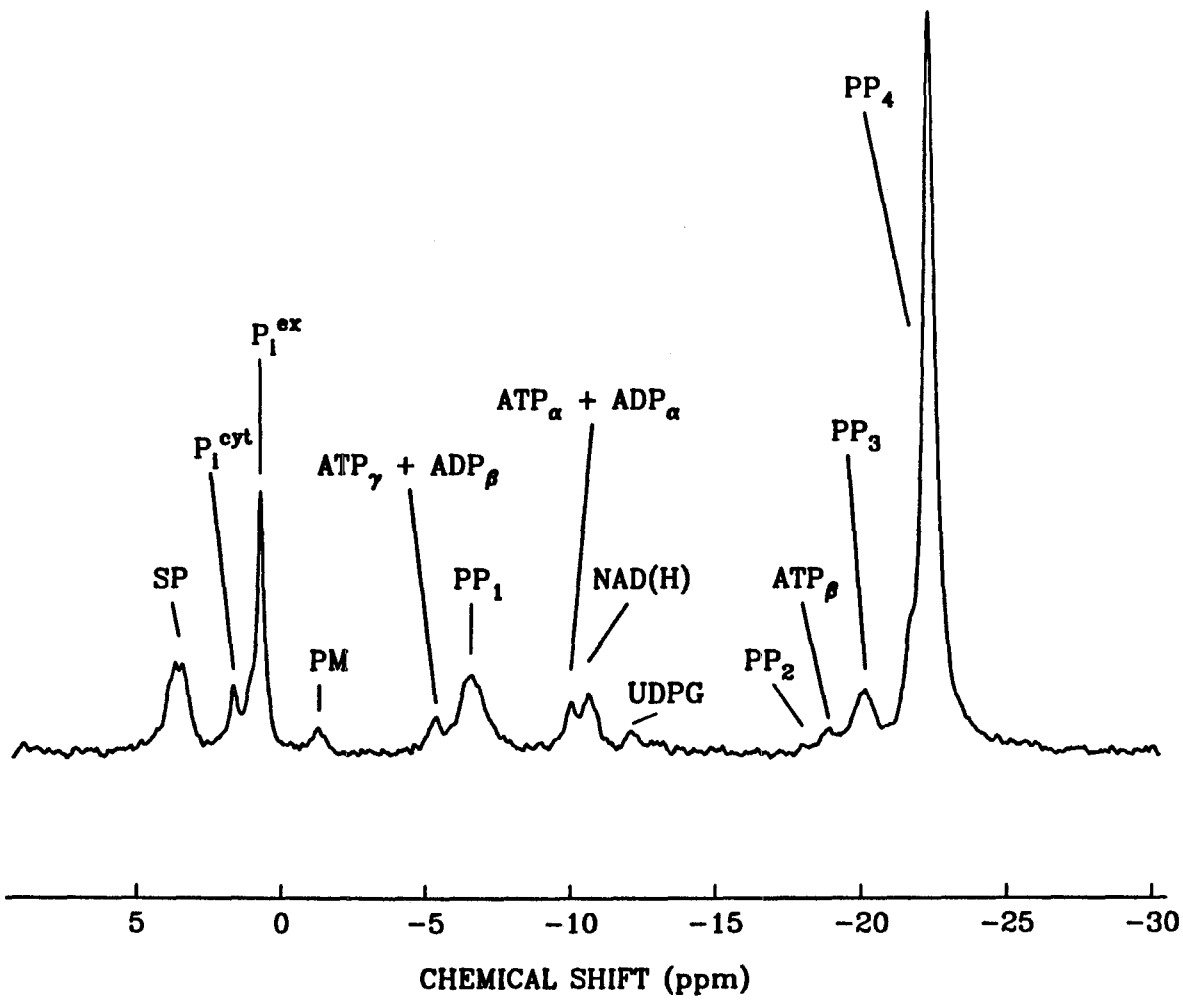
PP4
P1ex
P1cyt
ATPα + ADPα
PP3
ATPγ + ADPβ
SP
PP1
NAD(H)
ATPβ
PM
PP2
UDPG
5
0
-5
-10
-15
-20
-25
-30
CHEMICAL SHIFT (ppm)

Figure 1

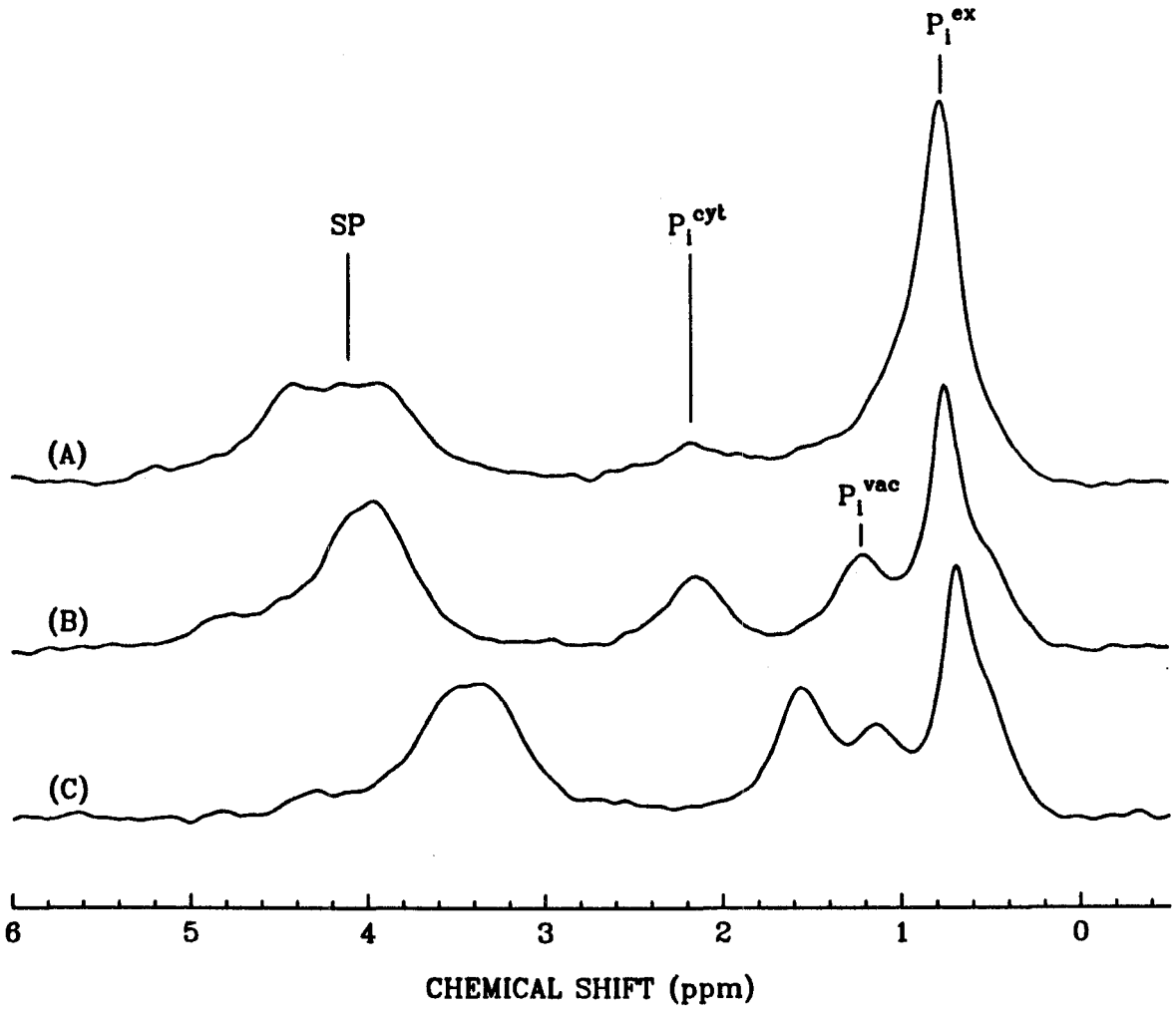

Figure 2

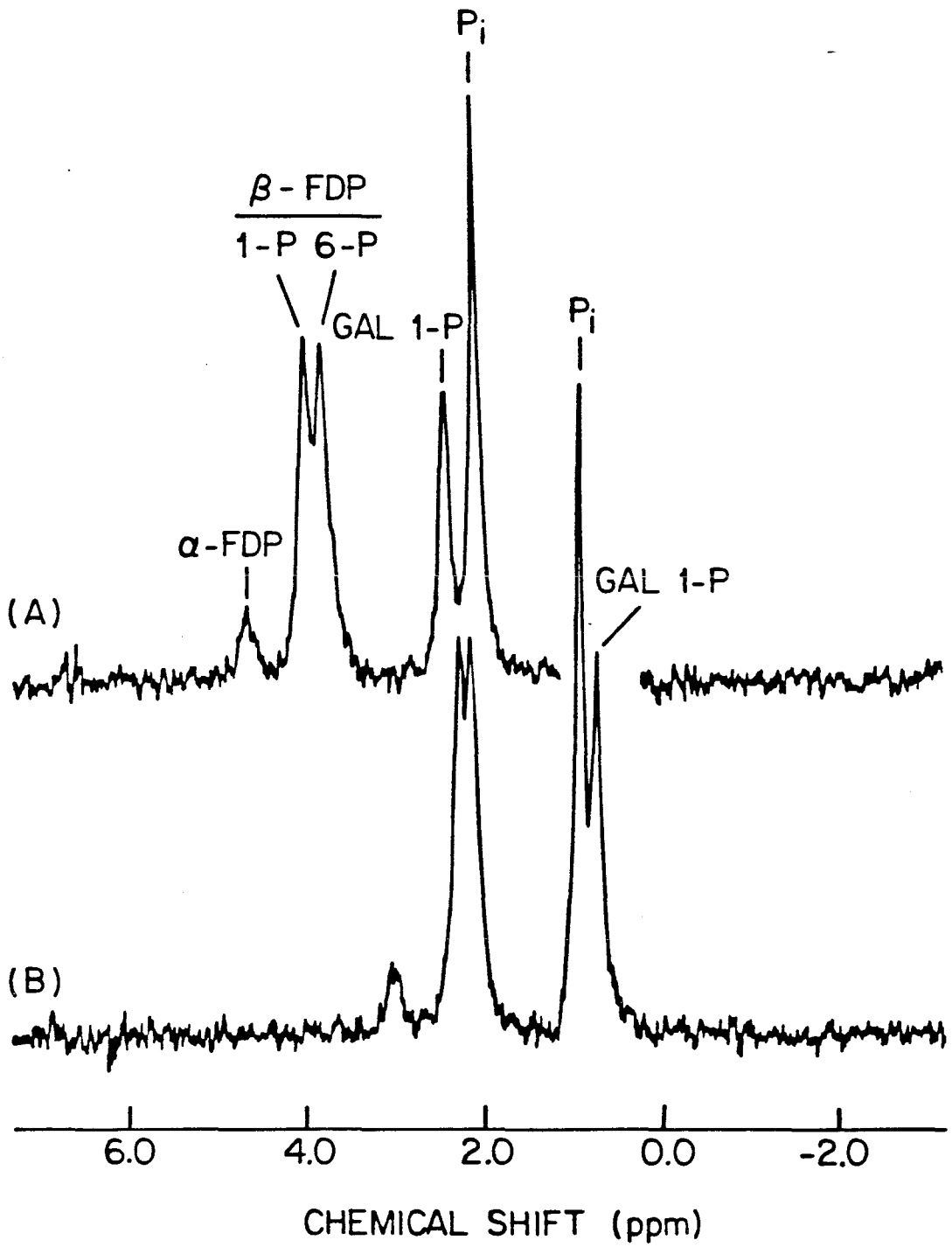
Pi
β - FDP
1-P 6-P
GAL 1-P
Pi
α-FDP
GAL 1-P
(A)
(B)
6.0
4.0
2.0
0.0
-2.0
CHEMICAL SHIFT (ppm)

Figure 3

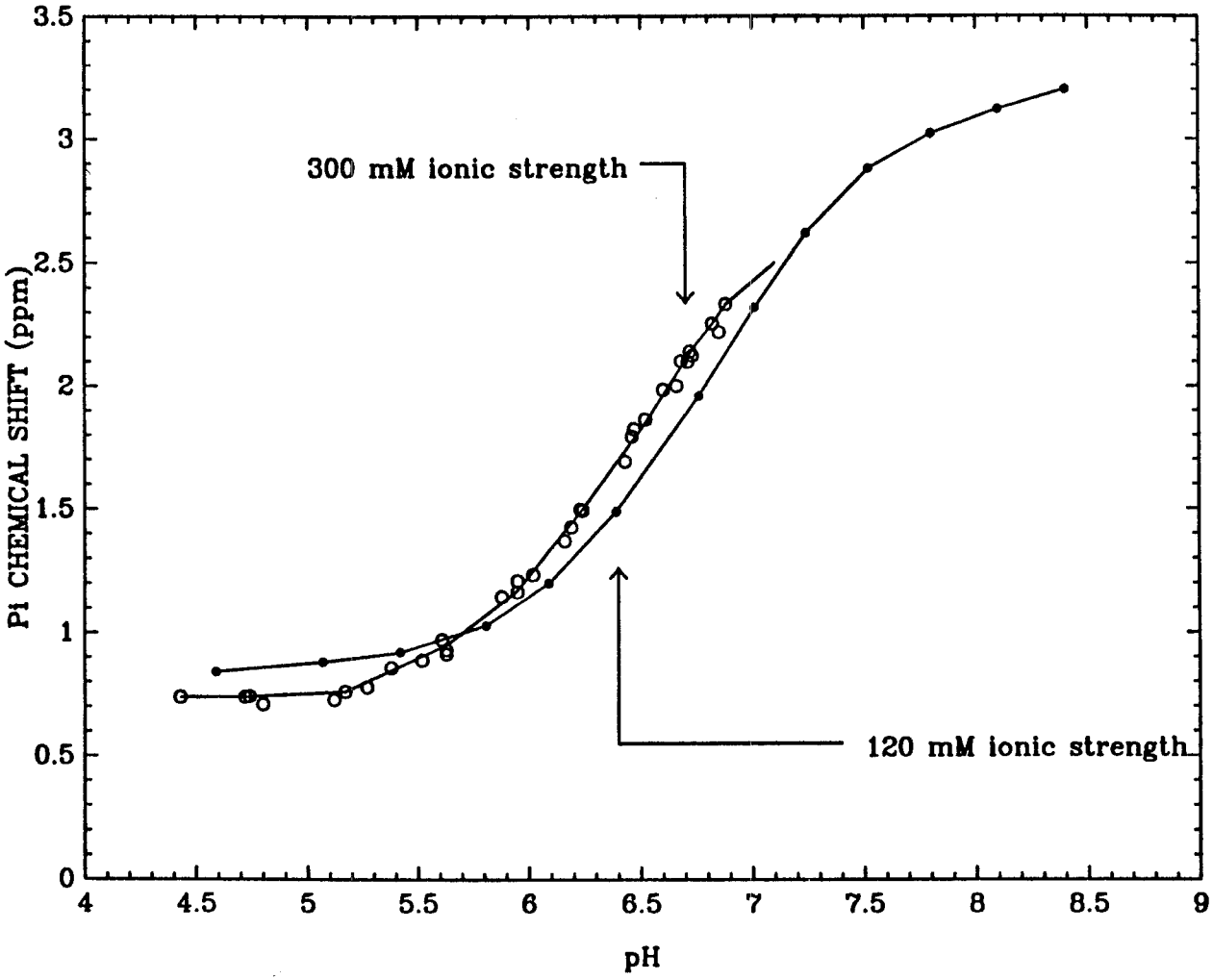
3.5
3
2.5
2
1.5
1
0.5
0
Pi CHEMICAL SHIFT (ppm)
300 mM ionic strength
120 mM ionic strength
4
4.5
5
5.5
6
6.5
7
7.5
8
8.5
9
pH

Figure 4

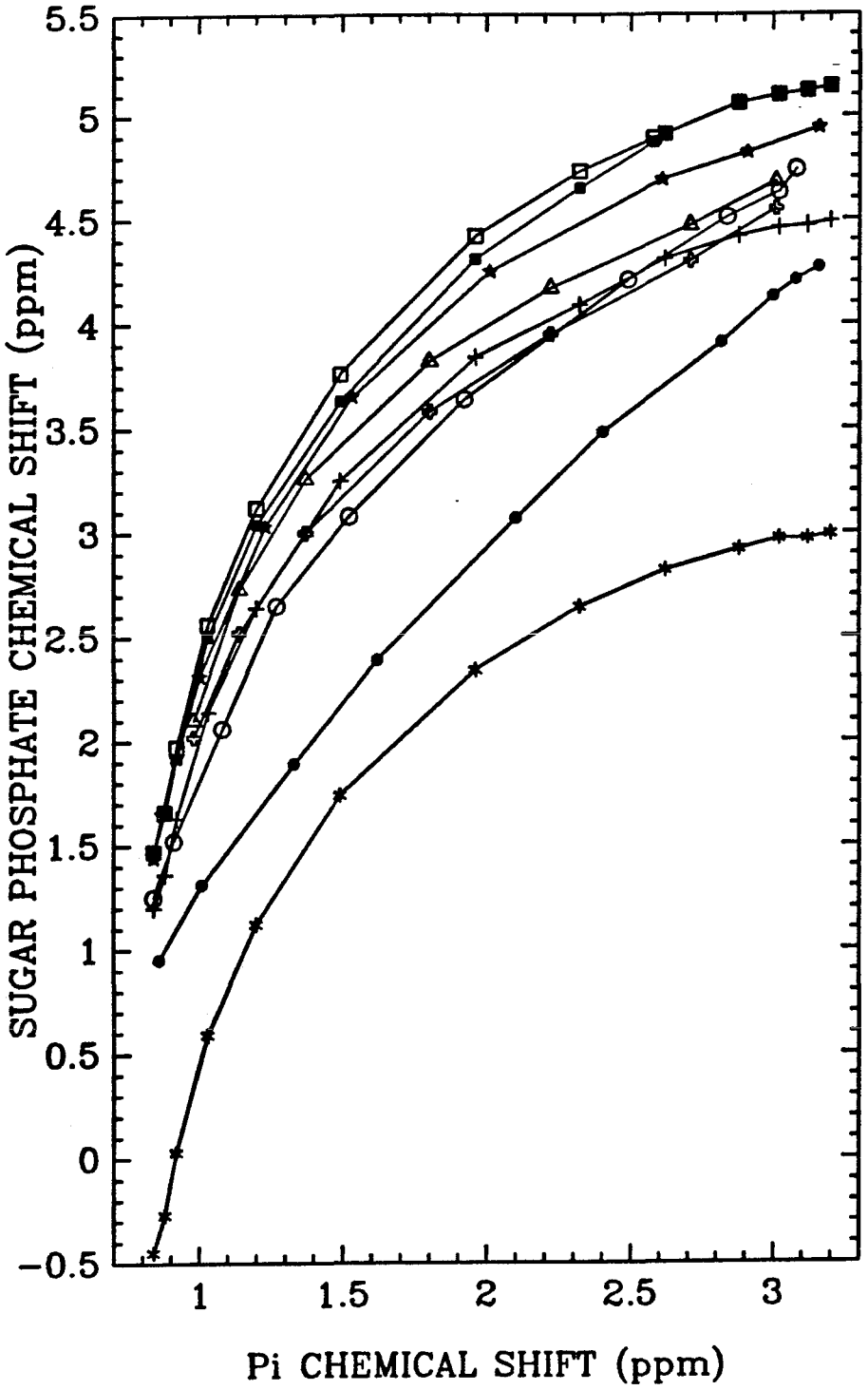
SUGAR PHOSPHATE CHEMICAL SHIFT (ppm)
Pi CHEMICAL SHIFT (ppm)
5.5
5
4.5
4
3.5
3
2.5
2
1.5
1
0.5
0
−0.5
1
1.5
2
2.5
3

Figure 5

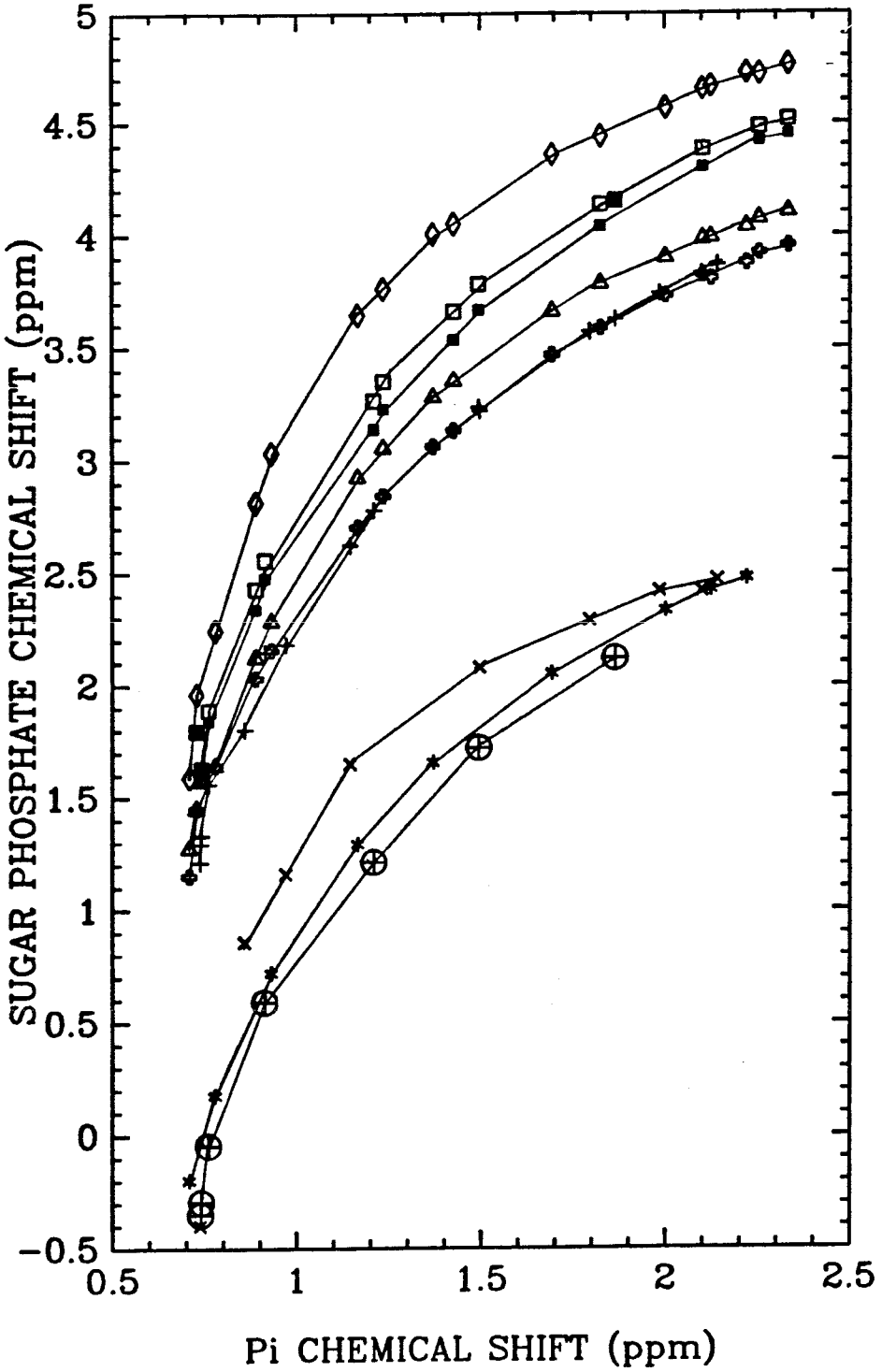
SUGAR PHOSPHATE CHEMICAL SHIFT (ppm)
Pi CHEMICAL SHIFT (ppm)
5
4.5
4
3.5
3
2.5
2
1.5
1
0.5
0
−0.5
0.5
1
1.5
2
2.5

Figure 6

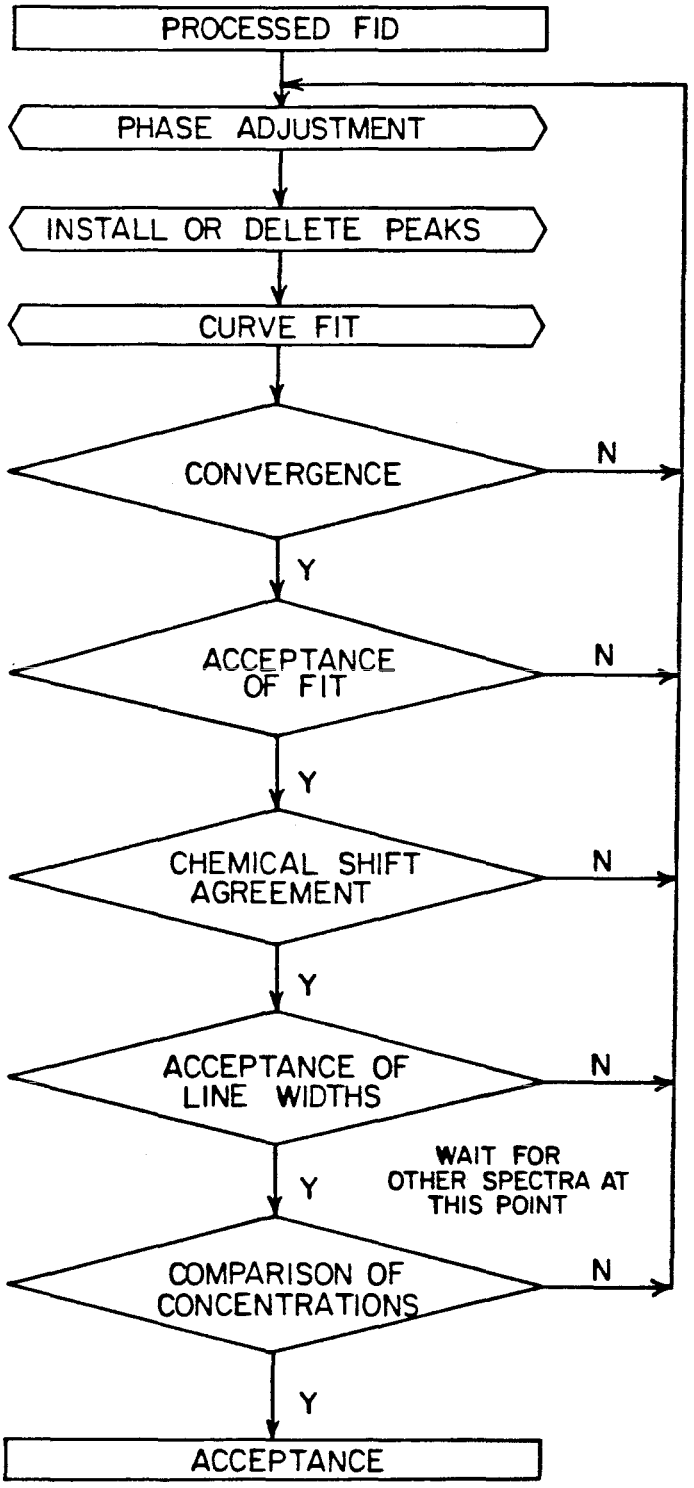
PROCESSED FID
PHASE ADJUSTMENT
INSTALL OR DELETE PEAKS
CURVE FIT
CONVERGENCE
N
Y
ACCEPTANCE OF FIT
N
Y
CHEMICAL SHIFT AGREEMENT
N
Y
ACCEPTANCE OF LINE WIDTHS
N
Y
WAIT FOR OTHER SPECTRA AT THIS POINT
COMPARISON OF CONCENTRATIONS
N
Y
ACCEPTANCE

Figure 7

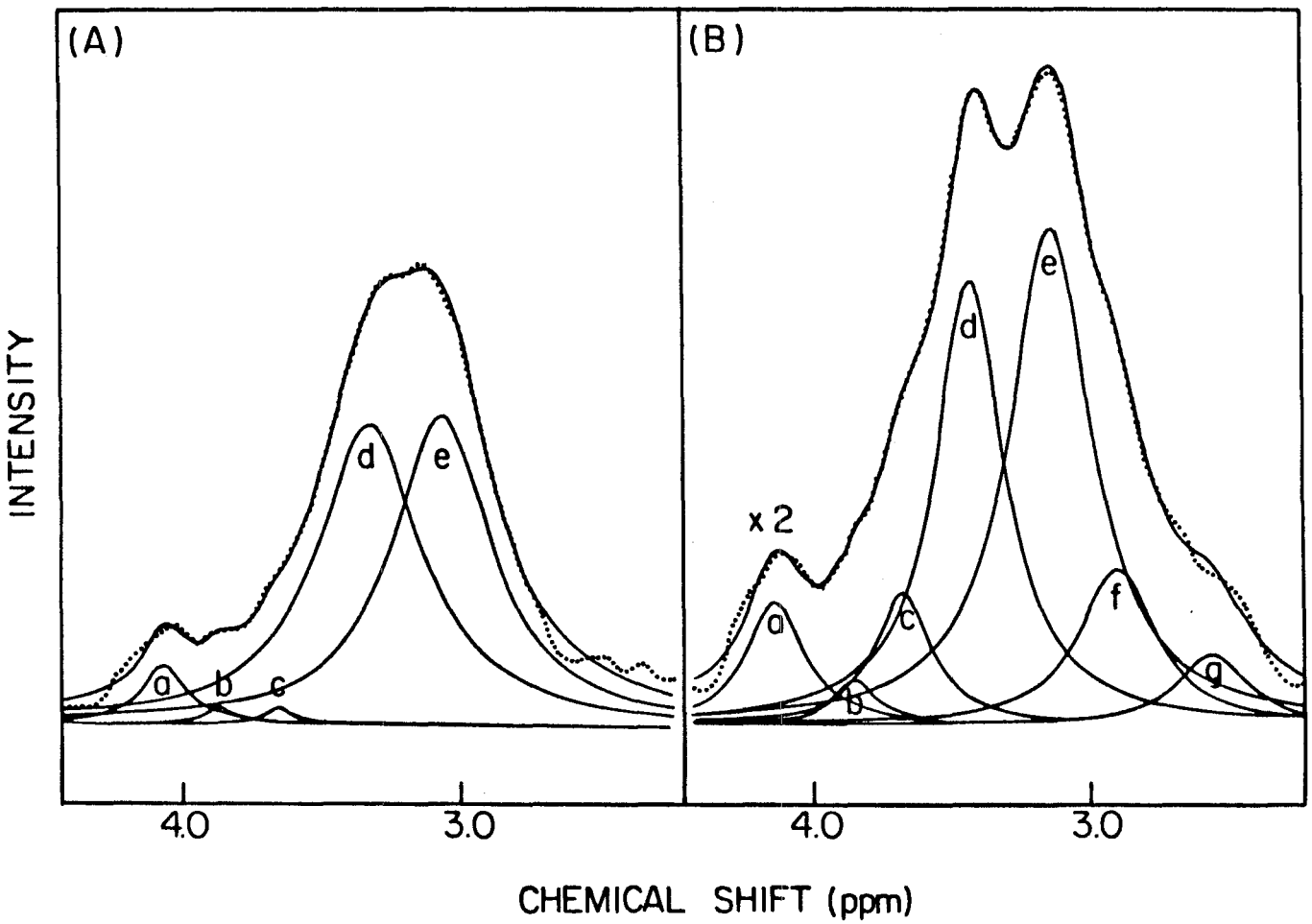

Figure 8

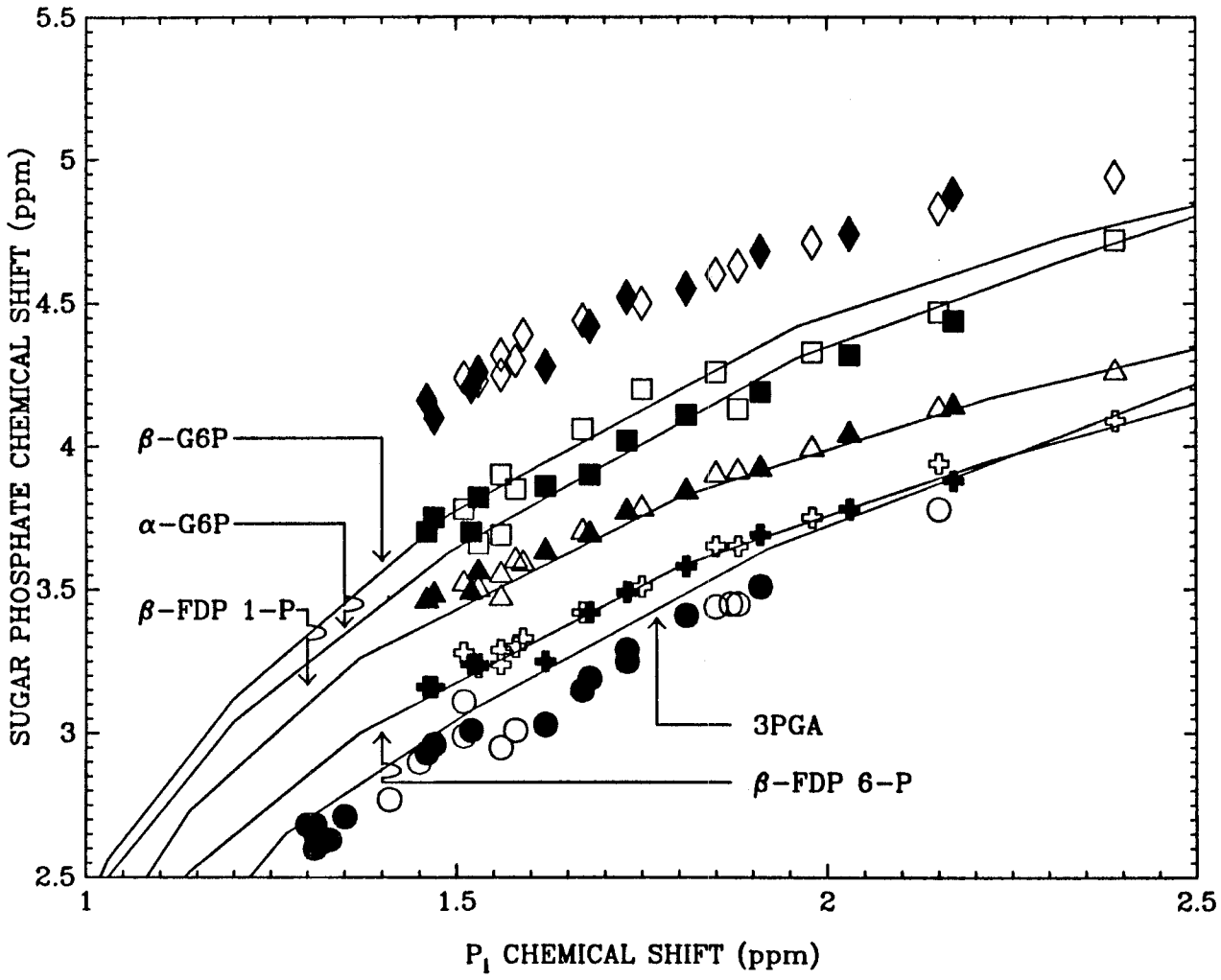
5.5
5
4.5
4
3.5
3
2.5
1
1.5
2
2.5
SUGAR PHOSPHATE CHEMICAL SHIFT (ppm)
P$_i$ CHEMICAL SHIFT (ppm)
β-G6P
α-G6P
β-FDP 1-P
3PGA
β-FDP 6-P

Figure 9

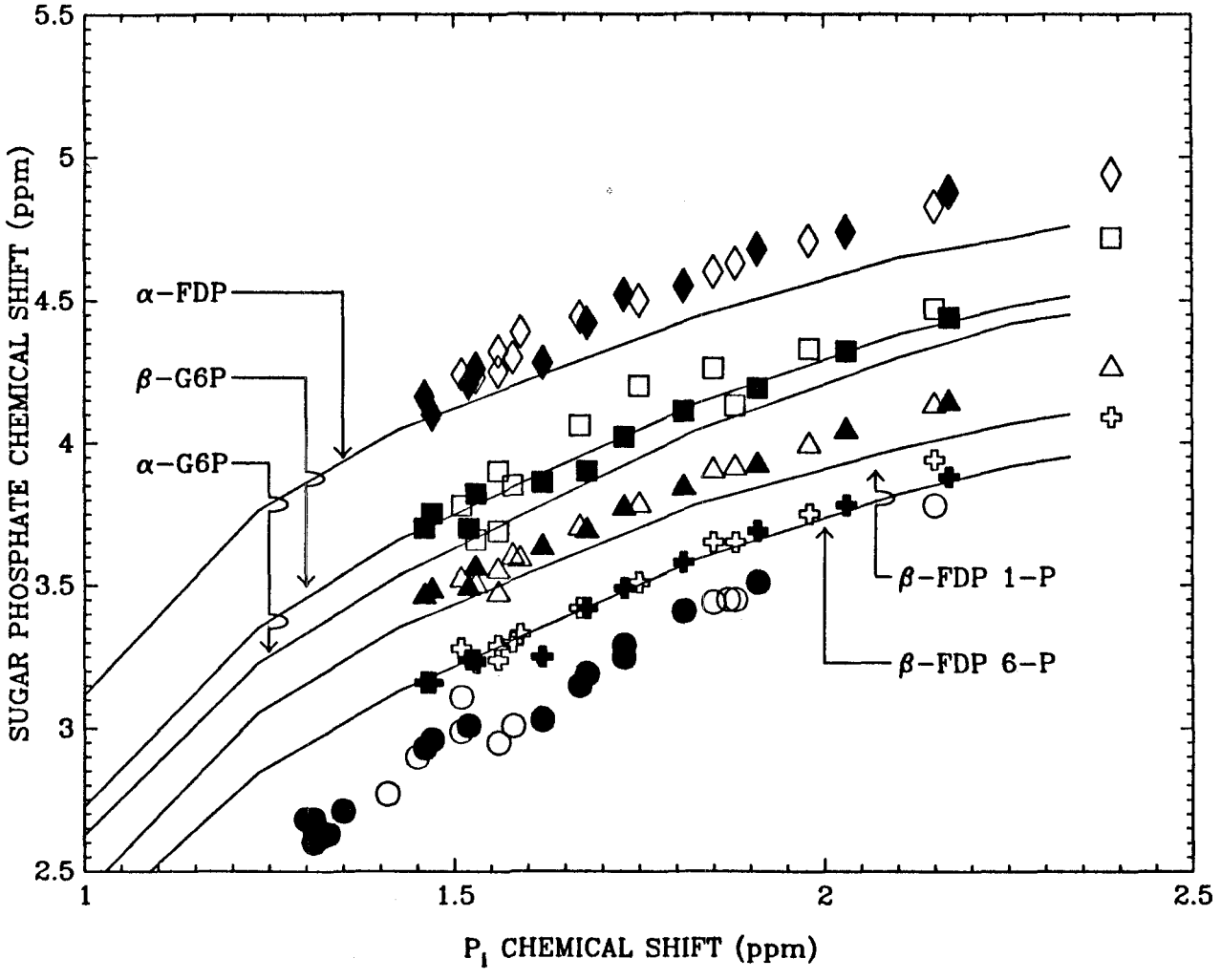
5.5
5
4.5
4
3.5
3
2.5
1
1.5
2
2.5
SUGAR PHOSPHATE CHEMICAL SHIFT (ppm)
P$_i$ CHEMICAL SHIFT (ppm)
α–FDP
β–G6P
α–G6P
β–FDP 1–P
β–FDP 6–P

Figure 10

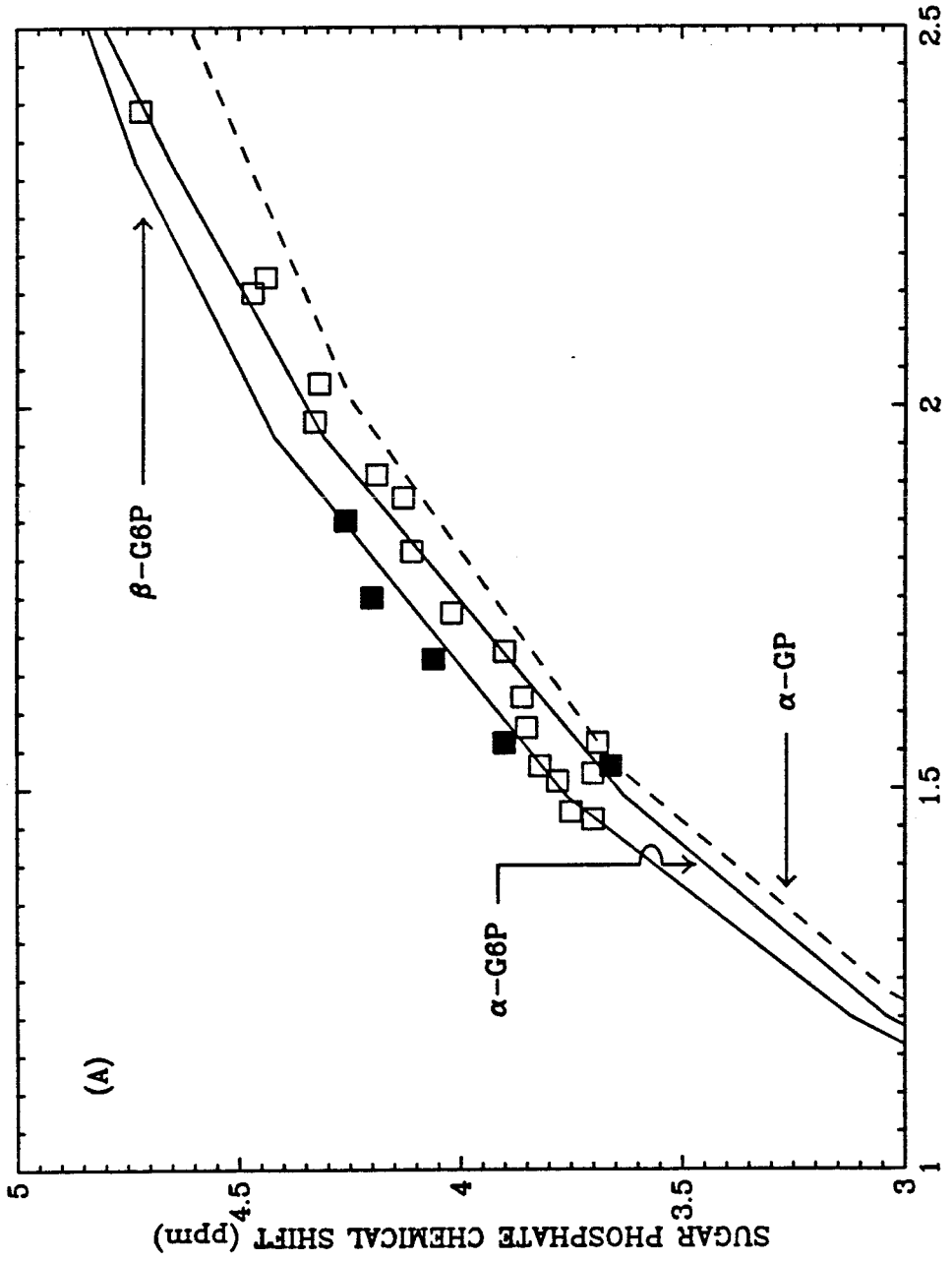
SUGAR PHOSPHATE CHEMICAL SHIFT (ppm)
5
4.5
4
3.5
3
1
1.5
2
2.5
P1 CHEMICAL SHIFT (ppm)
β-G6P
α-G6P
α-GP
(A)

Figure 11(A)

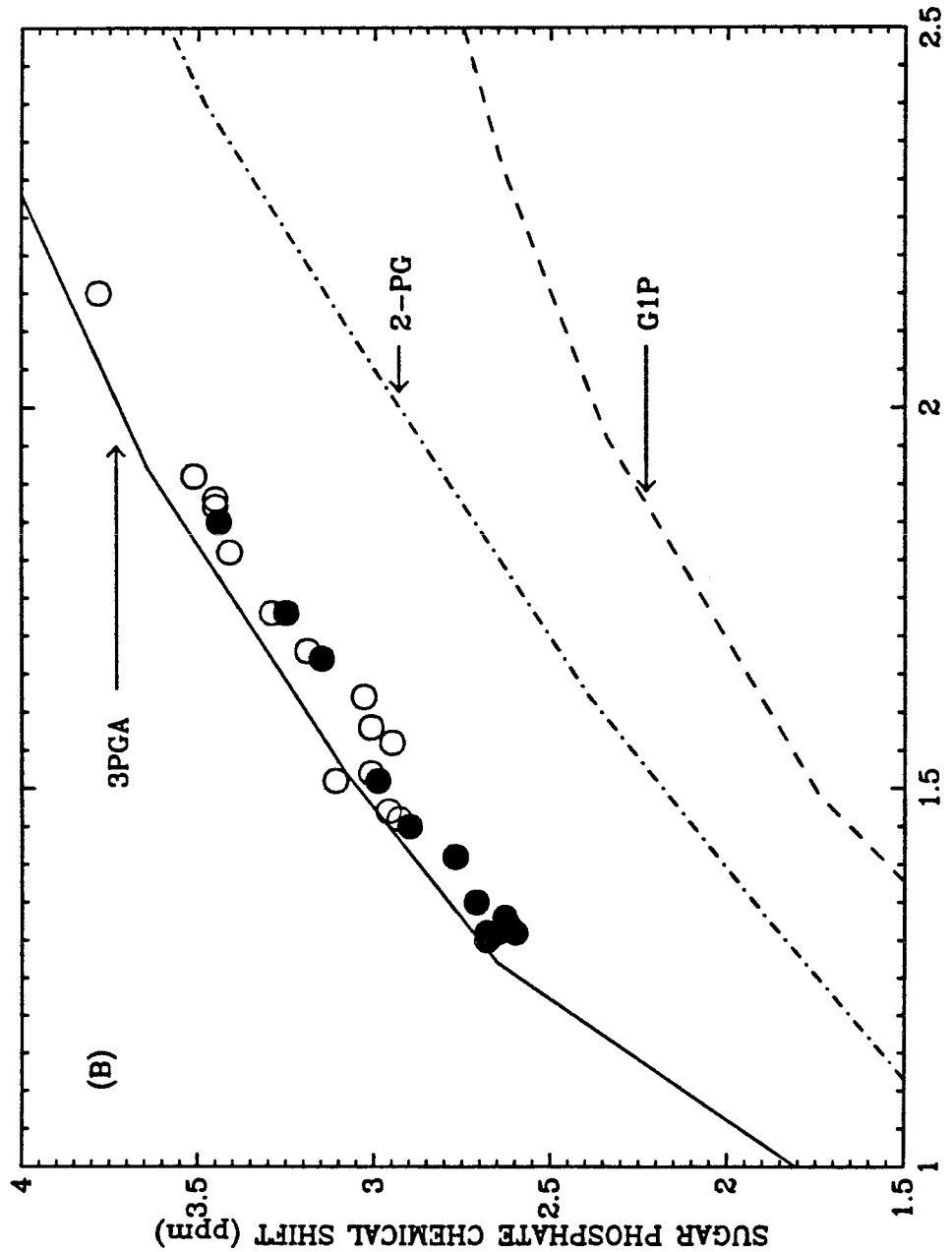
SUGAR PHOSPHATE CHEMICAL SHIFT (ppm)
4
3.5
3
2.5
2
1.5
1
2.5
2
1.5
P_i CHEMICAL SHIFT (ppm)
(B)
3PGA
2-PG
G1P

Figure 11(B)

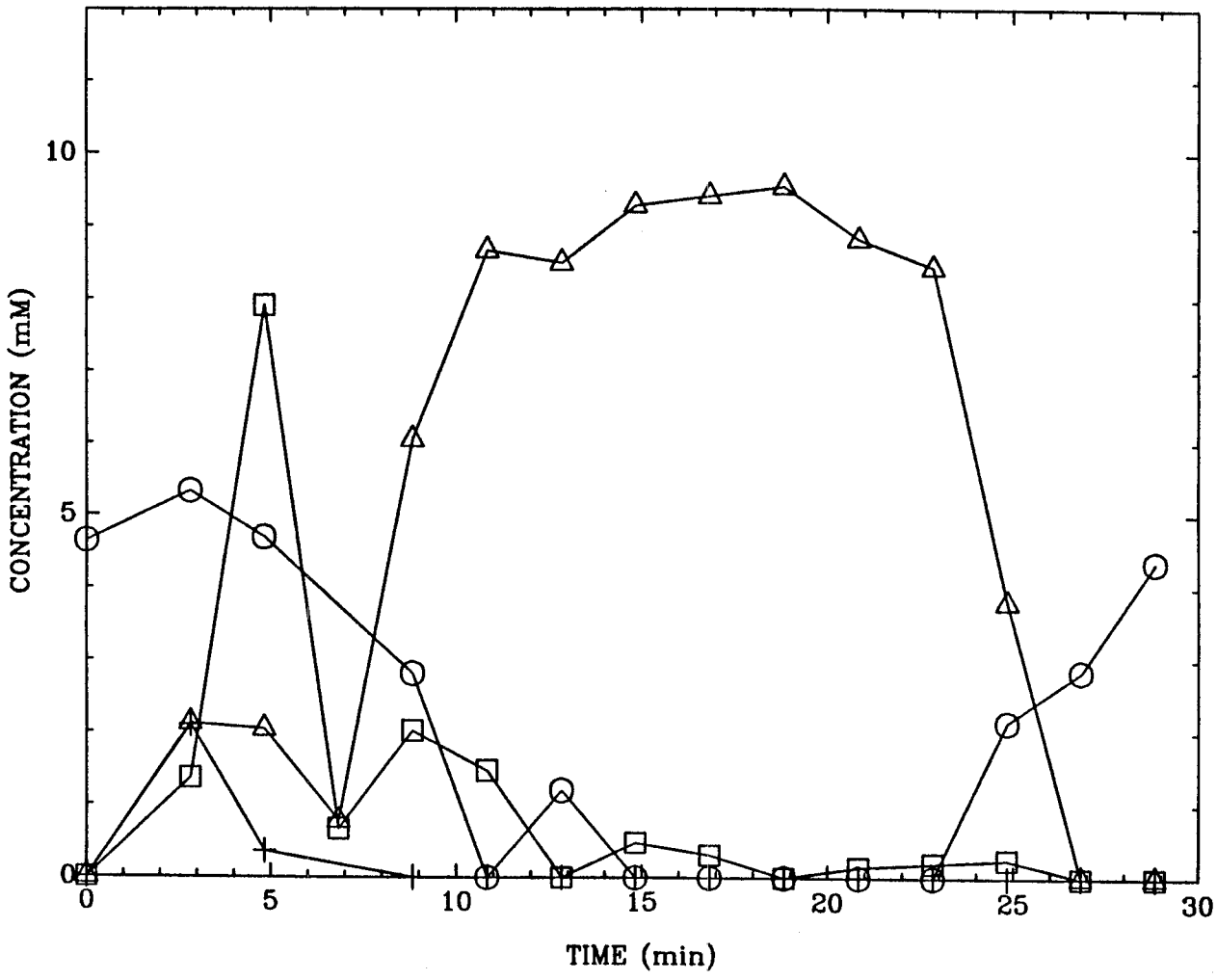

Figure 12

CHAPTER 3

ELUCIDATION OF THE CYTOPLASMIC AND VACUOLAR COMPONENTS IN THE INORGANIC PHOSPHATE REGION IN THE ^{31}P NMR SPECTRUM OF YEAST

ABSTRACT

Concentrations of inorganic phosphate and pH values of the vacuole and cytoplasm were determined for anaerobic *S. cerevisiae* cells based upon ^{31}P NMR spectroscopy. The intracellular inorganic phosphate resonance is first decomposed into two components by computer analysis. The assignments of the components were determined from the chemical shift estimation of the cytoplasmic resonance as determined from *in vivo* correlations of P_i chemical shift and the chemical shifts of the sugar phosphates, and the pH dependency of the resonance of pyrophosphate and the terminal phosphate of polyphosphate (PP_1). An *in vivo* correlation relating PP_1 and P_i^{vac} chemical shifts was established from numerous evaluations of intracellular compositions for several strains of *S. cerevisiae*. This correlation will aid future analysis of ^{31}P NMR spectra of yeast and will extend NMR studies of compartmentation to cellular suspensions in phosphate-containing medium. Application of this method shows that both vacuolar and extracellular P_i were phosphate reserves during glycolysis in anaerobic *S. cerevisiae*. Net transport of inorganic phosphate across the vacuolar membrane was not correlated with the pH gradient across the membrane.

INTRODUCTION

Since its infancy in 1973, *in vivo* ^{31}P NMR has become a popular method to study bioenergetics and metabolism in diverse living systems, from microbial cells to humans.[1–3] As such studies become more numerous and are performed by a diverse group of scientists and engineers, protocols established for the analysis of spectra will allow faster and more detailed data interpretation. The identity of compounds in the phosphomonoester region (low field region) in ^{31}P NMR spectra of cancer cells has been a subject of dispute.[4] Quick diagnosis of *in vivo* spectra is important for clinical applications. A method has been developed for estimation of sugar phosphate concentrations in ^{31}P NMR spectra of the yeast *Saccharomyces cerevisiae*.[5] In this paper, a method is described for elucidating information for the vacuole from the inorganic phosphate (P_i) region.

The chemical shift of inorganic phosphate and other phosphorylated metabolites are sensitive to pH near physiological pH values. Consequently, concentrations of P_i can be monitored in compartments within the cell that have different pH values (or which differ in ionic strength and in the levels of specific ions that affect pH determination by NMR).[6] In yeast, signals for inorganic phosphate in the cytoplasm, the vacuoles, and peroxisomes have been observed in ^{31}P NMR spectra.[2,5,7,8] Peroxisomes form under growth on methanol and contain enzymes essential for methanol metabolism.[8] Vacuoles are present under several growth conditions and during the entire growth cycle, but in a process of almost continual morphological change.[9] As much as 80 - 90 % of the soluble amino acids, up to 40 % of intracellular magnesium and up to 98 % of the cellular polyphosphate are located in the vacuole.[10] The vacuole contains an ATPase and several degradative and salvage enzymes for polyphosphate.[11] Polyphosphate may regulate phosphate homeostasis in the cell.[11]

The vacuole is usually more acidic than the cytoplasm through the action of the vacuolar ATPase.[12] This difference tends to shift the resonance P_i^{vac} upfield

(lower chemical shift values) relative to the resonance P_i^{cyt}. Other factors may cause the vacuolar resonance to shift slightly downfield from the cytoplasmic resonance because of differences in the chemical environment such as ionic strength or Mg^{2+} concentrations, which will affect the pH dependency of P_i chemical shift.

The vacuolar component may be difficult to distinguish in the ^{31}P NMR spectrum if one or more of the following factors are present: extracellular P_i is present, inorganic phosphate levels in the cytoplasm are greater than the vacuole, or the resonances P_i^{cyt} and P_i^{vac} are close together. This has limited ^{31}P NMR studies of the vacuole to cases in which the extracellular medium does not contain phosphate,[7,14] or contains low levels of phosphate.[13] Since the levels of expression of phosphatases are influenced by P_i in the medium,[11] the extension of these studies to cells exposed to varying levels of phosphate is important in studying phosphorus metabolism.

In this paper, a methodology is presented for determining the vacuolar component in ^{31}P spectra of yeast cells in which the cells are resuspended in medium containing phosphate. The intracellular inorganic phosphate resonance will be deconvoluted into two possible components. The assignments of the components are determined from a combination of factors: the chemical shift estimation of the cytoplasmic resonance (P_i^{cyt}) as determined from *in vivo* correlations of P_i chemical shift and the chemical shifts of the sugar phosphates,[5] and the pH dependency of the resonance of pyrophosphate and the terminal phosphate of polyphosphate (PP_1).

MATERIALS AND METHODS

Yeast Strains

Saccharomyces cerevisiae ATCC 18790, *S. cerevisiae* D603, [15] *S. cerevisiae* DFY 437:pBW111, *S. cerevisiae* DFY 437:pBW112, and *S. cerevisiae* DFY 437:

pBW113 were the yeast strains used in this study. *S. cerevisiae* 18790 is a standard diploid strain. *S. cerevisiae* D603 is the homozygous diploid version of YM603 (*ade2-101*, *ura3-52*, *his3*, *met*, *lys2-801*, *reg1-501*). The *reg1* mutation inhibits catabolic repression by glucose. *S. cerevisiae* DFY 437 and plasmids pBW111, pBW112, and pBW113 were kindly provided by Dan Fraenkel.[16] The haploid strain *S. cerevisiae* DFY 437 (*α lys1*, *leu2*, *hxk1*, *hxk2*, *glk*) is unable to phosphorylate glucose or fructose. The plasmids were constructed from the YEp13 shuttle vector, and the structural genes *HXK1*, *HXK2*, and *GLK* were cloned by complementation for the plasmids pBW111, pBW112, and pBW113, respectively. *HXK1* encodes for the gene for hexokinase P-I, *HXK2* for hexokinase P-II, and *GLK* for glucokinase.

Culture and NMR Preparation

Culture conditions and NMR preparation procedures have been described previously.[5,17] The strains were grown aerobically to midexponential phase in liquid medium containing 1% yeast extract, 2% bacto-peptone, and 2% glucose at pH 4.5. The cultures were chilled on ice, then harvested by low–speed centrifugation at 4°. The cells were washed twice in an ice-cold, sterile, buffered salt solution: 0.85 g/L KH_2PO_4, 0.15 g/L K_2HPO_4, 0.5 g/L $MgSO_4$, and 0.1 g/L NaCl in 50 mM MES buffer, pH adjusted to 6 with NaOH. The cells were resuspended in wash medium supplemented with an additional 15 mM P_i (7.5 mM KH_2PO_4: 7.5 mM K_2HPO_4) at a 1:1 ratio of cell pellet volume to resuspension volume. For one experiment, *S. cerevisiae* 18790 was resuspended in wash medium. Cell suspensions (2 mL) in the NMR tubes were tightly capped and kept on ice until used for the NMR experiment. Shimming was performed on identical samples except that they contained D_2O.

^{31}P NMR Spectroscopy

^{31}P NMR spectra were obtained in the Fourier-transform mode at 202.46

MHz on a Bruker WM-500 NMR spectrometer or a Bruker AM-500 NMR spectrometer at 20°C.[5,17] The pulse interval and angle were 0.5 s and 70°, respectively. Free induction decays (FID's) were accumulated either in consecutive 1 min. blocks (120 scans, 8K files) or in 2 min. blocks (240 scans, 8K files). Sample spinning and ^{1}H decoupling were not employed.

An initial spectrum was taken of the cellular suspension, then 75 μL of a 40 wt % glucose solution was added and a sequence of spectra was collected. At the end of each experiment in which concentrations were to be measured, phosphate buffer was added to the sample. Glycerol phosphorylcholine (P-L Biochemicals) was added for confirmation of endogenous GPC as a chemical shift reference. GPC resonates 0.49 ppm downfield from 85% phosphoric acid, which is assigned to zero ppm. Cell density (g CDW/L) was determined for samples for concentration measurements.

Calibration experiments for estimation of intracellular concentrations were performed by alternating fully relaxed spectra with partially saturated spectra, as described previously.[5,17] Relative concentrations can be determined within $\pm$ 5 %. For estimation of intracellular concentrations, 1.67 g wet weight/mL intracellular volume and 0.2 g dry weight/g wet weight were assumed.[18] For estimation of extracellular concentrations, the density of wet yeast was assumed to be 1.0 g wet weight/mL total yeast volume.

Data Processing

The 8K FID files taken by the Bruker Aspect-2000 (or -3000) computers were transferred to a VAX(11/780) computer for analysis using the LAB ONE (TM) NMR1 Spectroscopic Data Analysis Software System.[19] All subsequent processing was performed by the software system on the VAX computer. The FID's were multiplied by an exponential apodization function, Fourier transformed, phased, and baseline flattened (4^{th} degree polynomial).

pH Determination

As described previously, the cytoplasmic pH was determined by the chemical shift position of P_i^{cyt}, and then interpolating the corresponding pH from the *in vitro* relationship between pH and P_i chemical shift at 120 mM ionic strength.[5,20] The 120 mM ionic strength solution did not contain magnesium and will subsequently be referred to as a Mg^{2+} - free solution.

For spectra in which assignment of P_i^{vac} and P_i^{cyt} resonances is not apparent, the chemical shift positions of the sugar phosphates were used to estimate the P_i^{cyt} chemical shift and thus aided in the identification of the P_i^{cyt} resonance. *In vivo* correlations of P_i^{cyt} chemical shift and the chemical shifts of the sugar phosphates were determined by a systematic procedure based upon ^{31}P NMR measurements. [5] The sugar phosphate region of the ^{31}P NMR spectrum was first decomposed by computer analysis (NMR1 software), and the decomposition consistency and identification of individual sugar phosphate resonances were established, based on *in vitro* chemical shift calibrations determined in separate experiments.

For estimates of vacuolar pH, the P_i^{vac} resonance was the indicator. The *in vitro* relationship of pH and P_i chemical shift at 300 mM ionic strength[5] was used for reasons discussed below. The 300 mM ionic strength solution contained 20 mM Mg^{2+} and will subsequently be referred to as a 20 mM Mg^{2+} solution.

RESULTS

The low field regions of ^{31}P NMR spectra of *S. cerevisiae* 18790 during catabolism of glucose are shown in Figure 1. The yeast cells in Figure 1(A) and (C) were resuspended in buffer with 22 mM P_i; cells in Figure 1(B) and (D) were resuspended in buffer with 7 mM P_i. Spectra in Figure 1(A) and (B) were taken immediately after addition of glucose. The cells in Figure 1(C) and (D) are actively glycolyzing substrate.

The assignment of resonances in Figure 1 are as follows.[21–23] The resonances from 5 ppm to 3 ppm are in the sugar phosphate (SP) region. The resonances in the region from 2.5 ppm to 0.6 ppm are assigned to inorganic phosphate in different environments. In Figure 1(A), the resonance labelled P_i^{in} is the sum of vacuolar and cytoplasmic inorganic P_i resonances. Extracellular inorganic phosphate (P_i^{ex}) is the next clearly observable resonance in spectrum (A). The signal for cytoplasmic inorganic phosphate (P_i^{cyt}) resonates the farthest downfield in this region in Figure 1(B) and (C). This reflects the higher pH in the cytoplasm in comparison to the vacuole or the extracellular buffer. A separate resonance for inorganic phosphate in the vacuole is detected clearly at approximately 1 ppm in Figure 1(C) and (D). The shoulder on the right of P_i^{cyt} in Figure 1(B) is tentatively assigned to the vacuole. This assignment will be confirmed later. In spectra of perchloric acid cell extracts taken of glycolyzing cells of strain 18790 and D603, only a single resonance for inorganic phosphate is observed (data not shown). Since the extract procedure destroys the cell membrane and vacuolar membrane, this observation is consistent with the assignment of the cytoplasmic and vacuolar resonances in Figure 1(C) and (D).

Endogenous glycerophosphorylcholine (GPC) is detected at 0.49 ppm; its chemical shift is independent of pH. The resonance at -1.34 ppm is from phosphate in phosphomannan (PM) in the cell wall. The nucleotide resonance around -5 ppm is assigned to $ATP_\gamma + ADP_\beta$.

PP_1 is the sum of several phosphate resonances from pyrophosphate and the terminal phosphates of polyphosphate. The terminal phosphates of polyphosphate resonate between -5.5 and -7 ppm for stationary phase yeast cells titrated with acid or base.[24] The chemical shift of PP_1 is pH dependent, as determined in NMR experiments of cell extracts of *S. cerevisiae*; the divalent cation concentration lowered the pKa of PP_1.[22] Consequently, at a given pH value, higher divalent cation concentrations will cause the PP_1 resonance to shift downfield.

In Figure 1(A), cytoplasmic and vacuolar inorganic phosphate cannot be distinguished from each other. In Figure 1(B) the cells are in a similar state as in Figure 1(A), except that the level of phosphate in the buffer is lower; a shoulder is detected on P_i^{cyt}. The shoulder is tentatively assigned to the vacuole because the lower chemical shift would indicate a lower pH value. The resonance PP_1 has the same chemical shift value in Figure 1(A) and (B); since most of the cellular polyphosphate is located in the vacuole, this indicates a similar pH value for the vacuole. The chemical shifts of PP_1 for the first two spectra predict a pH of around 6.5, as estimated from the pH titration curve for PP_1 in Salhany *et al.*,[24] and as estimated from results in Nicolay et. al. [13] The pH estimated from the intracellular inorganic phosphate peak in the first two spectra are 6.52 and 6.69, respectively (using Mg^{2+}–free solution: for 20 mM Mg^{2+} solution, subtract 0.2 pH units). Hence, if a vacuolar component is present in Figure 1(A), it would be obscured by the cytoplasmic resonance.

Deconvolution of the P_i^{in} resonance into 2 components was performed using the NMR1 software.[19] P_i^{ex} and GPC must be included in the deconvolution exercise, since the resonances overlap slightly. A Lorentzian lineshape was assumed for each component. When necessary, the sugar phosphate region was also deconvoluted.[5] The chemical shifts of components #1 and #2 of P_i^{in} in different experiments of the same strain but differing levels of P_i in the buffer and of recombinant strains are given in Table 1. Values from the spectra in Figure 1(A) and (B) correspond to values listed in Table 1 for spectrum 2 for strain 18790 in the high P_i buffer and low P_i buffer, respectively. Also included in Table 1 is the estimation of the chemical shift of P_i^{cyt} as determined from the estimated chemical shifts of the sugar phosphates and the *in vivo* correlations of the chemical shift of P_i^{cyt} with the chemical shifts of the individual sugar phosphates. The first spectrum in an experiment is taken before glucose is added to the cellular suspension, and is labeled 1 in the table. Glucose is added, then a series of spectra is taken,

and the spectra are labeled 2, 3, and so forth. Before glucose addition, 3-PGA is the main component in the sugar phosphate region. After a minute after glucose addition, sugar phosphates G6P, F6P, and FDP also become detectable.

In all cases, component #1 is assigned to the cytoplasm because of the good agreement between the estimate of P_i^{cyt} from chemical shifts of the sugar phosphates and the chemical shift of component #1. Component #2 is tentatively assigned to the vacuole. However, for now this resonance will be referred to as $P_i^{\#2}$; the pH value, $pH^{\#2}$. Further explanation of this assignment follows.

Since at least 80% of the cellular polyphosphate concentrates in the vacuole,[25] profiles of pH^{vac} vs time and the chemical shift of PP_1 vs time should qualitatively be similar. This was illustrated in ^{31}P NMR experiments of *S. cerevisiae*, given ethanol as the carbon source.[13] This type of test was performed in the present experiment for strain 18790 in 22 mM P_i medium. The profiles of the chemical shifts of PP_1 and of $pH^{\#2}$ versus time follow the same pattern qualitatively, as shown in Figure 2. The $P_i^{\#2}$ resonance in this experiment is clearly observable in spectra for the third through fourteenth time points. In the fifteenth time point, the resonance is a shoulder on the cytoplasmic resonance. Only a single resonance is observed for intracellular phosphate for the first two time points. If component #1 in the second spectrum of this experiment were assigned to the vacuole, $pH^{\#2}$ would be 6.42. Such an assignment would cause major deviation between $pH^{\#2}$ and the trend in PP_1 chemical shift in time.

The results in Figure 2 suggest that the relationship between the chemical shifts of PP_1 and $pH^{\#2}$ is roughly linear for *in vivo* yeast suspensions. This result has not been discussed explicitly in prior literature. The next two figures expand on this matter. Figures 3 and 4 show the data from Figure 2 in a different way. These plots include the third variable - $P_i^{\#2}$ chemical shift. The chemical shifts of $P_i^{\#2}$ and PP_1 both depend upon vacuolar pH, if component #2 was assigned to the vacuole. A plot of PP_1 versus P_i^{vac} would have the shape of a quadratic

function, which is concave downward over the entire range of pH dependency. Figure 3 is such a plot over the range of pH values in the compartment assigned to $P_i^{\#2}$ during the ^{31}P NMR experiments. A plot of PP_1 versus pH^{vac} would have a sigmoidal shape, linear near the pKa. Figure 4 is the corresponding plot from the *in vivo* experiments. The knowledge of these functions is from the general shape of these types of correlations for the sugar phosphates.[5]

Besides showing the data from Figure 2, Figures 3 and 4 include the data from several other NMR measurements of yeast; data include the values in Table 1 and values from other spectra in which the $P_i^{\#2}$ resonance was distinguished from P_i^{cyt} and P_i^{ex}. Several observations can be made from these figures. First, the shape of the functional form including all of the data points in Figures 3 and 4 is quadratic, with the quadratic term much less heavily weighted than the linear term. From Figure 4, this indicates that the pKa for PP_1 is between 5.6 and 6.3 pH units. Second, with the exception of the experiment with strain DFY 437:pBW112, the data points for each experiment individually follow the functional form described above. Third, in Figure 3, the scatter over all of the different experiments is $\pm$ 0.1 ppm in the variance for PP_1 chemical shift from a given chemical shift in $P_i^{\#2}$ (and vice versa). Similar variances exist for the variables PP_1 and $pH^{\#2}$ ($\pm$ 0.1 pH) in Figure 4.

Because of the variances in Figures 3 and 4, the assignment for component #2 to the vacuole based upon these figures alone is plausible but not concrete. The assignment of component #1 to P_i^{cyt} based upon the chemical shifts of the sugar phosphates makes the assignment of component #2 to the vacuole concrete.

The scatter in Figures 3 and 4 may be explained by errors in chemical shift measurements and the possible differences in the chemical environment in the vacuole. The second point will be further discussed below. The error in chemical shift determinations is estimated to be $\pm$0.05 ppm; the stronger peaks are more accurately measured and the weaker peaks somewhat less. The resonance

PP_1 has a large linewidth - on the order of 150 Hz in the experiments performed at 202.46 MHz. The reason is that this asymmetric peak (see Fig. 1) is the sum of contributions from a $P_3O_{10}^{-5}$ doublet (tripolyphosphate), a $P_2O_7^{-4}$ singlet (pyrophosphate), and several end phosphate groups from different lengths of polyphosphate chains.[22] The chemical shift value is taken at the center of the highest peak height for this resonance. Any change in the relative distributions in the various contributors in this region will add to the error for the chemical shift value for PP_1. The linewidths of P_i^{cyt} and P_i^{vac} are on the order of 50 Hz; the deconvoluted components #1 and #2 also had similar linewidths.

The pH time courses for the experiment shown in Figure 2 are presented in Figure 5. The closer the chemical environment in the solution used for the *in vitro* P_i - pH chemical shift correlation to the *in vivo* situation, the more accurate the pH estimate. The *in vitro* relationship[5] between pH and P_i chemical shift that was developed from a solution containing 20 mM Mg^{2+} was used for the estimation of pH for the vacuole. As determined in an earlier paper, a correlation developed from a Mg^{2+}–free solution gave a more accurate pH estimate for the cytoplasm.[5] For comparison, the dashed line in Figure 5 is the vacuolar pH profile estimated from the relationship developed from the Mg^{2+}–free solution

The reasons for use of the curve from the 20 mM Mg^{2+} solution for the estimation of pH in the vacuole are as follows. The vacuole is a cation trap; 50 - 60% of the cellular magnesium was determined to be in the vacuole.[26] In addition, the concentration gradient of cytosolic to vacuolar magnesium is 1:5 in repressed *S. cerevisiae* cells.[26] The strains in this paper are repressed, since the cells are harvested in the middle of the exponential growth phase when glucose is still present in the medium. Because of the Mg^{2+} gradient, the pH - P_i curve for the vacuole would be expected to be shifted to the left of the pH - P_i curve for the cytoplasm. This would give a lower pH value for the same P_i^{vac} chemical shift. The total magnesium concentration in the vacuole was determined by *in vitro*

methods to be 80 mM;[26] the pH^{vac} values in Figure 5 are likely overestimates. However, the magnesium effect on the pH - P_i curve can be counterbalanced by the addition of molecules to which magnesium binds.[6] Some of the scatter in Figures 3 and 4 may due to differences in free Mg^{2+} levels in the vacuole from strain to strain. As a final note, the ionic strength in the vacuole is not known; however, increasing ionic strength would have a similar effect as increasing Mg^{2+} on the *in vitro* pH–P_i curve.

The transient profile for the cytoplasmic pH is explained elsewhere.[27] The pH gradient across the vacuolar membrane varies between 0.3 to 1.1 pH units. The pH gradient is constant for the first 3 min., then increases to its maximum value within 4 min. The pH gradient decreases in Figure 5 when the cytoplasmic pH decreases, until a final pH gradient value of 0.5 pH units is reached - at which time glucose is exhausted and the experiment is concluded. The large shift in the pH gradient occurs simultaneously with the detection of ATP in the ^{31}P NMR spectrum.[27] Most likely, the vacuolar ATPase is transporting protons into the vacuole with the hydrolysis of ATP. At this time the plasma membrane ATPase is also fueled with ATP provided by glycolysis, and consequently the pH value increases in the cytoplasm. A pH gradient increase from 0.3 to 1.2 pH units occurs upon supplying O_2 and glucose to logarithmic cells of *S. cerevisiae* in HEPES or MES buffer (no P_i in buffer).[14] The vacuolar pH dropped from 6.6 to 6.1 after addition of glucose and remained constant until glucose exhaustion.[14]

Figure 6 shows the levels of P_i^{cyt}, P_i^{vac}, and P_i^{ex} vs. time. These are from the same experiment as the data presented in Figures 2 and 5. Cytoplasmic and vacuolar concentrations are based on the cytoplasmic volume. The concentrations of P_i^{ex} are based upon the extracellular volume. The extracellular buffer volume is 2.4 times the cytoplasmic volume; the vacuolar volume may be estimated as 25% of the protoplast volume.[28] The concentrations of P_i^{in} are the sum of the concentrations of P_i^{cyt} and P_i^{vac}.

The sharp decline in P_i^{in} after 0^+ sec. is due to the consumption of P_i by the glycolytic pathway.[27] Vacuolar and cytoplasmic P_i are consumed at the same rate until 5 min. after glucose addition. At this point, extracellular P_i is transported into the cells to replenish intracellular P_i. Fairly steady levels for P_i^{cyt} and P_i^{vac}. are maintained between 8 and 20 min. - the "quasi-steady-state" period. In the quasi-steady state, glycolytic flux is constant and sugar phosphate intermediates are at constant levels.[5,27] Part of the P_i liberated in the cytoplasm from the completion of glycolysis is transferred to the vacuole. The ratio of cytoplasmic and vacuolar concentrations changed from approximately 0.9 initially to 1.5 at quasi-steady state to 2.3 after glucose exhaustion.

Consumption of vacuolar and cytoplasmic P_i at the same rate after addition of glucose has been observed for aerobic suspensions of the yeast *Candida utilis*.[7] However, for this yeast, polyphosphate levels rather than vacuolar P_i increased after glucose exhaustion. The availability of ATP explains this difference. The ratio of cytoplasmic and vacuolar P_i changed from 1.2 to 3 before and after glucose consumption, respectively.[7] Changes in the pH gradient between the cytoplasm and the vacuole occur from the beginning to the end of the experiment for *S. cerevisiae* 18790, as shown in Figure 5. However, the magnitude of this pH gradient is not correlated with the vacuolar to cytoplasmic P_i ratio, as indicated in Figures 4 and 5. In the study with *C. utilis*, the pH gradient remained constant throughout the experiment.[7] This indicates that the P_i gradient is not in equilibrium with the pH gradient, as reported for mitochondria in rat liver.[29]

CONCLUSIONS

The vacuolar and cytoplasmic components of intracellular inorganic phosphate were determined in ^{31}P spectra of anaerobic *S. cerevisiae* cells resuspended in medium containing phosphate. The assignments of the components were determined from the chemical shift estimation of the cytoplasmic resonance (P_i^{cyt}) as

determined from *in vivo* correlations of P_i chemical shift and the chemical shifts of the sugar phosphates, and the pH dependency of the resonance of pyrophosphate and the terminal phosphate of polyphosphate (PP_1). An *in vivo* correlation relating PP_1 and P_i^{vac} chemical shifts was established by using data from several strains of *S. cerevisiae.* This correlation will aid future analysis of ^{31}P NMR spectra of yeast and has expanded NMR studies of compartmentation to suspensions in phosphate-containing medium.

Transient pH profiles for the cytoplasm, vacuole, and extracellular space were determined for anaerobic *S. cerevisiae* undergoing glucose utilization. In addition, concentration profiles of the three compartments were provided by this analysis. This information showed the interplay of the various compartments in the metabolism of glucose; both vacuolar and extracellular P_i were reserves for glycolysis. Phosphate transport across the vacuolar membrane is not in equilibrium with the pH gradient. This information demonstrates the usefulness of *in vivo* studies on compartmentation in the cell.

Acknowledgement:

This research was supported by the Energy Conversion and Utilization Technology (ECUT) program of the U.S. Department of Energy. The nuclear magnetic resonance experiments reported here were made possible by the facilities of the Southern California Regional Nuclear Magnetic Resonance Center (NSF Grant No. CHE-84-40137) and software for NMR spectral analysis was provided by the NIH Resource Laboratory at Syracuse University (Grant No. RR-01317).

REFERENCES

1. R.B. Moon and J.H. Richards, *J. Biol. Chem.*, **248**, 7276 (1973).

2. S.L. Burk and R.G. Shulman, *Ann. Rev. Microbiol.*, **41**, 595 (1987).

3. M.J. Avison, H.P. Hetherington, and R.G. Shulman, *Annu. Rev. Biophys. Chem.*, **15**, 377 (1986).

4. P.F. Daly, R.C. Lyon, P.J. Faustino, and J.S. Cohen, *J. Biol. Chem.*, **262**, 14875 (1987).

5. J.V. Shanks and J.E. Bailey, "Estimation of Intracellular Sugar Phosphate Concentrations in *Saccharomyces cerevisiae* using ^{31}P Nuclear Magnetic Resonance Spectroscopy," *Biotech. Bioeng.*, in press (1988).

6. J.K.M. Roberts, and O. Jardetsky, *Biochem. Biophys. Acta*, **639**, 53 (1981).

7. K. Nicolay, W.A. Scheffers, P.M. Bruinenberg, and R. Kaptein, *Arch. Microbiol.*, **134**, 270 (1983).

8. K. Nicolay, M Veenhuis, A.C. Douma, and W. Harder, *Arch. Microbiol.*, **147**, 37 (1987).

9. T.G. Cooper, "Nitrogen Metabolism in *Saccharomyces cerevisiae*" in *The Molecular Biology of the Yeast Saccharomyces, Metabolism and Gene Expression*, p. 68, (Cold Spring Harbor, New York, 1982).

10. T.G. Cooper, "Transport in *Saccharomyces cerevisiae*" in *The Molecular Biology of the Yeast Saccharomyces, Metabolism and Gene Expression*, p. 399, (Cold Spring Harbor, New York, 1982).

11. H.O. Halvorson, K.A. Bostian, J.G. Yarger, and J.E. Hopper, "Enzyme Expression during Growth and Cell Division in *Saccharomyces cerevisiae*: A Study of Galactose and Phosphorus Metabolism " in *Recombinant DNA and Cell Proliferation*, p. 49, (Academic Press, New York, 1984).

12. E. Uchida, Y. Ohsumi, and Y. Anraku, *J. Biol. Chem.*, **263**, 45 (1988).

13. K. Nicolay, W.A. Scheffers, P.M. Bruinenberg, and R. Kaptein, *Arch. Microbiol.*, **134**, 83 (1982).

14. N.J. Greenfield, M. Hussein, and J. Leonard, *Biochim. Biophys. Acta*, **926**, 205 (1987).

15. F. Srienc, J.L. Campbell, and J.E. Bailey, *Cytometry*, **7**, 132 (1986).

16. R.B. Walsh, G. Kawasaki, and D.G. Fraenkel, *J. Bacteriol.*, **154**, 1002 (1983).

17. J.V. Shanks and J.E. Bailey, "^{31}P and ^{13}C NMR Studies of Recombinant *Saccharomyces cerevisiae* with Altered Glucose Phosphorylation Activities," to be submitted (1988).

18. J.M. Gancedo and C. Gancedo, *Biochimie*, **55**, 205 (1973).

19. LABONE(TM) NMR1 Spectroscopic Data Analysis Software System, Revision 2.70, (Syracuse University, New Methods Research Inc., 1985).

20. D.G. Gadian, G.K. Radda, R.E. Richards, and P.J. Seeley, "^{31}P NMR in Living Tissue: The Road from a Promising to an Important Tool in Biology," in *Biological Applications of Magnetic Resonance*, (Academic Press, New York, 1979).

21. J.A. den Hollander, K.Ugurbil, T.R.Brown, and R.G.Shulman, *Biochemistry*, **20**, 5871 (1981).

22. G. Navon, R.G. Shulman, T. Yamane, T.R. Eccleshall, K.B. Lam, J.J. Baronofsky, and J.Marmur, *Biochemistry*, **18**, 4487 (1979).

23. R.A. Gage, W. Van Wijngaarden, A.P.R. Theuvenet, G.W.F.H. Borst-Pauwels, and C.A.G. Haasnoot, *Biochim. Biophys. Acta.*, **804**, 341 (1984).

24. J.M. Salhany, T. Yamane, R.G. Shulman, and S. Ogawa, *Proc. Natl. Acad. Sci.*, **72**, 4966 (1975).

25. K. Urech, M. Durr, Th. Boller, and A. Wiemken, *Arch. Microbiol.*, **116**, 275 (1978).

26. F. Moreno, T. Fernandez, R. Fernandez, and P. Herrero, *Eur. J. Biochem.*, **161**, 565 (1986).

27. J.V. Shanks and J.E. Bailey, "Comparision of Wild-Type and *REG1* Mutant *Saccharomyces cerevisiae* Metabolic Levels During Glucose and Galactose Metabolism Using ^{31}P NMR," to be submitted (1988).

28. L.A. Okorokov, L.P. Lichko, and I.S. Kulaev, *J. Bacteriol.*, **144**, 661 (1980).

29. S. Ogawa, C.C. Boens, T. M. Lee, *Arch. Biochem. Biophys.*, **210**, 740 (1981).

TABLE 1: Comparison of Deconvoluted P_i^{in} Chemical Shifts and Estimated P_i^{cyt} Chemical Shift

			Deconvolution of P_i^{in}		Estimate of P_i^{cyt} (ppm) from SP (ppm)				
Strain	Spectrum	P_i^{in}	#1	#2	3PGA	αFDP	G6P	βFDP 1-P	βFDP 6-P
18790-High P_i	1	1.85	1.87	1.73	1.87	–	–	–	–
18790-High P_i	2	1.64	1.71	1.56	1.71	n.d.	1.73	1.67	1.72
18790-Low P_i	1	1.86	1.86	1.52	1.86	–	–	–	–
18790-Low P_i	2	1.79	1.81	1.53	1.83	–	–	–	–
18790-Low P_i	3	1.58	1.58	1.44	1.58	1.62	1.61	1.61	1.59
DFY437: pBW111	1	1.85	1.88	1.67	1.84	–	–	–	–
DFY437: pBW112	2	1.69	1.78	1.62	1.77	–	–	–	–
D603	1	1.70	1.73	1.35	1.72	–	–	–	–

High P_i – cells in 22 mM P_i buffer

Low P_i – cells in 7 mM P_i buffer

n.d. – below detectable amounts

FIGURE CAPTIONS

Figure 1: The downfield regions of ^{31}P NMR spectra at 202.46 MHz of anaerobic suspensions of *Saccharomyces cerevisiae* 18790 at 20°C. Suspensions in (A) and (C) were resuspended in a buffer with 22 mM phosphate, and represent 2 min. time accumulations (240 scans); line broadening of 20 Hz was applied. Suspensions in (B) and (D) were resuspended in buffer with 7 mM phosphate, and represent 1 min. time accumulations (120 scans); line broadening of 15 Hz was applied. All spectra were recorded using 70° pulses and 0.5 sec. acquisition time. 75 mM of glucose was added to the 50 % w/v suspensions that had been grown on glucose. (A) and (B) Spectra taken immediately after addition of glucose. (A) The vacuolar component of P_i is obscured by high levels of P_i^{cyt} and P_i^{ex}. (B) P_i^{vac} is a shoulder upfield of P_i^{cyt}. (C) and (D) Spectra taken several min. after addition of glucose. Note: intensities in spectra cannot be compared. Abbreviations: SP : sugar phosphate; P_i^{cyt} : cytoplasmic inorganic phosphate; P_i^{vac} : vacuolar inorganic phosphate; P_i^{in} : intracellular (cytoplasmic plus vacuolar) inorganic phosphate; P_i^{ex} : extracellular inorganic phosphate; PM : phosphomannan; ATP_γ : γ phosphate of adenosine triphosphate; ADP_β : β phosphate of adenine diphosphate; PP_1 : pyrophosphate and terminal phosphates of polyphosphate.

Figure 2: Time evolution of PP_1 chemical shift (top frame) and of pH for component #2 as labelled in Table 1 (bottom frame) for *S. cerevisiae* 18790. Measurements obtained from ^{31}P NMR spectra of cells resuspended in 22 mM phosphate buffer – Fig. 1(A) and (C). Glucose addition at 0^+ sec. Times are given as the time at the end of each 2 min. accumulation. pH of component #2 estimated from *in vitro* relationship of P_i chemical shift as a function of pH in a solution containing 20 mM Mg^{2+}.[5]

Figure 3: *In vivo* correlation of the chemical shift of PP_1 versus chemical shift of component #2, ($P_i^{\#2}$). *In vivo* chemical shift values for $P_i^{\#2}$ include the values in Table 1, which were based upon deconvolution analysis of ^{31}P NMR spectra and also include additional values from clearly delineated resonances for $P_i^{\#2}$. Symbols: (■) 18790, high P_i - 22 mM P_i buffer; (▲) 18790, low P_i - 7 mM P_i buffer; (●) DFY 437:pBW111; (□) DFY 437:pBW112; (△) DFY 437:pBW113; (○) D603.

Figure 4: PP_1 chemical shift as a function of pH of component #2 ($pH^{\#2}$). $pH^{\#2}$ estimated as in Figure 2. Symbols: as in Figure 3.

Figure 5: Profiles of pH in the cytoplasm and in the vacuole versus time for *S. cerevisiae* 18790. Measurements for the same experiment as in Fig. 1(A), 1(C),

and 2. pH^{cyt} estimated from P_i chemical shift as a function of pH for Mg^{2+} - free solution.[5,19] pH^{vac} is assigned to $pH^{\#2}$ and is estimated as in Figure 2. Dashed line - pH^{vac} estimated as for pH^{cyt}. Abbreviations: pH^{cyt} : cytoplasmic pH; pH^{vac} : vacuolar pH. Symbols: (▲) pH^{cyt}; (■) pH^{vac}.

Figure 6: Concentrations of P_i with time for the same experiment as in Fig. 1(A), 1(C), 2, and 5. All concentrations except for P_i^{ex} are based upon cytoplasmic volume; P_i^{ex} based upon buffer volume. Abbreviations: as in Figure 1. Symbols: (▲) P_i^{cyt}; (■) P_i^{vac}; (○) P_i^{ex}; (●) P_i^{in}.

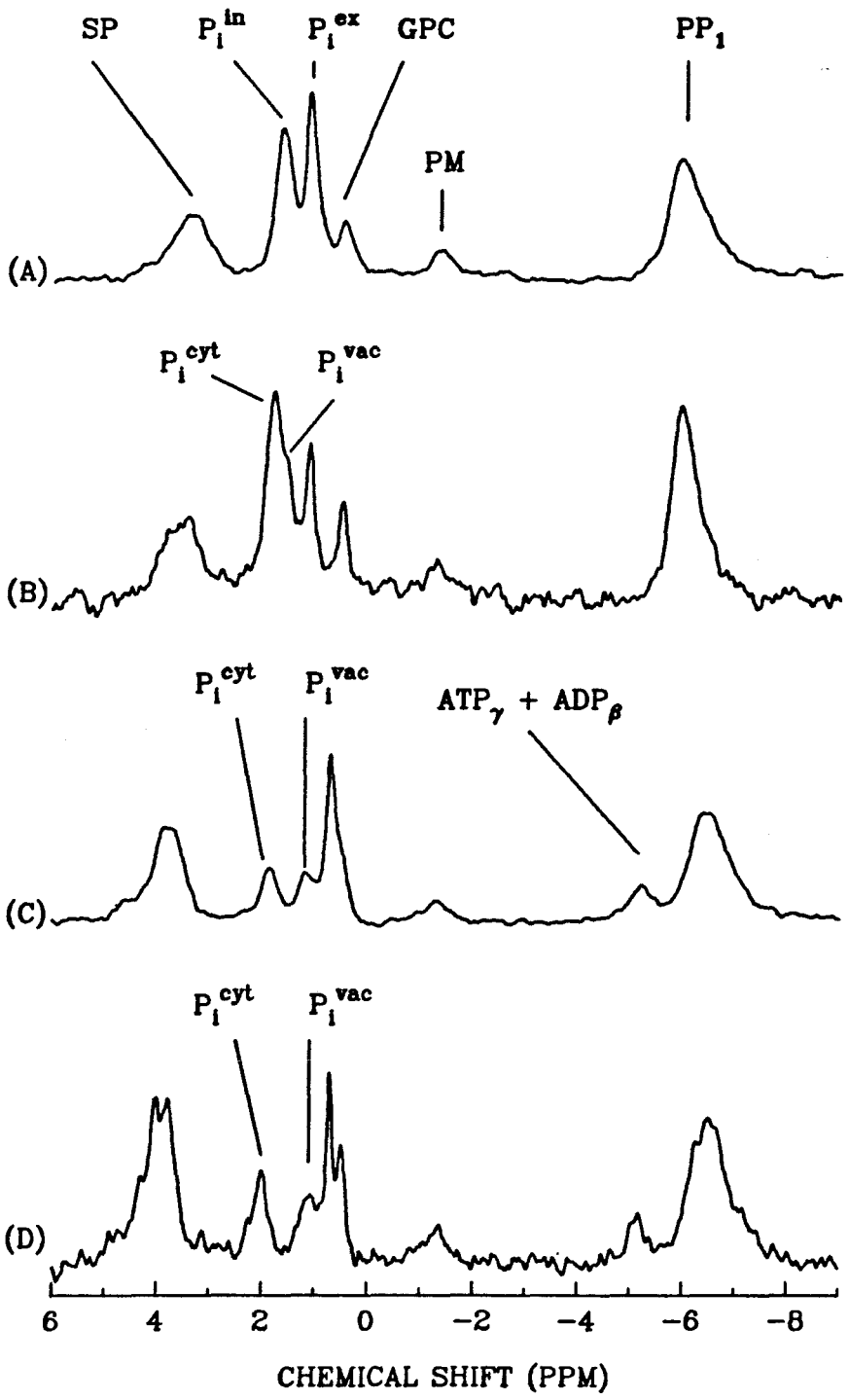
SP
P_i^{in}
P_i^{ex}
GPC
PM
PP_1
(A)
P_i^{cyt}
P_i^{vac}
(B)
P_i^{cyt}
P_i^{vac}
ATP_γ + ADP_β
(C)
P_i^{cyt}
P_i^{vac}
(D)
6
4
2
0
−2
−4
−6
−8
CHEMICAL SHIFT (PPM)

Figure 1

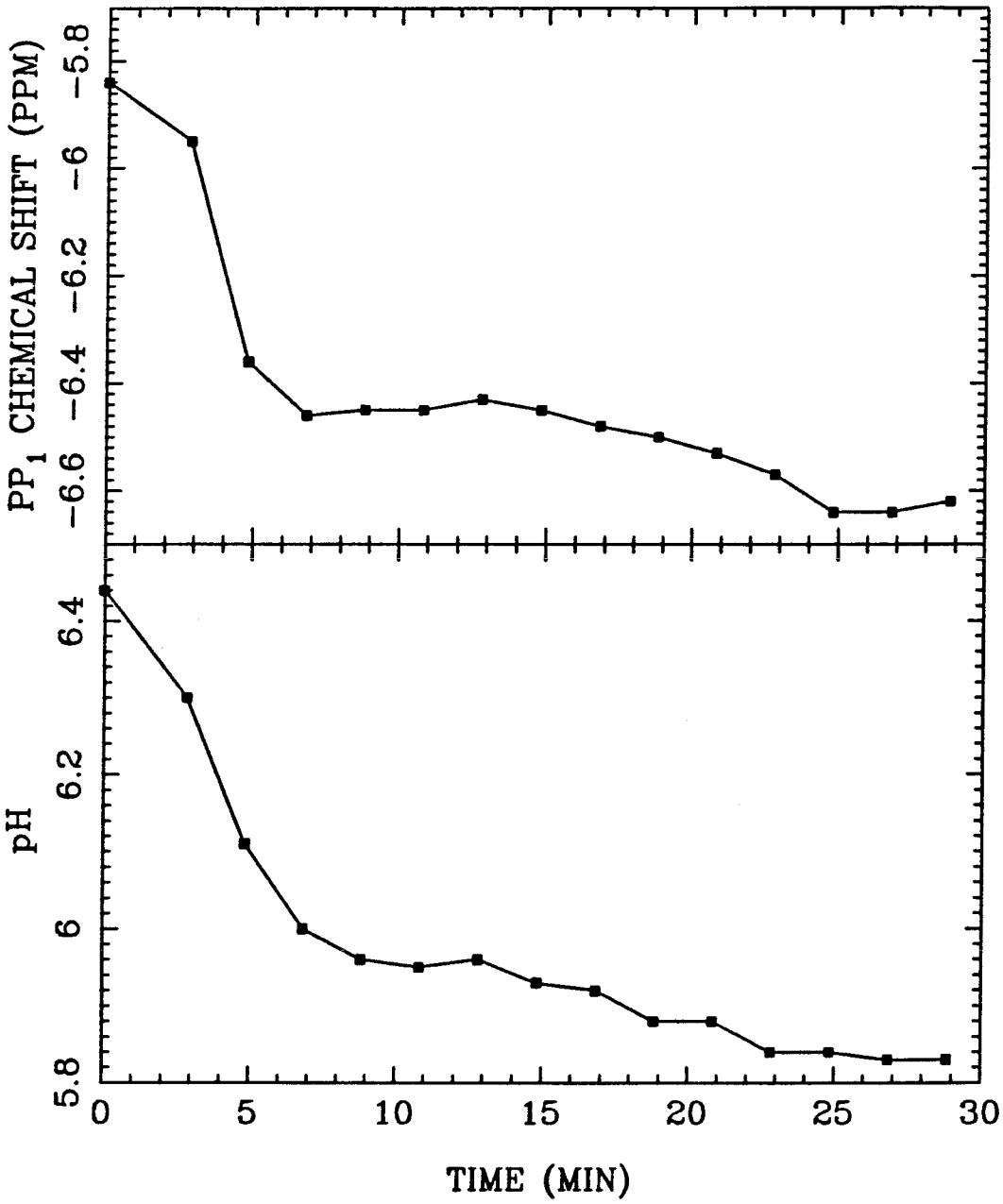
PP1 CHEMICAL SHIFT (PPM)
−6.6
−6.4
−6.2
−6
−5.8
pH
6.4
6.2
6
5.8
0
5
10
15
20
25
30
TIME (MIN)

Figure 2

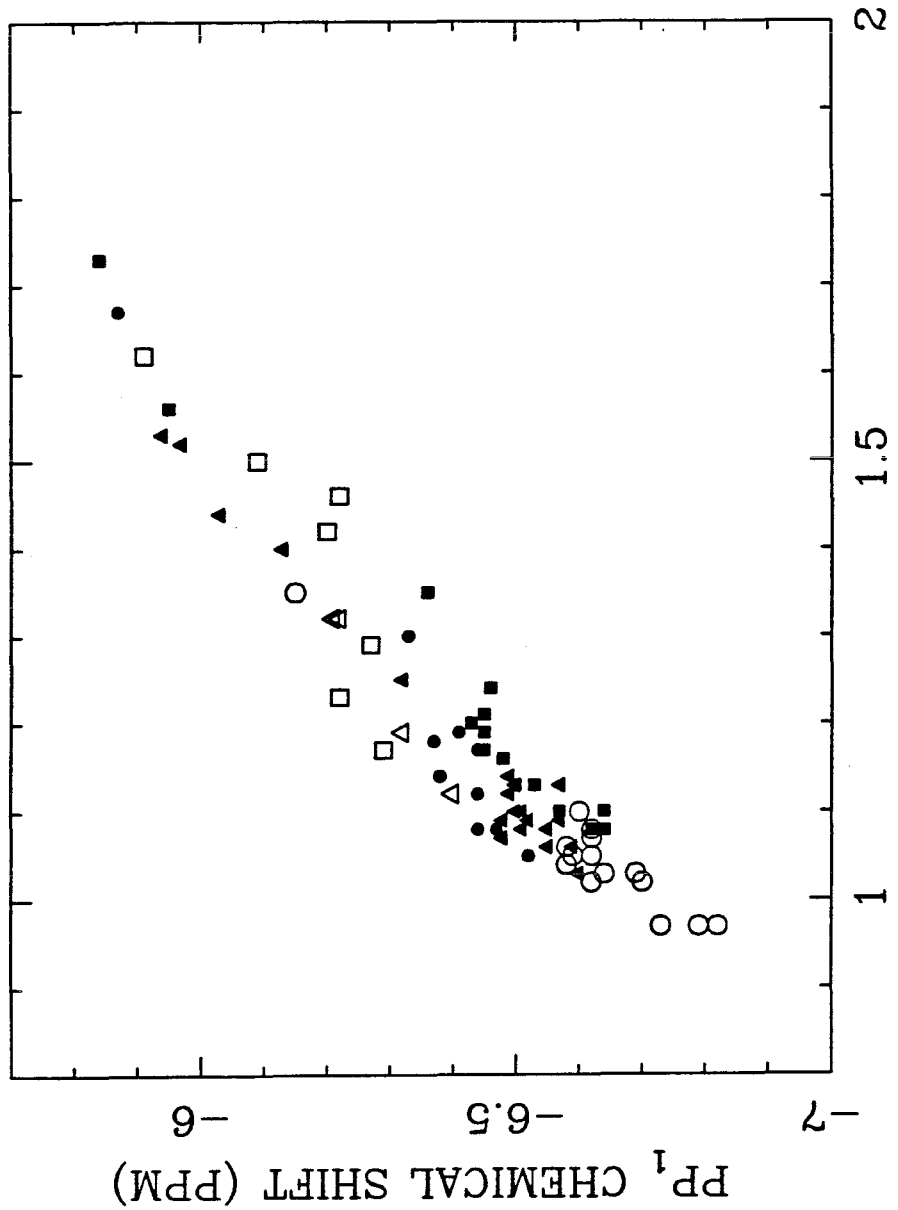

Figure 3

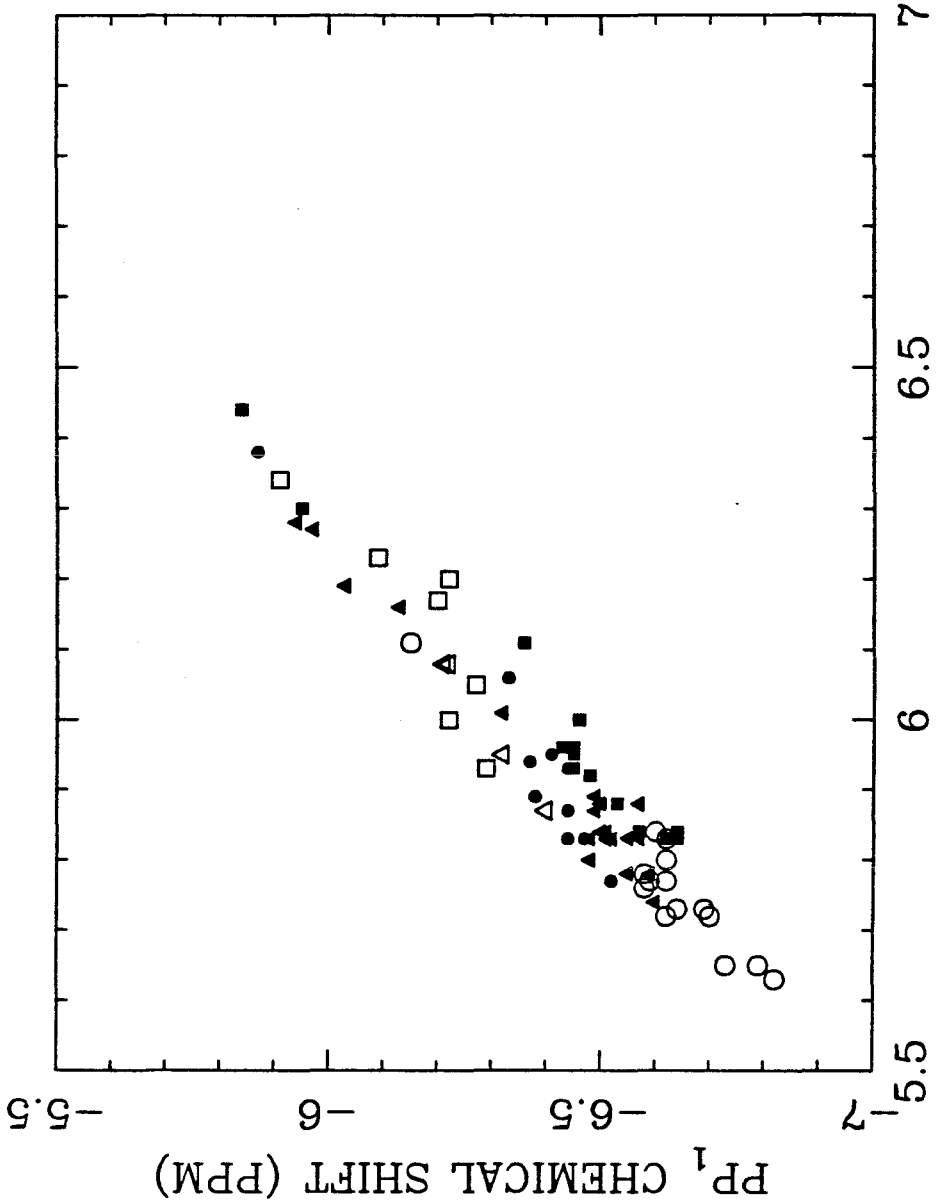

Figure 4

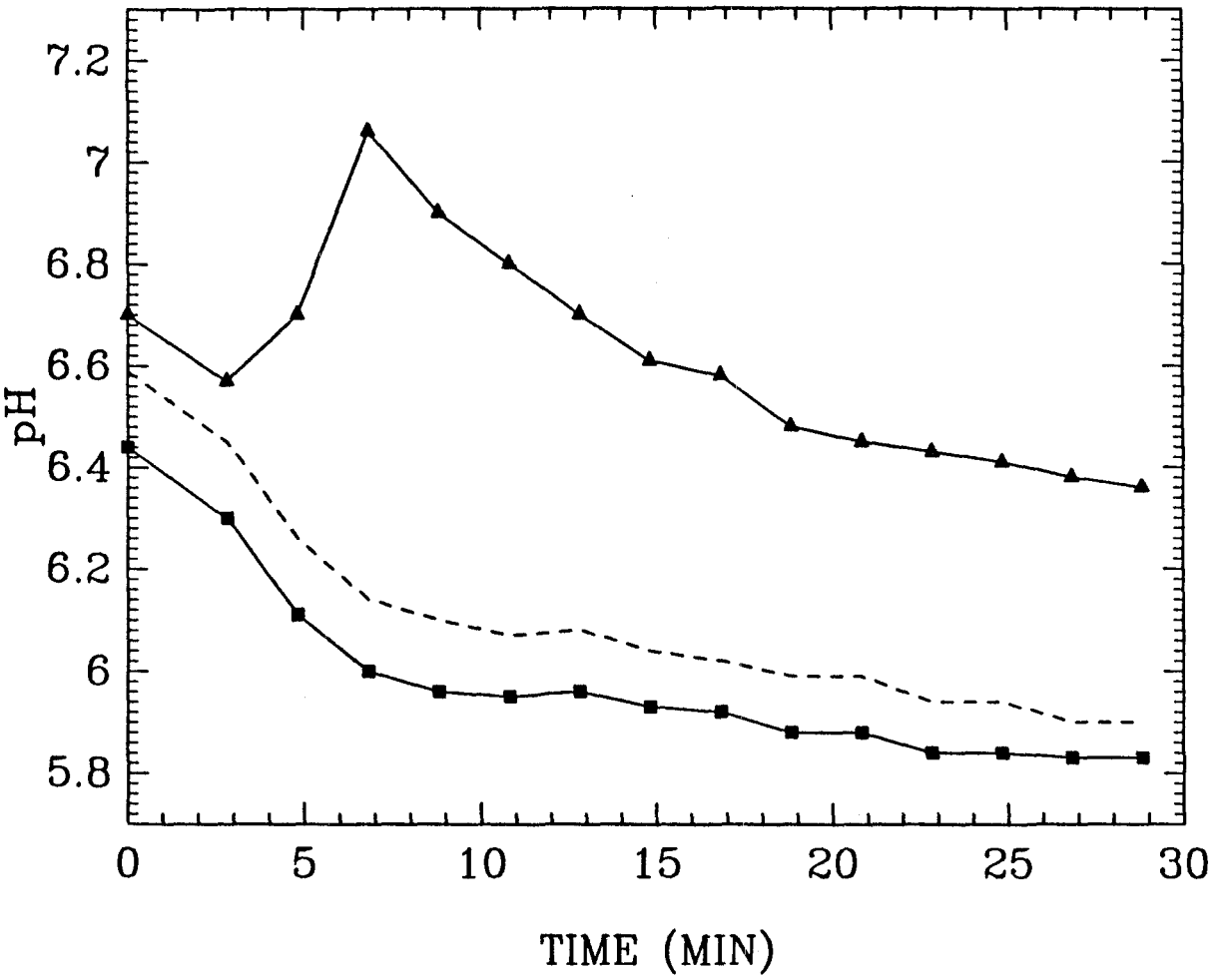

Figure 5

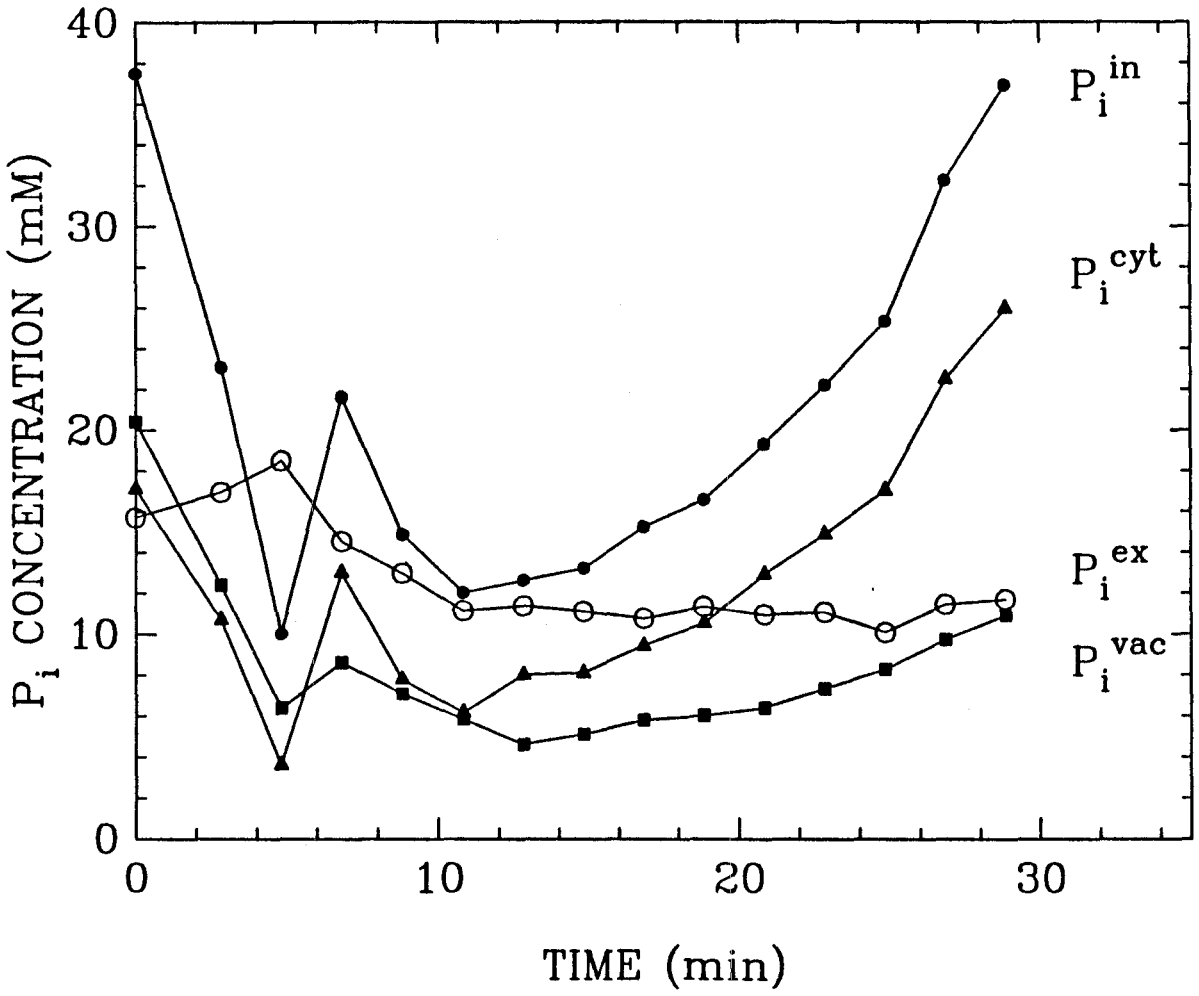
40
30
20
10
0
0
10
20
30
P_i CONCENTRATION (mM)
TIME (min)
P_i^{in}
P_i^{cyt}
P_i^{ex}
P_i^{vac}

Figure 6

CHAPTER 4

COMPARISON OF WILD–TYPE AND *REG1* MUTANT *SACCHAROMYCES CEREVISIAE* METABOLIC LEVELS DURING GLUCOSE AND GALACTOSE METABOLISM USING ^{31}P NMR

ABSTRACT

The *reg1* mutation will allow the expression of a cloned gene on a plasmid under the control of a *GAL* promoter in the presence of glucose. The metabolism of wild-type and *reg1* mutant strains were examined by *in vivo* ^{31}P NMR spectroscopy. Transient profiles of glucose 6-phosphate, fructose 6-phosphate, fructose 1,6-diphosphate and 3–phosphoglycerate indicated that glucose was processed differently for the *reg1* strain despite similar cytoplasmic pH values and ATP levels. Intracellular phosphate became depleted in the transition to quasi-steady state and limited glycolysis in the *reg1* strain. The glucose uptake step or hexokinase step appears to be altered in the *reg1* strain. The *reg1* strain utilized galactose faster than the wild-type strain under the conditions used for NMR analysis. These results are consistent with the hypothesis that the *REG1* product operates early in the regulatory circuitry for glucose repression. This study illustrates the usefulness of transient information provided by NMR in understanding changes in metabolism of genetically manipulated organisms.

INTRODUCTION

Numerous choices for manipulating organisms for enhanced production of biochemicals complicate the selection of optimal genetic and environmental conditions in bioprocesses. Knowledge of the structure of the metabolic reaction network and of its regulation and kinetic activities would provide the metabolic engineer with a basis for optimization. Noninvasive experimental techniques, metabolic pathway synthesis models, metabolic pathway kinetic models, and cellular growth models are the means to such knowledge.[1] Nuclear magnetic resonance (NMR) spectroscopy, an emerging technique, can be implemented in these efforts.

In vivo NMR has exploded into the science and medical fields since 1973, when Moon and Richards[2] determined the intracellular pH of red blood cells by ^{31}P NMR. Metabolic studies by *in vivo* NMR have been performed in subjects ranging from microorganisms to humans. [3–6] One obvious advantage of *in vivo* NMR stems from the quantitative nature of measuring metabolites noninvasively in real time. While NMR does not alone revolutionize the understanding of metabolic regulation, the increasing use of NMR for quantitative understanding of metabolic control will challenge conventional views of metabolism.[3] For example, phosphofructokinase (PFK) has been postulated to control the glycolytic rate and to be responsible for the Pasteur effect in yeast. Also, the levels of ADP and inorganic phosphate are thought to affect PFK activity and to be limiting substrates in glycolysis.[3] Using NMR, Shulman and coworkers[4] have shown that during the Pasteur effect in yeast, PFK responds only to changes in the glycolytic flux; hence, the glycolytic rate is controlled at either the glucose uptake step or the hexokinase step. By measuring *in vitro* fluxes through PFK that mimicked the *in vivo* states under the Pasteur effect, the enzyme activity of PFK was determined to be insensitive to levels of ADP and P_i, sensitive to levels of fructose 2,6-bisphosphate and fructose 6-phosphate, and independent of physiological pH values between 7.0 and 7.6.[4] Thus, NMR can be a valuable tool to either support or challenge past

conceptions about metabolism and consequently will aid the metabolic engineer in understanding changes in the metabolic function of manipulated organisms.

Promoters from the *GAL* operon have been applied in cloning and expression vehicles for *Saccharomyces cerevisiae.*[8] Galactose is the inducer for such a promoter, and hence, to achieve induction in glucose–containing media, a host strain must be chosen that will not exhibit catabolic repression by glucose. When galactose is added to a medium containing glucose, a host strain which has the *reg1* mutation can express a cloned gene from a *GAL* promoter. The mechanism by which *reg1* inhibits catabolic repression by glucose has not been characterized.[9] Host-plasmid interactions have been studied in fermentations of recombinant strains with the *reg1* mutation.[10] In this paper, the metabolism of wild-type and *reg1* mutant strains has been studied by transient *in vivo* ^{31}P NMR experiments in order to elucidate the influence of the *reg1* mutation on glucose catabolism.

GLUCOSE REPRESSION AND *REG1* FUNCTION

The anaerobic fermentation pathways for glucose and galactose in *S. cerevisiae* are shown in Figure 1.[11,12] These pathways are of primary interest in this study and Figure 1 is included to aid in the discussion of glucose repression and function of the *REG1* product. Glucose repression is a global regulatory system that governs the response of cells to the availability of glucose. Glucose repression regulates expression of fermentation genes at the transcriptional level. The presence of glucose also affects transport of sugars such as galactose into the cell, thereby influencing the function of regulatory mechanisms for induction.[9]

The regulatory system of glucose repression in *S. cerevisiae* contrasts to that of *E. coli* in two known ways. First, as suggested by genetic and biochemical evidence, the molecular signal for glucose deprivation in yeast is not cyclic AMP.[13,14] Second, biochemical functions are known for two genes - *HXK2* and *SNF1* - that affect global glucose repression. The constitutive enzyme hexokinase

PII, encoded by *HXK2*, phosphorylates glucose to glucose 6-phosphate; hexokinase PII is the predominant enzyme for glucose phosphorylation in growth on glucose.[17] Mutations for hexokinase PII have been isolated that do not delete catalytic function but cause constitutivity for glucose-repressible enzymes.[15–17] *HXK2* has been suggested to function at early steps in the regulatory circuitry for glucose repression, perhaps by signaling functions that enable the cell to evaluate the availability of glucose.[9] The uptake of glucose may be coupled with the glucose phosphorylation step;[17] however, the uptake of glucose is not well understood, as indicated by the question mark for this step in Figure 1; *SNF1* encodes for a protein kinase that is required for release from glucose repression, suggesting that protein phosphorylation has a critical role in glucose repression. [18]

In *S. cerevisiae*, the utilization of galactose requires the induction of an enzyme system, which consists of a specific galactose transport activity and the Leloir pathway enzymes.[12] This enzyme system is illustrated in Figure 1. The expression of these genes is induced by galactose and repressed by glucose. Galactose enters the cell via the galactose permease encoded by *GAL2*. Galactokinase, encoded by *GAL1*, converts galactose to galactose 1-phosphate. Uridyl transferase, encoded by *GAL7*, converts galactose 1-phosphate and UDP-glucose into glucose 1-phosphate and UDP-galactose. UDP-galactose is reconverted to UDP-glucose by an epimerase encoded by *GAL10*. To complete the path for entry into the glycolytic pathway, glucose 1-phosphate is converted to glucose 6-phosphate by a constitutively produced isozyme of phosphoglucomutase.[17]

Induction of the galactose structural genes is controlled by at least three regulatory genes: *GAL4*, which encodes for a positive regulatory protein; *GAL80*, which encodes for a negative regulator that interferes with the *GAL4* product; and *GAL3*, which may function in the synthesis of a coinducer.[9] The mechanism of the interaction between the *GAL4*- and *GAL80*- encoded proteins is still unclear. The two proteins may form a complex that is dissociated in the presence

of inducer,[19] or the *GAL80* protein may inhibit *GAL4*-mediated transcriptional activation by modifying the interaction of the *GAL4* protein with the upstream activating sequence (UAS_g) between the *GAL1* and *GAL10* genes.[20]

The role of the *REG1* product in glucose repression has not been characterized.[19,21] The *reg1* mutation causes glucose-insensitive expression of permease, Leloir enzymes, and invertase (an enzyme required for sucrose utilization).[10,21] Therefore, the *REG1* product has a global role in glucose repression, *i.e.*, not just for glucose repression of galactose utilization.[21] Strains that have the *reg1* mutation will still preferentially catabolize glucose in favor of galactose when both are present.[10,21] For galactose utilization, the *REG1* product may convey the signal for glucose availability to the positive factor (*GAL4*) or directly to the structural genes.[21] Thus, *REG1* and *HXK2* are proposed to have similar regulatory functions in glucose repression.[9]

MATERIALS AND METHODS

Yeast Strains

Saccharomyces cerevisiae ATCC 18790 and *S. cerevisiae* D603 [22] were the yeast strains used in this study. *S. cerevisiae* 18790 is a standard diploid strain and has no known mutations. *S. cerevisiae* D603 is the homozygous diploid version of YM603 (*ade2-101*, *ura3-52*, *his3*, *met*, *lys2-801*, *reg1-501*). The *reg1* mutation inhibits catabolic repression by glucose.

Culture and NMR Preparation

Culture conditions and NMR preparation procedures have been described previously.[23] The strains were grown aerobically to midexponential phase in liquid medium containing 1% yeast extract, 2% bacto-peptone, and either 2% glucose or 2% galactose, at pH 4.5. The cultures were chilled on ice, then harvested by low–speed centrifugation at 4°. The cells were washed twice in an ice-cold, sterile,

buffered salt solution: 0.85 g/L KH_2PO_4, 0.15 g/L K_2HPO_4, 0.5 g/L $MgSO_4$, and 0.1 g/L NaCl in 50 mM MES buffer, pH adjusted to 6. The cells were resuspended in wash medium supplemented with an additional 15 mM P_i at a 1:1 ratio of cell pellet volume to resuspension volume. Cell suspensions (2 mL) in the NMR tubes were tightly capped and were kept on ice until used for the NMR experiment.

^{31}P NMR Spectroscopy

^{31}P NMR spectra were obtained in the Fourier-transform mode at 202.46 MHz on a Bruker WM-500 NMR spectrometer at 20°C.[23] The pulse interval and angle were 0.5 s and 70°, respectively. Free induction decays (FID's) were accumulated in consecutive 2 min. blocks (240 scans, 8K files). Sample spinning and ^{1}H decoupling were not employed.

An initial spectrum was taken of the cellular suspension, then 75 μL of a 40 wt % glucose or galactose solution was added to cells grown on their respective carbon source, and a sequence of spectra was collected during subsequent 2 min. intervals. At the end of each experiment, phosphate buffer was added to the sample for calibration purposes. Glycerol phosphorylcholine (P-L Biochemicals) was added for a chemical shift reference: it resonates 0.49 ppm downfield from 85% phosphoric acid, which is assigned to zero ppm. Cell density (g CDW/L) was determined for each sample.

Calibration experiments for estimation of intracellular concentrations were performed as described previously.[23] Relative concentrations can be determined within ± 5 %. For estimation of intracellular concentrations, 1.67 g wet weight/mL intracellular volume and 0.2 g dry weight/g wet weight were assumed.[24] For estimation of extracellular concentrations, the density of wet yeast was assumed to be 1.0 g wet weight/mL total yeast volume.

Data Processing

The 8K FID files taken by the Bruker Aspect-2000 computer were transferred to a VAX(11/780) computer for analysis using the LAB ONE (TM) NMR1 Spectroscopic Data Analysis Software System.[25] All subsequent processing was performed by the software system on the VAX computer. The FID's were multiplied by an exponential apodization function corresponding to a line broadening of 20 Hz, Fourier transformed, phased, and baseline flattened (4^{th} degree polynomial).

pH Determination

As described previously, the cytoplasmic pH was determined by the chemical shift position of P_i^{cyt}, and then by interpolating the corresponding pH from the *in vitro* relationship between pH and P_i chemical shift at 120 mM ionic strength.[23] When the P_i^{cyt} resonance was not detected in the ^{31}P NMR spectrum, the chemical shift positions of the sugar phosphates were used to estimate the cytoplasmic pH. Absolute values for the cytoplasmic pH can be determined within ± 0.1 pH units. The error for relative changes of pH in a given experiment is dependent upon the error in chemical shift determination; therefore, changes in pH can be measured to better than 0.05 pH units. Thus, a relative change in 0.05 pH units in a given experiment is significant.

The P_i^{ex} resonance was the indicator for estimating the extracellular pH. The *in vitro* relationship of pH and P_i chemical shift was determined as described previously,[23] except that the solution was the same resuspension buffer as used in the *in vivo* experiments. The relationship between pH and the P_i resonance position in resuspension buffer was determined over the range between 4.5 and 8.5 pH units. The accuracy of pH determination around the pKa is ± 0.1 pH units and around the endpoints ± 0.2 pH units.

Estimation of Sugar Phosphate Concentrations

Estimates of the concentrations of the sugar phosphates were determined by a systematic procedure based upon ^{31}P NMR measurements. [23] The sugar phosphate region of the ^{31}P NMR spectrum was first decomposed by computer analysis (NMR1 software), and the decomposition consistency and identification of individual sugar phosphate resonances were established based on *in vitro* chemical shift calibrations determined in separate experiments.

FEATURES OF ^{31}P NMR SPECTRA FOR *S. CEREVISIAE*

^{31}P NMR spectra of *S. cerevisiae* D603 during catabolism of glucose and catabolism of galactose are shown in Figure 2. ^{31}P metabolites are distinguished in the NMR spectrum by their chemical shift position (a dimensionless frequency), which is a function of the different electronic environments of phosphorus in these various compounds. The peaks are assigned from previous work in the literature.[26–28] The assignment of resonances for (A) glucose metabolism and (B) galactose metabolism are the same. Starting from the low field (at the left) in Figure 2, the assignments are as follows. The resonances from 4.5 ppm to 3 ppm are in the sugar phosphate (SP) region. Cytoplasmic inorganic phosphate (P_i^{cyt}) and extracellular inorganic phosphate (P_i^{ex}) are the next clearly observable resonances. Cytoplasmic inorganic phosphate resonates downfield from extracellular inorganic phosphate because the cytoplasm has a higher pH than the buffer. A separate resonance for inorganic phosphate in the vacuole is detected in spectra for both strains.[29] The vacuolar resonance can be seen as the shoulder downfield of P_i^{ex} in the spectra at 21.5 min. and 37.5 min. in Figure 2(A), and in the spectra at 55.5 min. and 109.5 min. in Figure 2(B).

The resonance at -1.34 ppm is from phosphate in phosphomannan (PM) in the cell wall. The nucleotide resonances around -5 ppm, -10 ppm, and -19 ppm were assigned to $ATP_\gamma + ADP_\beta$, $ATP_\alpha + ADP_\alpha$, and ATP_β, respectively, since

other nucleotides were not observed for *S. cerevisiae* experiments under similar conditions.[26] The ADP resonances are included for completeness even though they probably contribute less than 10% of the overall signal.[26] Also, a difference in area is not detected between the ATP_β resonance and either of the two nucleotide resonances in the *in vivo* spectrum of either strain. PP_1 is the sum of several phosphate resonances from pyrophosphate and the terminal phosphates of polyphosphate. PP_3 is penultimate phosphates from polyphosphate chains, and PP_4 is the inner phosphate from longer polyphosphate. NAD(H) includes both NAD^+ and NADH. Finally, UDPG resonates in the region of -12 ppm.

Figure 2 illustrates how the features in ^{31}P spectra can indicate metabolic changes. The cells in Figure 2(A) were grown on complex medium with glucose as the carbon source, harvested during exponential phase, then resuspended in a buffered solution (without carbon) for the NMR experiment. The cells in Figure 2(B) were grown on complex media with galactose then prepared for the NMR experiment in the same manner as for the cells grown on YPD. Thus, the cells at time 0 are in a resting state. Prior to carbon addition, at time 0, the SP levels are at their initial basal levels. Based upon the chemical shift values for the SP resonances, 3-phosphoglycerate (3-PGA) is identified as the predominant compound in the pool of sugar phosphate compounds in the cells' resting state. ATP levels are not detectable, and artificial pH gradients of 0.4 pH units exist. The term artificial is used since an energy source is not present to create the pH gradient. As depicted at 7.5 min. in Figure 2(A) and at 13.5 min. in Figure 2(B), after carbon addition the sugar phosphate levels increase, cytoplasmic inorganic phosphate levels drop drastically, and ATP is formed. The intermediates in glycolysis will maintain nearly constant levels during a quasi-steady-state period during which the carbon consumption rate is constant. As shown at 21.5 min. in Figure 2(A) and at 55.5 min. in Figure 2(B), SP and ATP levels are near their maximum and quasi-steady-state levels. Also, the shape of the SP region - which is indicative

of the specific sugar phosphate compounds present and their concentrations - is similar to that in other spectra of the same experiment in the quasi-steady-state period. After glucose is exhausted, as depicted at 37.5 min in Figure 2(A), the SP resonance returns to near basal levels, ATP levels decline to undetectable levels, and the resonance for cytoplasmic inorganic phosphate increases to an intensity slightly greater than its initial level. D603 is still utilizing galactose at 109.5 min., as shown by the levels of SP, P_i^{cyt}, and ATP resonances in Figure 2(B). More information on these and other different features besides the ones noted here can be obtained from quantitative analysis of the spectra, as described in the next section.

DYNAMICS OF METABOLIC POOLS AND pH

Glucose Utilization

Concentration and pH measurements obtained from spectra obtained at different times after glucose addition are shown in Figure 3. Figure 3 compares concentrations and pH values for *S. cerevisiae* strains 18790 (A) and D603 (B) undergoing glucose utilization. The upper frame compares polyphosphate, extracellular inorganic phosphate, and ATP concentrations. The middle frame compares intracellular (cytoplasmic + vacuolar) inorganic phosphate and total sugar phosphate concentrations. For material balance considerations, it should be noted that the ratio of extracellular (buffer) volume to intracellular volume is approximately 2.4 for both strains. The bottom frame compares cytoplasmic pH and extracellular pH values.

Figures 3(A) and (B) show for each strain five periods in the catabolism of glucose: the state before glucose addition (time 0); the transition from the resting state to quasi-steady state; a period where metabolite levels are fairly constant or the quasi-steady-state interval; the transition from quasi-steady state to glucose exhaustion; and the final state after glucose exhaustion. The transition period

to quasi-steady state lasts from 0^+ min to approximately 10 min for 18790 and from 0^+ min to approximately 12 min for D603. The time frames of 10 to 20 minutes for 18790 and 12 to 30 minutes for D603 are tentatively assigned as the quasi-steady-state interval because of the constant values of PolyP, SP, and ATP, and of the fairly constant levels of P_i^{in}. The transition state to glucose exhaustion is marked by the decreasing levels of SP and increasing levels of P_i^{in}: 23 to 27 min for 18790 and 30 to 37 min for D603. Glucose is exhausted by 29 minutes for 18790 and by 39 minutes for D603.

At time 0, before glucose is added, the cells are in a resting state. Sources of nitrogen, amino acids, and carbon have not been added, so the cells are starved with respect to these nutritional compounds. The initial distributions of inorganic phosphate and polyphosphate are different between 18790 and D603. D603 has 30 % more polyphosphate, 55 % more inorganic phosphate in the extracellular space, and 30 % less inorganic intracellular phosphate. The inorganic phosphate concentration in the resuspension medium is 22 mM, so the cells have redistributed the phosphate in the time in which the sample was on ice (2 hrs) and warmed to 20°C in the magnet (15 min). Sugar phosphate levels are similar for both strains initially, and ATP levels are not detectable. The initial cytoplasmic pH values for strain 18790 is 6.7; for strain D603, 6.5. The ΔpH across the membrane is similar for both strains - for 18790 it is 0.5; for D603, 0.4.

As the term transition implies, several fluctuations in metabolite levels and pH values are observed in the transition period from the resting state to the quasi-steady-state period. Immediately after addition of glucose, as indicated by the second time point in Figure 3(A) and (B), several changes occur in both strains: PolyP and P_i^{in} levels drop, SP and P_i^{ex} levels increase, and the cytoplasmic and extracellular pH values decrease. For for the following rate values, the volume basis is intracellular volume. Polyphosphate degradation occurs at twice the rate for D603 (4 mM/min) than for 18790 (2 mM/min). An efflux of inorganic phosphate

occurs for both strains; the initial rate for D603 (5 mM/min) is 5 times that for 18790. The maximum level of P_i^{ex} is attained at this time for D603. For both strains, the initial rates of consumption of P_i^{in} are approximately 50 % greater than the same rate of production of SP (4 mM/min). Both cytoplasmic and vacuolar P_i are consumed at the same number of mols of P_i per minute for both strains (data not shown; for 18790, see Ref. 29). The cytoplasmic pH acidifies in strain 18790 by 0.15 pH units; in D603, 0.2 pH units. The ΔpH is approximately the same as at time 0.

For the next two minutes, in the transition to quasi-steady state, for both strains the trends in the levels of P_i^{in} and SP continue; P_i^{in} and SP values are now at their minima and maxima, respectively. For 18790, the level of P_i^{ex} reaches a maximum. In contrast, for D603, extracellular inorganic phosphate has begun to be transported inside the cells. For both strains, polyphosphate levels are near their value for the rest of the experiment. Also, for both strains, the values of cytoplasmic pH increase, the ΔpH across the membrane increases, and ATP is now being produced faster than it is consumed. The difference between the minimum and maximum cytoplasmic pH values between 2 and 8 minutes is approximately 0.6 pH units for both strains.

The end of the transition period to quasi-steady state and the quasi-steady-state period reveal several similarities and differences between the two strains. The influx of extracellular inorganic phosphate into the cytoplasm continues until around 10 minutes for both strains. Extracellular P_i levels then stay fairly constant for the rest of the experiment; the same amount of extracellular P_i is consumed by both strains between the level at time 0 and the final level. The strains maintain approximately the same SP levels (20 mM) and ATP levels (3 mM) during the quasi-steady-state period. The cytoplasmic acidification profiles are similar. The extracellular pH declines sharply to pH values of 4.5 or lower within 12 minutes after addition of glucose.

A major difference between the two strains is in the intracellular inorganic phosphate profiles at end of the transition period to quasi-steady state. In 18790, the P_i^{in} level increases to a local maximum at 8 min., then declines to lower concentrations between 10 and 20 minutes (the time-frame enclosing the quasi-steady-state period). In contrast, for D603, the P_i^{in} pool is depleted to undetectable amounts, and a local overshoot does not exist; however, the levels of P_i^{in} between 12 and 30 minutes are similar for those for 18790 during its quasi-steady-state period. In addition, the vacuolar and cytoplasmic levels of P_i are similar for both strains; in strain 18790, roughly 40% of the mols of P_i in the intracellular space is from the vacuole.[29]

In the transition period to glucose exhaustion, the sum of P_i^{in} and SP is constant for both strains. After glucose exhaustion, levels of P_i^{in}, SP, and ATP return to their initial values.

Mass balances performed on the data reveal differences in the dynamic intracellular pools of phosphate between the strains. Let the phosphate in the dynamic pools in the cytoplasm (and vacuole) be denoted by

$$C_C = C_{in} + C_{sp} + C_{ATP}, \tag{1}$$

where C_C is the sum of the concentration of intracellular inorganic phosphate (C_{in}), the concentration of the sugar phosphates (C_{sp}), and the concentration of ATP (C_{ATP}). For each experiment, the C_C value is within $\pm$ 5 % from the mean determined for all the timepoints except for those at which C_{in} is at a minimum. At these timepoints for 18790, decreases in C_C from the mean are: 5 min., 20 %; and 9 - 15 min., 12 %. For D603, up to 35 % lower levels of C_C occur during the time period of 3.5 - 9.5 min. The sum of all the levels indicated in Figure 3, C_T, may be denoted by

$$C_T = C_C + C_{PolyP} + C_{ex}, \tag{2}$$

where C_C is defined previously, C_{PolyP} is the concentration of polyphosphate and C_{ex} is the concentration of extracellular phosphate (based upon intracellular volume). The difference in C_T in Figure 3 from the beginning to the end of the experiment is 13 mM for 18790 and 19 mM for D603 (intracellular volume basis). C_T began to decrease after the second spectrum in each experiment. Although phosphomannan, NAD(H), and GPC are not included in equation (2), the levels of these compounds remain constant during the experiments. The decrease in C_T from time 0 and the end of the experiment results from the eventual transformation of the extracellular inorganic phosphate and polyphosphate into phosphate pool(s) not detected in the ^{31}P NMR spectrum.

As a final note, NMR experiments were performed at least three times for both strains under glucose utilization. Detailed calculations are only performed for one experiment for each strain. However, qualitative differences such as shift in P_i^{cyt} and disappearance of the P_i^{in} resonance for D603, and the difference in shape of the SP region between the strains were observed in all of the experiments.

Galactose Utilization

Figures 4(A) and (B) compare galactose metabolism as observed from ^{31}P NMR for 18790 and D603, respectively. At time 0, the cells are in a resting state; galactose is added within 1 min. (recall that the cells now were grown in galactose prior to suspension in buffer, so that there are differences at time zero relative to the experiments with glucose). Strains 18790 and D603 are still metabolizing galactose after 60 min. and 120 min., respectively, as indicated by ATP and SP levels. Thus, the time periods included in Figure 4 are the resting state and the transition period to quasi-steady state. Since the experiments were not concluded with glucose exhaustion, a definite quasi-steady-state period cannot be defined.

As observed for glucose utilization, the distribution at time 0 of inorganic phosphate and polyphosphate is different between strains 18790 and D603. D603

has 40% more polyphosphate, 170% more extracellular inorganic phosphate, and 35% less intracellular inorganic phosphate. In comparison to the initial state observed for glucose utilization, both strains have approximately 15 mM less polyphosphate; 10 mM (18790) and 5 mM (D603) more intracellular inorganic phosphate; and 5 mM less (18790) and 5 mM more (D603) extracellular inorganic phosphate (extracellular volume basis). Sugar phosphate levels are similar for both strains and have values similar to those observed for glucose utilization. ATP levels are undetectable; the initial cytoplasmic pH values are 6.6 and 6.5 for 18790 and D603, respectively.

The metabolic changes observed after addition of galactose to the strains reveal many parallels with glucose metabolism. In the initial minutes after galactose addition, polyphosphate degradation and efflux of inorganic phosphate occur for both strains. P_i^{in} levels decrease concomitant with the rise in SP levels. ATP is produced. The cytoplasmic pH is acidified first and then becomes basic. The ΔpH across the membrane increases at the same time as the cytoplasmic pH becomes basic. The decrease in concentration of intracellular phosphate occurs at a faster rate than the increase in sugar phosphate levels.

The initial fluctuations observed under galactose utilization occur on longer time scales than those for glucose utilization. In addition, the time scales observed under galactose utilization are different between the strains for the different transients. As shown in Figure 4, under galactose utilization strain 18790 exhibits a much slower decline of P_i^{in} over 24 min., in contrast to that of 10 min. for strain D603. P_i^{ex} levels remain at about 18 mM for 18790, but the trajectory of P_i^{ex} with D603 goes through a maximum before declining to a value of 20 mM. For both strains, extracellular phosphate is transported into the cells when intracellular P_i is at constant, minimal levels. However, for 18790, only a few mM of external phosphate are consumed before the experiment ends.

Sugar phosphate levels gradually increase to a value of 13 mM for strain

18790 but reach 20 mM for strain D603. The increase in sugar phosphates from 13 mM to 20 mM for D603 occurs after consumption of extracellular P_i begins. ATP levels during galactose utilization are 50 % of those observed during glucose utilization.

The cytoplasmic pH acidification and subsequent alkalinization occurs on a longer time scale for 18790 than for D603. The cytoplasmic pH drop after galactose addition is 0.1 pH units for 18790 but 0.05 units for D603. The change in pH of the cytoplasm during the transition between acidification and alkalinization is 0.2 units for both strains. These changes in pH are less than those observed under utilization of glucose.

Under galactose utilization, as under glucose utilization, intracellular P_i is diverted to a sink other than the sugar phosphates and ATP. For 18790, C_C, as defined in equation (1), continually decreases from the initial value until 30 min., at which time C_C is constant for the rest of the experiment. For D603, C_C is at the same value at time 0 and at times between 50 and 120 min. C_C decreases immediately after galactose addition until 11.5 min., when a global minimum for C_C is attained. For D603, the minimum value for C_C is 40% lower than the initial value of C_C; the sum C_C then increases linearly until 50 min.

DYNAMICS OF SUGAR PHOSPHATE POOLS UNDER GLUCOSE UTILIZATION

Glucose 6-phosphate, fructose 1,6-diphosphate, fructose 6-phosphate, and 3-phosphoglycerate levels are shown in Figure 5 for both 18790 and D603 under glucose utilization. The identification and estimates of the individual sugar phosphates were determined by a method of analysis based upon the deconvolution of the sugar phosphate region of the same spectra that were used in Figure 3.[23] Representative fits of the SP region for these strains are given in the references.[1,23]

Even though the transients of the total sugar phosphate concentration are

similar for both strains, as indicated in Figure 3, the levels of the individual sugar phosphates are very different between the strains during glucose utilization, as shown in Figure 5. For both strains, glucose 6-phosphate is not detectable in cells in the resting state. After addition of glucose, glucose 6-phosphate increases to 8 mM, then decays to undetectable levels. The notable differences between 18790 and D603 are the difference in time to reach the maximum value of G6P and in the time for decay of G6P level from the maximum to zero. D603 has the longest times for both processes.

As indicated in Figure 3, phosphate flows between the P_i^{in} and SP + ATP pools. Phosphorylation of glucose and fructose 6-phosphate by ATP occurs in the hexokinase and phosphofructokinase steps in glycolysis, respectively, as shown in Figure 1. As also shown in Figure 1, P_i is consumed directly in glycolysis in the phosphorylation of glyceraldehyde–3–phosphate. A comparison of P_i levels and the G6P and FDP levels is as follows. For 18790, the maximum G6P level and minimum P_i^{in} level are attained at the same time; P_i^{in} levels increase when G6P levels decline, and then the quasi-steady-state region is reached. For D603, P_i^{in} levels are depleted when G6P is halfway to its maximum value. The rise in FDP levels for D603 is stalled at this time. G6P levels for D603 increase as P_i^{in} levels increase to its quasi-steady-state value, at which point G6P began its decline.

Additional differences between the strains are noted in the concentrations of the other sugar phosphates. D603 has approximately 50% of the amount of FDP as 18790 in the period between 8 and 26 minutes. Furthermore, detectable levels of F6P (1 mM) and 3PGA (1 mM) are observed for D603 but not for 18790 in this period. Note that a quasi-steady-state period for the individual sugar phosphates is much shorter in D603 (between 14 - 18 min) than the corresponding period for 18790 (11 - 23 min). Clearly, D603 is processing carbon in the upper part of the glycolytic pathway differently than is 18790.

DISCUSSION

Energy, phosphate, and carbon metabolism are linked directly or indirectly. Consequently, observations in any of these areas may provide insight into the regulatory or catalytic differences among the strains. Since NMR is a multicomponent, noninvasive measurement, it is imperative to tie together the many observations that may be obtained by spectra analysis. In some cases, a negative result may exist; however the beauty of the multicomponent measurement is that additional experiments do not have to be performed in order to identify a possible influence. Any suggested influences can be tested further in the future by additional and complementary techniques. The energetics, phosphate, and carbon metabolism are discussed next for the two strains in this study. References are made to models in the literature, and implications for metabolic engineering on the *REG1* strain are discussed.

Energetics

The initial fluctuations in cytoplasmic pH in *S. cerevisiae* observed here have been noted in many other studies,[26,30–33] by both ^{31}P NMR and acid-base determinations of intracellular pH. The uptake of glycolytic substrate, conversion into acids, and extrusion of surplus acidity are the proposed events that result in such a pH^{cyt} profile.[31,34] There is broad consensus that uptake of glucose in *S. cerevisiae* occurs by facilitated diffusion, although a membrane carrier for this uptake process has not been isolated.[35] (Researchers have shown recently that the yeast *SNF3* gene encodes a glucose transporter homologous to the mammalian protein.[36]) Cotransport of protons has been found with maltose, an actively transported sugar, but not with glucose.[11] The uptake process of glucose may trigger rapid extrusion of protons from endogeneous sources.[31] Consequently, the intracellular acidification in the initial moments after glucose addition is a result of metabolism, not of glucose uptake itself. The uptake of galactose via galactose permease may be by active transport,[12] although it most likely occurs by facilitated diffusion since the

ratio of intracellular to extracellular galactose concentration is less than one.[35] Thus, galactose uptake, like glucose uptake, is probably not directly related to intracellular acidification.

The transient profiles of cytoplasmic and extracellular pH are explained as follows. In Figure 3, under glucose catabolism, at the time ATP becomes detectable, the cytoplasmic pH increases and extracellular pH decreases; hence, the membrane ATPase is now extruding protons. Passive extrusion of CO_2 and organic acids and their anions decrease the acidity in the cell. After the cytoplasmic pH reaches a maximum, the cytoplasmic pH slowly becomes more acidic. This has been observed but the data not shown by other workers.[26] The cellular suspensions in this study were not bubbled with nitrogen. If the suspensions are bubbled with nitrogen, the cytoplasmic pH will maintain a constant level during the quasi-steady-state period;[26,33] the pH then declines after exhaustion of glucose.[26] When the cells are tightly capped without N_2 bubbling, as in this study, CO_2 becomes saturated in the extracellular medium, and hence some CO_2 remains inside the cells. Ethanol will increase the membrane fluidity and consequently make the membrane more permeable to protons.[37] However, acidification is most likely the result of CO_2 accumulation and not ethanol production, since the cytoplasmic pH remains constant when the sample is bubbled with N_2. As the cells continuously produce CO_2, the cytoplasmic pH becomes more acidic until acid loading balances acid extrusion. Thus, the acidification of the extracellular medium is an indication of the extent of fermentation.

The cytoplasmic and extracellular pH transients and ATP levels are similar under glucose metabolism for both 18790 and D603. Therefore, the differences observed in the individual sugar phosphate levels in Figure 5 do not appear to be caused by pH or ATP regulatory effects on the activities of the glycolytic enzymes. This does not exclude the unlikely possibility that the regulatory properties of a glycolytic enzyme in D603 are mutated so that it is sensitive to the pH values and

ATP levels observed.

The longer time of acidification and the subsequent alkalinization for pH^{cyt} and the smaller difference between the minimum and maximum of pH^{cyt} observed in the initial stages in Figure 4 in comparison to Figure 3 are most likely the result of the slower rate of galactose versus glucose consumption and subsequent lower rate of acid production by glycolysis. Under galactose utilization, the sugar phosphates have increased to only 11 mM for both strains at the minimum of the pH trajectory. Under galactose utilization, the strains must convert galactose to glucose 1-phosphate by the Leloir enzymes, followed by conversion of glucose 1-phosphate to glucose 6-phosphate, which then enters the glycolytic pathway. The ratio of moles ATP produced per mole of galactose and glucose is 2. As shown in Figures 2 and 3, half the amount of ATP is detected in galactose metabolism compared to glucose metabolism. Thus, under galactose metabolism, the cells must be expending energy in another process besides plasma membrane ATPase function. Not as much ATP is available for the ATPase in galactose metabolism, so the increase in pH^{cyt} is smaller than it was in glucose metabolism.

Strain D603 is able to ferment galactose faster than strain 18790, as evidenced by the transients in Figure 3. The time scale for initial drop and recovery in the cytoplasmic pH transient for D603 metabolizing galactose is more similar to those for glucose utilization for both 18790 and D603 than for the time scale observed for 18790 under galactose utilization The faster drop in extracellular pH signifies more CO_2 production for D603. The faster decline in P_i^{in} levels and rise in SP levels also point to the faster rate of fermentation by D603 than for 18790 under galactose utilization. However, since the cytoplasmic pH values are not different enough between the strains, the change in rate of galactose utilization cannot be attributed to differences in rates caused by pH influencing activity of the glycolytic enzymes.

Flow of Phosphate

The spectra of strains 18790 and D603 in the resting state following growth on glucose and galactose indicate that the initial distribution of phosphate is strain specific, not carbon–source specific. D603 has approximately the same polyphosphate and P_i^{in} levels relative to 18790 for both carbon sources. Strains 18790 and D603 only had small changes from glucose to galactose metabolism on intracellular P_i, extracellular P_i, and polyphosphate levels.

The major differences between growth on glucose to that on galactose are the induction of the *GAL2*, *GAL1*, *GAL7*, and *GAL10* genes by galactose and the derepression of the enzymes for respiration for the times when galactose is the carbon source.[11] Since the NMR experiment is conducted under anaerobic conditions, the differences in respiratory enzyme levels are irrelevent. For strain 18790 grown on glucose, the galactose–utilizing enzymes should be repressed; growth on galactose, derepressed. For strain D603 grown on glucose, the *GAL* genes should be expressed at some level because of the influence of the *reg1* mutation; for growth on galactose, these genes should also be expressed. Thus, a relationship between the strain specific distribution of phosphate and the role of the *REG1* product is not apparent.

Both 18790 and D603 consumed approximately 30 mM of intracellular P_i in the initial moments after glucose addition. Most of this phosphate is transferred to the sugar phosphate and ATP pools. Strain D603 was depleted of intracellular P_i for four minutes, while 18790 attained a minimum value of 10 mM. At these times, some of the intracellular P_i is being diverted to a P_i sink not detected by ^{31}P NMR, as determined by 20 % lower levels of C_C for 18790 and 35 % for D603. The identity of this additional sink is not known although some of this phosphate may be transported to the extracellular space. ATP may transfer P_i to undectable pools.

Extracellular P_i has begun to be transported into the cells after the first five minutes for both strains under glucose utilization in order to increase the intracellular P_i pool. The value of C_T is lower after the second spectrum until the end of the experiment, indicating that phosphate is eventually consumed from polyphosphate and extracellular P_i stores into unknown pools. As stated earlier, such unknown pools are larger for D603 (19 mM) than for 18790 (13 mM).

In the initial moments after carbon addition, as shown for both glucose and galactose utilization, the cell adjusts the levels of its phosphate ions and reserves by consuming polyphosphate and P_i^{in} and increasing P_i^{ex} levels. Polyphosphate degradation after addition of glucose has been reported in glucose-derepressed cells of *S. cerevisiae*;[30] the sample was infused with medium in that study, so a possible efflux of P_i was not reported. Phosphate efflux after addition of glucose has also been reported in glucose-derepressed cells of *S. cerevisiae*.[31] The cell membrane is impermeable to phosphate.[31] Efflux of P_i can be increased by glucose and inhibited by inhibitors of glycolysis; however, the transport mechanisms of efflux of P_i is not known.[31]

The efflux of P_i occurs at the same time as P_i^{in} levels are decreasing. It would appear that shunting some of the intracellular P_i to the extracellular space would be detrimental to the cells as they need P_i for glycolysis. Since polyphosphate is located in the vacuole and not in the periplasmic space,[35] the efflux of P_i is not from an exocellular location of polyphosphate. Since the flux of other ions such as Na^+ or K^+ at the time of P_i efflux is not known or has not been reported in the literature, a mechanism of charge distribution across the membrane cannot be postulated here as an explanation for the observed P_i efflux.

Finally, the role of polyphosphate in the cellular metabolism of *S. cerevisiae* is noted. The cells adapted their phosphate levels from a growth state in complex media to a resting state in starvation buffer. The cells were harvested in the middle of the exponential phase; in contrast to levels in the stationary phase,

polyphosphate levels are typically low during exponential growth.[12] Hence, the polyphosphate levels observed in the NMR spectra are in response to phosphate limitation or nutrient stress. Polyphosphate may serve as an energy store, a phosphate store, and as a regulator of polysaccharide content of the cell wall.[12] The consumption of polyphosphate in the vacuole and of vacuolar P_i [29] for use in glucose catabolism supports the role of polyphosphate as a phosphate store.[12]

Influence of *reg1* Mutation on Carbon Utilization

In the *reg1* strain, D603, the signal for the availability of glucose is defective, as suggested by the genetic studies referred to earlier in this paper. Two possible consequences of this action in comparison to the wild-type strain, 18790, are the scramble in the sugar phosphate region under glucose catabolism and the faster rate of glycolysis under galactose catabolism. The differences in phosphate metabolism between the strains (redistribution of P_i in the resting state and the lack of P_i^{in} under glucose utilization) may have been a result of the *reg1* mutation affecting metabolism. The other known genetic differences between the strains are in the amino acid mutations. The amino acid mutations are assumed to be unimportant in comparing the wild–type strain and *reg1* mutant strain, since both strains were grown similarly in complex media.

Under glucose utilization, phosphate is the limiting metabolite in glycolysis in D603, but not in 18790. The initial rates of P_i depletion and SP formation after glucose addition are similar for both strains. However, P_i^{in} is then depleted in D603 for 4 minutes, and the total time for glycolysis in D603 is 39 min. in contrast to 30 min. for 18790 (note: the total cell density for D603 was 5% greater than for 18790). Both D603 and 18790 maintain the same cytoplasmic concentrations of P_i during the quasi-steady-state period. Thus, the limitation is prior to the quasi-steady-state period, but after the initial moments of glucose addition.

The transients in Figure 5 are consistent with the notion that PFK may be limiting glycolysis in strain D603 under glucose utilization. PFK is activated by P_i for the cytoplasmic pH values in this study.[7,38] Hexokinase is not activated by P_i.[11] After the depletion of intracellular P_i for D603, the G6P trajectory continues to its maximum at 14 minutes after glucose addition. FDP levels cannot increase to the levels attained in 18790 because PFK is not activated. By 14 min., the P_i^{in} levels increase to quasi-steady-state values; consequently, FDP levels increase and G6P levels decrease by the same magnitude. Quasi-steady-state levels of FDP in D603 are half those in 18790.

At this point, comparison of the experimental data in this study to models of glycolysis in the literature is appropriate in the discussion of rate–limiting steps. The glucose uptake and/or hexokinase step, the phosphofructokinase step, the pyruvate kinase step, and the glyceraldehyde 3-phosphate dehydrogenase step have been suggested to exert control in glycolysis in yeast.[39,40] Shulman and coworkers[4] inferred that the glycolytic rate is controlled at either the glucose uptake step or the hexokinase step during anaerobic cultures of *S. cerevisiae.* By using characteristic reaction path (CRP) analysis, Liao and coworkers[41] suggested that PFK does not limit glycolysis in anaerobic high cell density suspensions of commercial strains of *S. cerevisiae.*

By applying metabolic control theory to a model of glycolysis, Galazzo and Bailey[42] calculated for steady-state conditions that most of the flux control lies in the glucose uptake step in suspended cell cultures of 18790. However, flux control switches to PFK in immobilized cells of the same strain. Immobilization was suggested to affect the glucose uptake step. The glycolytic intermediates and pH^{cyt} values at quasi-steady state for the immobilized cells at an extracellular pH of 4.5 were similar to those of D603 under quasi-steady state in this study. It can be shown that only the functional form of the metabolite concentrations and pH dependency of the enzymes and not maximal activity of the enzymes are

important in determing the flux control coefficients in an unbranched pathway. Extrapolation of the experimental results to the model by Galazzo and Bailey suggest that PFK may exert greater flux control in D603 than in 18790.

These results suggest that the glucose uptake step or the hexokinase step may be altered in D603. Hexokinase PII, the glucose–phosphorylating kinase present in in exponential growth on glucose, is proposed to have a similar function as the *REG1* product in glucose repression. It is not clear that the *reg1* mutation would also simultaneously effect a change in hexokinase PII activity under glucose utilization. Galactose utilization was faster in D603 than in 18790. 18790 is so much slower in the initial stages of galactose catabolism. Hexokinase PII is not needed in galactose metabolism for catalytic activity but may be needed in a regulatory role. A change in the regulation of the components for catabolite repression could conceivably change the metabolism of the cells under galactose catabolism, as is observed for D603. This evidence points to the initial functions of carbon catabolism being affected for D603; however a mechanism for these changes cannot be postulated on the data observed here.

The detailed information provided by NMR combined with the flux control analysis shows that PFK is the controlling step in D603. From a metabolic engineering viewpoint augmenting PFK activity in D603 will allow for better carbon utilization. This may provide beeter productivity in this strain in use of expression vectors with *GAL* promoters.

CONCLUSIONS

The metabolism of wild-type and *reg1* mutant *Saccharomyces cerevisiae* has been studied by transient ^{31}P NMR experiments in order to characterize the influence of the *reg1* mutation on catabolite repression. Separate experiments were conducted using glucose or galactose as carbon sources. Transient profiles were determined for extracellular phosphate, cytoplasmic phosphate, sugar phosphates, ATP and

polyphosphate. Cytoplasmic pH and extracellular pH transients were measured. Profiles of G6P, F6P, FDP, and 3PGA were analyzed under glucose catabolism. As indicated by these measurements under glucose utilization, the phosphate and carbon metabolism of the *reg1* strain was regulated differently despite ATP and pH profiles similar to those of the wild-type strain. The pH and metabolic transients under galactose utilization support the hypothesis that the *REG1* product operates early in the regulatory circuitry for glucose repression. The ability to coordinate measurements of metabolic flows with information on the energy status of the cell *in vivo* is an important step in understanding cellular metabolic kinetics and regulation. The wealth of information provided by NMR will aid the metabolic engineer in understanding the metabolic function of manipulated organisms.

Acknowledgement:

This research was supported by the Energy Conversion and Utilization Technology (ECUT) program of the U.S. Department of Energy. The nuclear magnetic resonance experiments reported here were made possible by the facilities of the Southern California Regional Nuclear Magnetic Resonance Center (NSF Grant No. CHE-84-40137) and software for NMR spectral analysis was provided by the NIH Resource Laboratory at Syracuse University (Grant No. RR-01317).

REFERENCES

1. J.E. Bailey, D.D. Axe, J.L. Galazzo, K.F. Reardon, A. Seressiotis and J.V. Shanks, *Biochem. Engr. V* (Ann. N.Y. Acad. Sci.), **506**, 1 (1987).

2. R.B. Moon and J.H. Richards, *J. Biol. Chem.*, **248**, 7276 (1973).

3. R.G. Shulman, *TIBS*, **13**, 37 (1988).

4. S.L. Burk and R.G. Shulman, *Ann. Rev. Microbiol.*, **41**, 595 (1987).

5. M.J. Avison, H.P. Hetherington, and R.G. Shulman, *Annu. Rev. Biophys. Chem.*, **15**, 377 (1986).

6. J.W. Pritchard, and R.G. Shulman, *Annu. Rev. Neurosci.*, **9**, 61 (1986).

8. L. Guarante, R.R. Yocum and P. Gifford, *Proc. Natl. Acad. Sci.*, **79**, 7410 (1982).

9. M. Carlson, *J. Bacteriol.*, **169**, 4873 (1987).

10. N.A. Da Silva, "Host-Plasmid Interactions and Regulation of Cloned-Gene Expression in Recombinant Cells", Ph.D. Dissertation, Caltech, Pasadena, California. (1988).

11. D.F. Fraenkel, "Carbohydrate Metabolism" in *The Molecular Biology of the Yeast Saccharomyces, Metabolism and Gene Expression*, p. 1, (Cold Spring Harbor, New York, 1982).

12. H.O. Halvorson, K.A. Bostian, J.G. Yarger, and J.E. Hopper, "Enzyme Expression during Growth and Cell Division in *Saccharomyces cerevisiae*: A Study of Galactose and Phosphorus Metabolism " in *Recombinant DNA and Cell Proliferation*, p. 49, (Academic Press, New York, 1984).

13. P. Eraso, and J.M. Gancedo, *Eur. J. Biochem.*, **141**, 195 (1984).

14. K. Matsumoto, I. Uno, T. Ishikawa, and Y. Oshima, *J. Bacteriol.*, **156**, 898 (1983).

15. K.D. Entian, *Mol. Gen. Genet.*, **178**, 633 (1980).

16. K.D. Entian, and K. -U. Frohlich, *J. Bacteriol.*, **158**, 29 (1984).

17. K.D. Entian, F. Hilberg, H. Opitz, and D. Mecke, *Mol. Cell. Biol.*, **5**, 3035 (1985).

18. J.L. Celenza, and M. Carlson, *Science*, **233**, 1175 (1986).

19. Y. Oshima, " Regulatory Circuits for Gene Expression: The Metabolism of Galactose and Phosphate" in *The Molecular Biology of the Yeast Saccharomyces, Metabolism and Gene Expression*, p. 159, (Cold Spring Harbor, New York, 1982).

20. E. Giniger, S.M. Varnum, and M. Ptashae, *Cell*, **40**, 767 (1985).

21. K. Matsumoto, T. Yoshimatsu, and K. Oshima, *J. Bacteriol.*, **153**, 1405 (1983).

22. F. Srienc, J.L. Campbell, and J.E. Bailey,*Cytometry*, **7**, 132 (1986).

23. J.V. Shanks and J.E. Bailey, *Biotechnol. Bioeng.*, in press.

24. J.M. Gancedo and C. Gancedo, *Biochimie*, **55**, 205 (1973).

25. LABONE(TM) NMR1 Spectroscopic Data Analysis Software System, Revision 2.70, (Syracuse University, New Methods Research Inc., 1985).

26. J.A. den Hollander, K. Ugurbil, T.R. Brown, and R.G. Shulman, *Biochemistry*, **20**, 5871 (1981).

27. G. Navon, R.G. Shulman, T. Yamane, T.R. Eccleshall, K.B. Lam, J.J. Baronofsky, J. Marmur, *Biochemistry*, **18**, 4487 (1979).

28. R.A. Gage, W. Van Wijngaarden, A.P.R. Theuvenet, G.W.F.H. Borst-Pauwels, and C.A.G. Haasnoot, *Biochim. Biophys. Acta.*, **804**, 341 (1984).

29. J.V. Shanks and J.E. Bailey, "Elucidation of Cytoplasmic and Vacuolar Components in the Inorganic Phosphate Region in the ^{31}P NMR Spectrum of Yeast," submitted, (1988).

30. R.J. Gillies, K. Ugurbil, J.A. den Hollander, and R.G. Shulman, *Proc.*

Natl. Acad. Sci., **78**, 2125 (1981).

31. K. Sigler, A. Knotkova, and A. Kotyk, *Biochim. Biophys. Acta.*, **643**, 572 (1981).

32. G.W.F.H. Borst-Pauwels, *Biochim. Biophys. Acta.*, **650**, 88 (1981).

33. J.L. Galazzo, J.V. Shanks and J.E. Bailey, *Biotechnology Techniques*, **1**, 1 (1987).

34. K. Sigler, A. Kotyk, A. Knotkova, and M. Opekarova, *Biochim. Biophys. Acta.*, **643**, 583 (1981).

35. T.G. Cooper, "Transport in *Saccharomyces cerevisiae*" in *The Molecular Biology of the Yeast Saccharomyces, Metabolism and Gene Expression*, p. 399, (Cold Spring Harbor, New York, 1982).

36. J.L. Celenza, L. Marshall-Carlson, and M. Carlson, *Proc. Natl. Acad. Sci.*, **85**, 2130 (1988).

37. R.P. Jones and P.F. Greenfield, *Yeast*, **3**, 223 (1987).

38. M. Banuelos and C. Gancedo, *Arch. Microbiol.*, **117**, 197 (1978).

39. A. Boiteux and B. Hess, *Phil. Trans. R. Soc. Lond. B*, **293**, 5 (1981).

40. Y. Termonia and J. Ross, *Proc. Natl. Acad. Sci.*, **78**, 3563 (1981).

41. J.C. Liao, E.N. Lightfoot, Jr., S.O. Jolly, and G.K. Jacobson, *Biotechonl. Bioeng.*, **31**, 855 (1988).

42. J.L. Galazzo and J.E. Bailey, "Fermentation Pathway Kinetics and Metabolic Flux Control in Suspended and Immobilized *Saccharomyces cerevisiae*," manuscript in preparation.

FIGURE CAPTIONS

Figure 1: Fermentation pathways for glucose and galactose in *Saccharomyces cerevisiae*.[11,12] A glucose transporter has not been isolated and thus, the gene symbol for this step is marked as a question mark. Consumption of glycerol and ethanol as substrates requires O_2.

Figure 2: ^{31}P NMR spectra at 202.46 MHz of anaerobic *S.cerevisiae* D603 suspensions at 20°C for (A) glucose metabolism and (B) galactose metabolism. (A) Glucose was added at 0^+ sec. at a final concentration of 75 mM to a 50 % w/v suspension that had been grown on glucose. Glucose was exhausted at 37.5 min. (B) Same as (A), except that galactose was the carbon source for growth and for the NMR experiment; galactose was not exhausted at 109.5 min. Spectra for (A) and (B) were recorded using 70° pulses and 0.5 sec. acquisition time. Times given for each spectrum represents the end of the 2 minute accumulation period. Abbreviations: SP : sugar phosphate; P_i^{cyt} : cytoplasmic inorganic phosphate; P_i^{ex} : extracellular inorganic phosphate; PM : phosphomannan; ATP : adenosine triphosphate; ADP : adenine diphosphate; PP_1 : pyrophosphate and terminal phosphates of polyphosphate; NAD(H) : nicotinamide adenine dinucleotide; UDPG : uridine diphosphoglucose and uridine diphosphogalactose; PP_3 : penultimate phosphates of polyphosphate; and PP_4 : middle phosphates of polyphosphate.

Figure 3: Concentrations and pH values with time for cells utilizing glucose. Measurements obtained from ^{31}P NMR spectra. (A) *S. cerevisiae* 18790. (B) *S. cerevisiae* D603. All concentrations except for P_i^{ex} are based upon intracellular volume; P_i^{ex} based upon buffer volume. Carbon addition at 0^+ sec. Abbreviations: P_i^{in} : cytoplasmic + vacuolar inorganic phosphate; PolyP : polyphosphate summed for PP_1, PP_2 and PP_4; pH^{cyt} : cytoplasmic pH; pH^{ex} : extracellular pH; others as in Figure 2. Symbols: (■) PolyP; (▲) P_i^{ex}; (●) ATP; (□) P_i^{in}; (○) SP; (△) pH^{cyt}; (◊) pH^{ex}.

Figure 4: Same as Figure 3 except for galactose utilization.

Figure 5: Intracellular sugar phosphate concentrations obtained from the deconvolution analysis process for *S. cerevisiae* 18790 and *S. cerevisiae* D603 undergoing glucose utilization. Glucose added at 0^+ seconds for 18790 and 90 seconds for D603. 18790 (solid symbols) and D603 (open symbols).

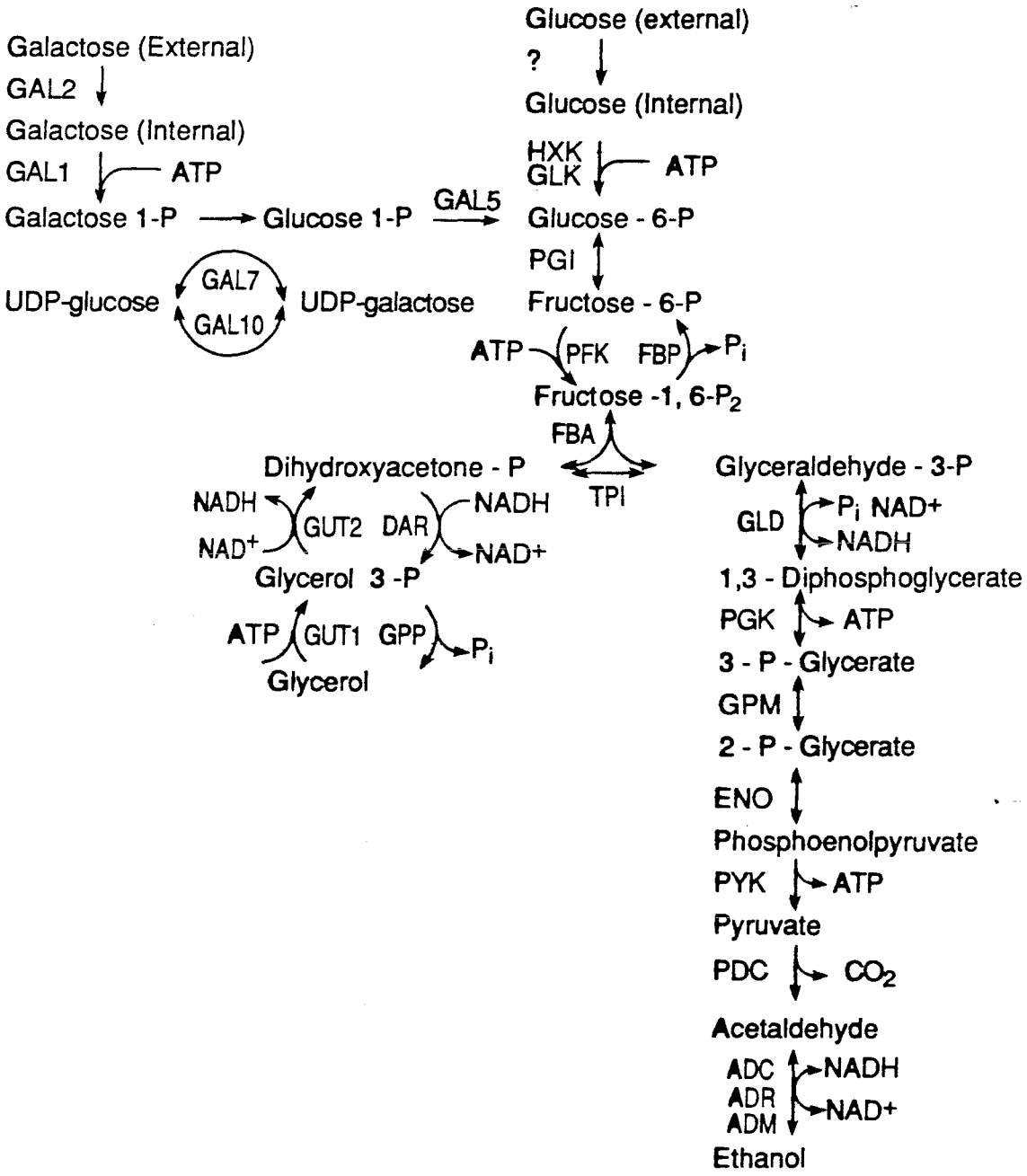
Galactose (External)
GAL2
Galactose (Internal)
GAL1
ATP
Galactose 1-P
Glucose 1-P
GAL5
UDP-glucose
GAL7
GAL10
UDP-galactose
Glucose (external)
?
Glucose (Internal)
HXK
GLK
ATP
Glucose - 6-P
PGI
Fructose - 6-P
ATP
PFK
FBP
Pi
Fructose -1, 6-P2
FBA
Dihydroxyacetone - P
TPI
Glyceraldehyde - 3-P
NADH
NAD+
GUT2
DAR
NADH
NAD+
Glycerol 3 -P
GLD
Pi NAD+
NADH
1,3 - Diphosphoglycerate
PGK
ATP
3 - P - Glycerate
GPM
2 - P - Glycerate
ENO
Phosphoenolpyruvate
PYK
ATP
Pyruvate
PDC
CO2
Acetaldehyde
ADC
ADR
ADM
NADH
NAD+
Ethanol
ATP
GUT1
GPP
Pi
Glycerol

Figure 1

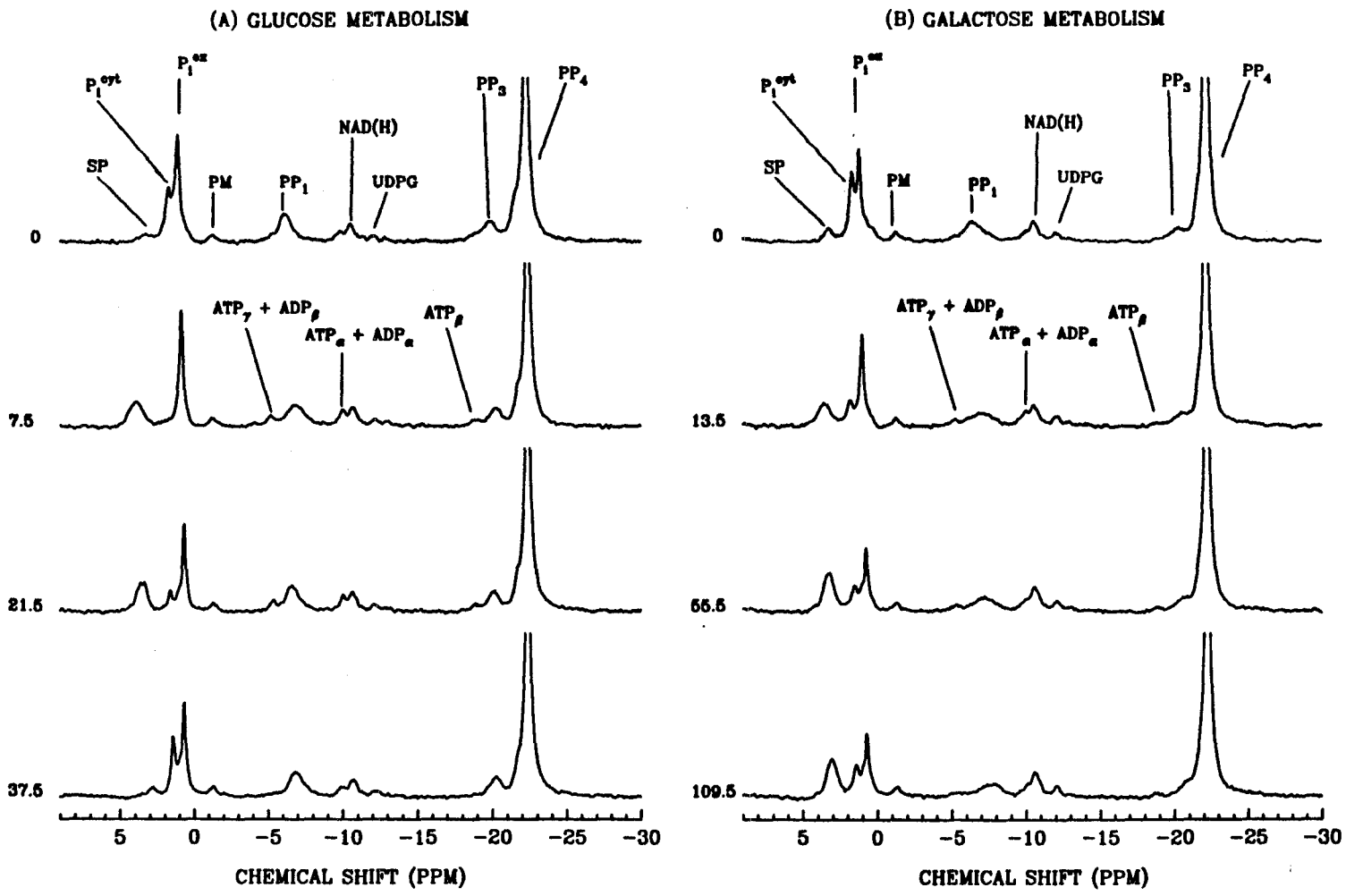
(A) GLUCOSE METABOLISM
(B) GALACTOSE METABOLISM
P_i^{cyt}
P_i^{ex}
SP
PM
PP_1
NAD(H)
UDPG
PP_3
PP_4
$ATP_\gamma + ADP_\beta$
$ATP_\alpha + ADP_\alpha$
ATP_β
0
7.5
21.5
37.5
13.5
55.5
109.5
5
0
-5
-10
-15
-20
-25
-30
CHEMICAL SHIFT (PPM)

Figure 2

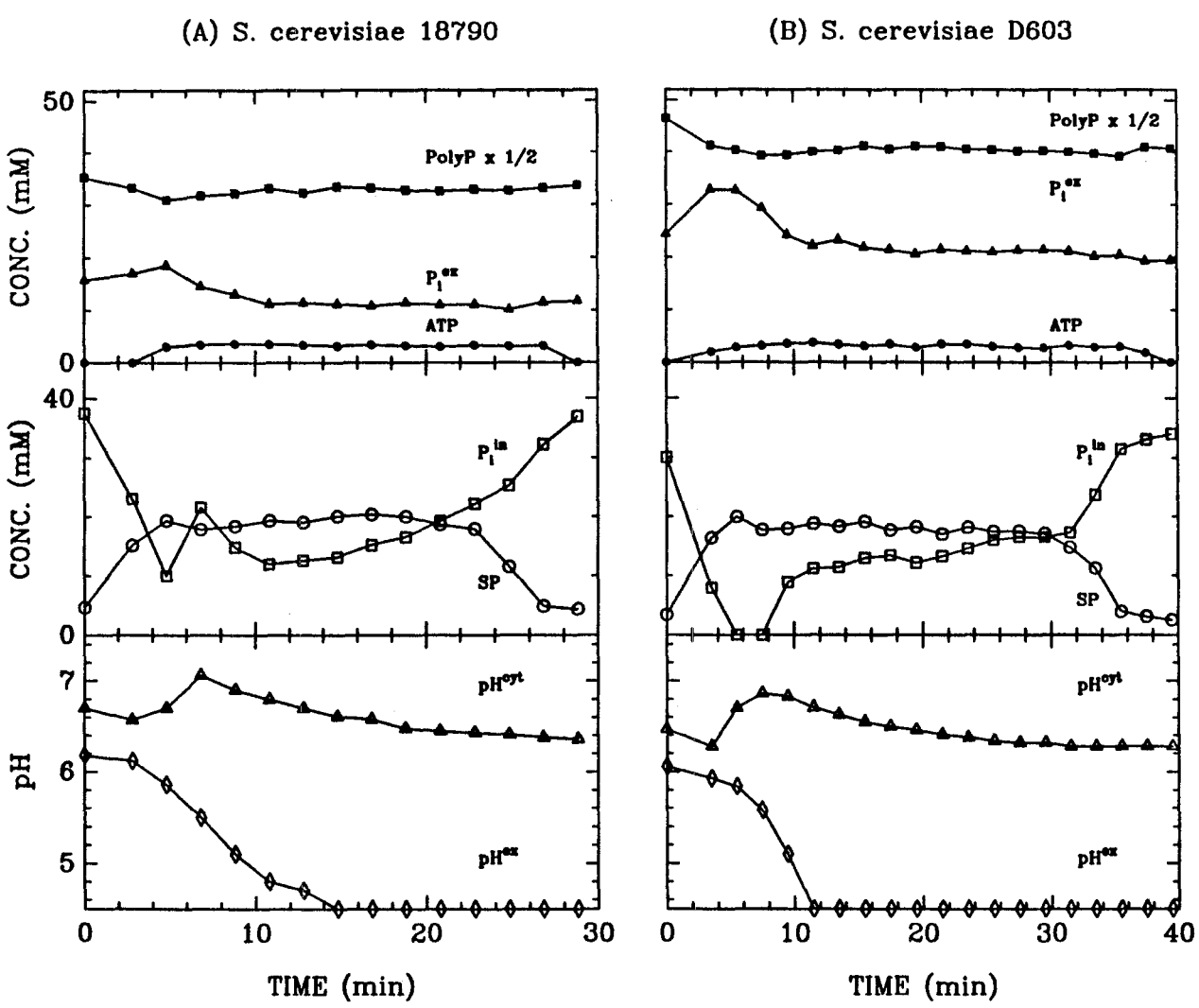
(A) S. cerevisiae 18790
(B) S. cerevisiae D603
CONC. (mM)
PolyP x 1/2
P_i^{ex}
ATP
P_i^{in}
SP
pH
pH^{cyt}
pH^{ex}
TIME (min)

Figure 3

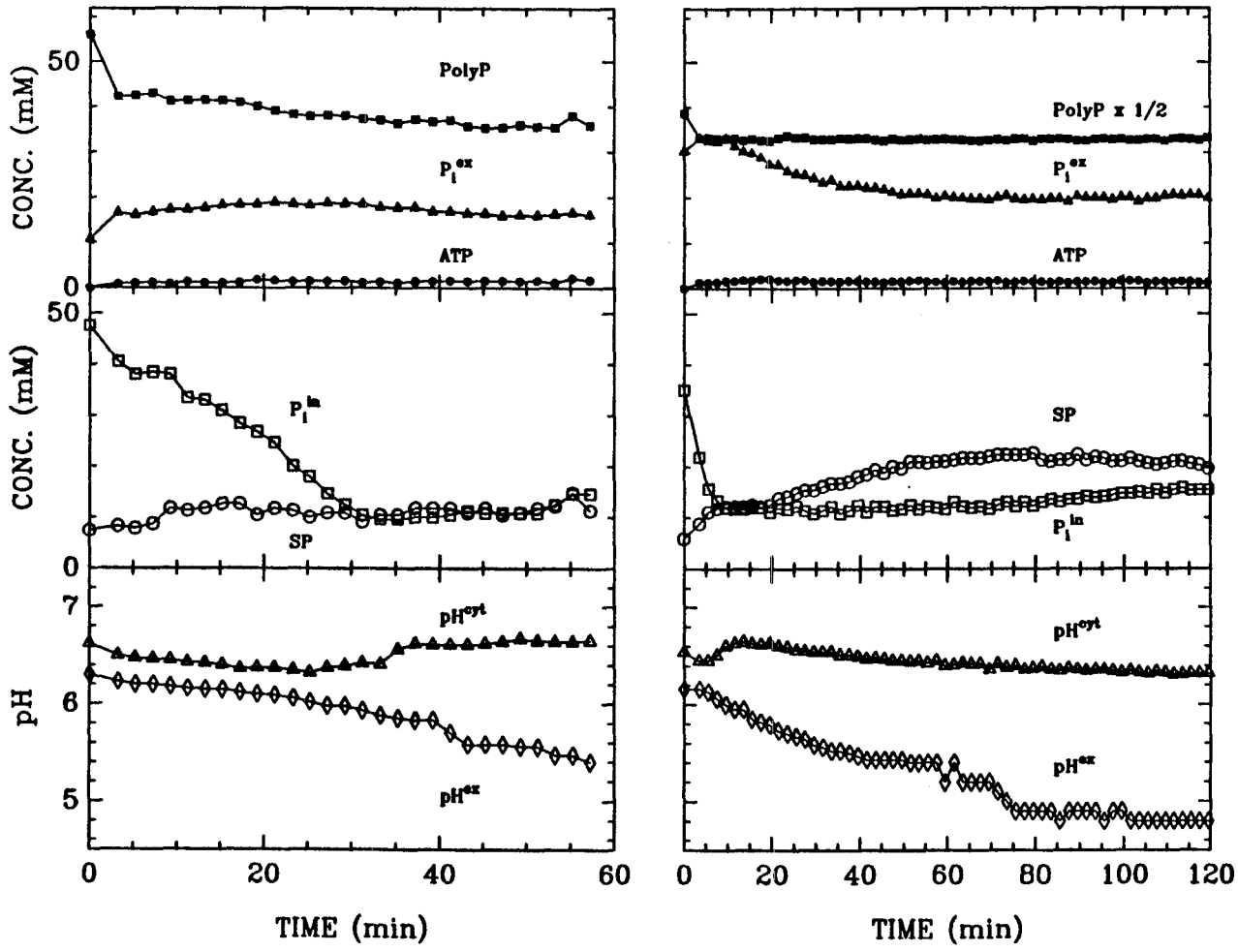
(A) S. cerevisiae 18790
(B) S. cerevisiae D603
CONC. (mM)
PolyP
P_i^{ex}
ATP
P_i^{in}
SP
pH
pH^{cyt}
pH^{ex}
PolyP x 1/2
TIME (min)

Figure 4

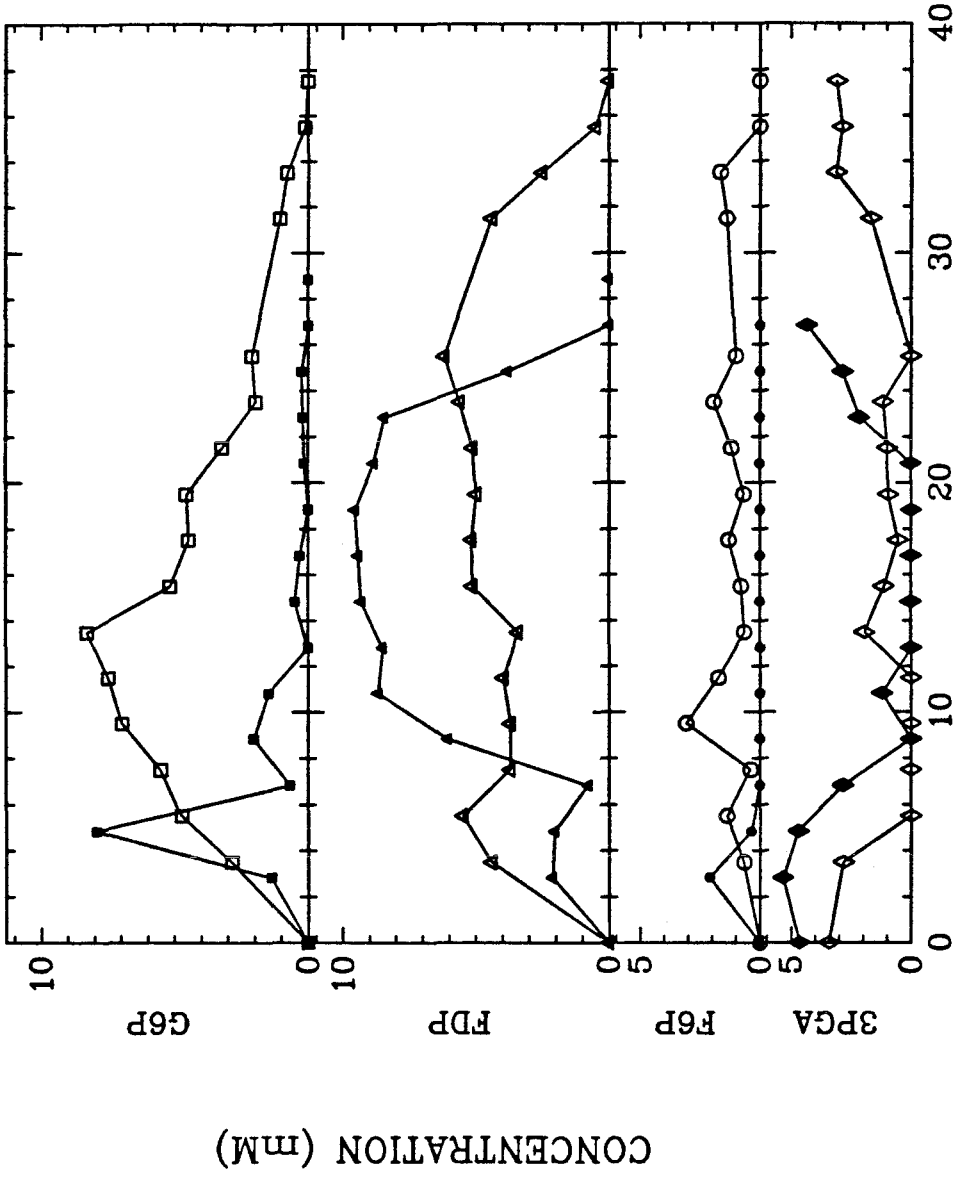
G6P
FDP
F6P
3PGA
10
0
10
0
5
0
5
0
0
10
20
30
40
TIME (min)
CONCENTRATION (mM)

Figure 5

CHAPTER 5

^{31}P and ^{13}C NMR STUDIES OF RECOMBINANT *SACCHAROMYCES CEREVISIAE* WITH ALTERED GLUCOSE PHOSPHORYLATION ACTIVITIES

ABSTRACT

Manipulation of cellular metabolism to maximize the yield and rate of formation of desired products may be achieved through genetic modification. Batch fermentations utilizing glucose as a carbon source were performed for three recombinant strains of *Saccharomyces cerevisiae* in which the glucose phosphorylation step was altered. The host strain (*hxk1 hxk2 glk*) is unable to grow on glucose or fructose; the three plasmids investigated expressed hexokinase PI, hexokinase PII, or glucokinase, respectively, enabling more rapid glucose and fructose phosphorylation *in vivo* than that provided by wild–type yeast.

Intracellular metabolic state variables were determined by ^{31}P NMR measurements of *in vivo* fermentations under nongrowth conditions. Glucose consumption, ethanol and glycerol production, and polysaccharide formation were determined by ^{13}C NMR measurements under the same experimental conditions as used in the ^{31}P NMR measurements. The trends observed in ethanol yields for the strains under growth conditions were mimicked in the nongrowth NMR conditions.

Only the strain with hexokinase PI had higher rates of glucose consumption and ethanol production in comparison to healthy diploid strains in the literature. The hexokinase PII strain drastically underutilized its glucose–phosphorylating capacity. A regulation difference in the use of magnesium–free ATP for this strain could be a possible explanation. Differences in ATP levels and cytoplasmic pH values among the strains were observed that could not have been foreseen. However, cytoplasmic pH values were dismissed as the inhibitory difference observed among the strains in the glucose–phosphorylating activity used *in vivo*.

INTRODUCTION

Metabolic engineering is the process of manipulating one or more steps in the metabolic pathway of an organism in order to produce or enhance production of desired biochemicals.[1] The vehicles for this process include recombinant DNA techniques for insertion of foreign genes to create new steps, for amplification of existing enzymes and for control of expression of enzyme activity; mutagenesis for deletion of steps; and environmental manipulations such as immobilization to alter the activity or regulation of certain steps.[1] Successful examples of metabolic engineering include the production of indigo in *Escherichia coli*,[2] 2–keto–L–gulonate in *Erwinia herbicola*,[3] and enhanced methanol production in *Methylophilus methylotrophus*.[4] These examples resulted from cloning a foreign gene for creation of new reactions inside the host cell. These studies have relied on the premise of increasing enzyme amount or activity as much as possible for the new step for enhanced production. However, information on the regulatory features of the enzymes and the energetics of the cell *in vivo* will be important in developing tactics for production by metabolic engineering.

Ethanol production by the yeast *Saccharomyces cerevisiae* is a classic system for affecting changes to the cell and observing rates of productivity.[1,5,6] The glucose–uptake/glucose–phosphorylation steps have been proposed as the limiting steps in glycolysis.[7,8] *S. cerevisiae* has three enzymes for the phosphorylation of glucose – hexokinases PI and PII and glucokinase.[9,10] A study was conducted in which a wild–type strain, with all three kinases, was compared to mutant strains of *S. cerevisiae*, each carrying a single glucose–phosphorylating enzyme.[11] The order (from highest to lowest) of *in vitro* glucose phosphorylation activities were the wild–type strain, the hexokinase PI strain, the hexokinase PII strain, and the glucokinase strain.[11] Of the three single kinase strains, the glucokinase strain showed the highest glucose–phosphorylation activity *in vivo*.[11] *In vivo* glucose consumption rates were determined for the strains in a resting (nongrowth) state.

The *in vivo* glucose consumption rate increased linearly with increasing *in vitro* enzyme activity for all strains except the glucokinase strain.[11] Each of the single–kinase strains had lower glucose consumption rates than the wild–type strain.[11] The study did not indicate if ethanol production increased with higher glucose consumption rate. Each of the three kinases have been cloned into multicopy plasmids into yeast.[12,13,14] In this paper, the anaerobic catabolism of glucose and consequent ethanol production is monitored for recombinant *S. cerevisiae* strains in which the glucose–phosphorylation activities have been altered.

Noninvasive experimental techniques are imperative for evaluating the detailed intracellular consequences of metabolic engineering. ^{31}P and ^{13}C NMR spectroscopy are used in this study for *in vivo* examination of the recombinant yeast strains. The yeast cell as viewed by ^{31}P and ^{13}C NMR is shown in Figure 1. The ^{31}P and ^{13}C NMR studies are performed in separate experiments on identically prepared samples of yeast. The boxed components in Figure 1 can be determined from ^{13}C NMR by feeding [1–^{13}C] labelled glucose to the yeast cells. The other boldface components in Figure 1 can be measured by ^{31}P NMR. In a suitably controlled and calibrated NMR experiment, the number of nuclei of a compound is proportional to the area of the compound's resonance in the NMR spectrum; thus, concentration can be determined from NMR measurements.

^{13}C NMR cannot distinguish between intracellular and extracellular pools of ^{13}C labelled compounds. Besides the substrate glucose and the fermentation products, glycerol, acetate, and ethanol, the storage polymers glycogen and trehalose can be detected.[15] The sugar phosphates (glucose–6–phosphate, fructose–6–phosphate, fructose–1,6–diphosphate, and 3–phosphoglycerate (3PGA)) are in too of low levels for detection by ^{13}C NMR and the resonances for tthe sugar phosphates are partially obscured by the glycerol resonance in the ^{13}C NMR spectrum.[15] However, the concentrations of these components can be determined by analysis of the ^{31}P NMR spectrum.[16] Because the chemical shift resonance of

inorganic phosphate (P_i) is sensitive to pH, the pH as well as to P_i, concentrations can be determined in the different compartments in the cell.[17] Phosphomannan in the cell wall and polyphosphate in the vacuole can also be detected. The chemical shifts of ATP in the ^{31}P NMR spectra are sensitive to the fraction of ATP bound to magnesium ions.[18] Mg–ATP is a cofactor in many glycolytic reactions. This information can be combined in order to obtain a picture of the working cell with the inhibitors and effectors present. Thus, NMR provides information on different intracellular compartments and is a noninvasive, multicomponent measurement.

GLUCOSE–PHOSPHORYLATION ENZYMES

S. cerevisiae has three enzymes in the wild–type that phosphorylate glucose; Mg–ATP is the cosubstrate.[9,10] Hexokinases PI and PII phosphorylate mannose and fructose,[9] while glucokinase does not use fructose as a substrate.[10] Values reported for the ratios of phosphorylation of fructose to glucose are 2.5–4.2 for hexokinase PI, 1.2–1.9 for hexokinase PII, and 0–0.2 for glucokinase.[11,12,19]

The hexokinases are dimers.[9] The structural gene sequences for the hexokinases included 1452 and 1455 bp, corresponding to MW of 53605 and 53800 for the *HXK1* and *HXK2* monomers, respectively.[20,21] The *HXK1* sequence was 76% homologous to *HXK2*.[21] Glucokinase has a variable MW of 144000–200000;[11] the MW of the monomer is 51000. The amino acid composition of glucokinase is similar to those of hexokinases PI and PII except for the number of aspartic acid and histidine residues.[22] A common ancestor for these enzymes has been suggested.[20–22]

The physiological roles of the enzymes in the wild–type organism are not well understood. In the wild–type, hexokinase PII activity predominates in exponential phase cultures on YPD medium; in stationary phase cultures, *in vitro* glucose–phosphorylation activities for hexokinase PII, hexokinase PI, and glucokinase are in approximate ratios of 4:3:3.[19] Hexokinase PII is reported to be necessary for

glucose repression and to have distinct catalytic and regulatory domains.[13,23]

In haploid strains carrying single enzymes for glucose phosphorylation, the *GLK* strain grew on glucose faster than the *HXK1* strain or *HXK2* strain; the *HXK2* strain grew 30% faster than the *HXK1* strain.[11] Under anaerobic conditions, the *GLK* strain had the highest glucose consumption rate *in vivo* and the lowest enzyme activity (*in vitro*).[11] The *HXK1* and *HXK2* strains exhibited a linear relationship between *in vivo* glucose consumption rates and *in vitro* enzyme activities for glucose phosphorylation, the *HXK1* strain having the highest values in both cases.[11]

The kinases are involved in glucose uptake. Two types of glucose transport systems have beeen observed for wild–type *S. cerevisiae*, based upon their apparent affinity (K_m) values of 2 mM ("high affinity") and 15 mM ("low affinity").[24] The high–affinity process is kinase–dependent and glucose–repressible. The kinase dependence is not merely a consequence of phosphorylation and metabolism, but reflects some other unknown role for the kinases in the uptake process.[25]

X–ray structural analysis reveals two binding sites for ATP in the hexokinase PII dimer.[26,27] High ATP concentrations (5 mM) inhibited the glucose–phosphorylation activities of the hexokinases by 50%.[13] However, magnesium levels in the assay procedure were not given. A more recent study determined that glucose–phosphorylation activity for hexokinase PI is not affected either by magnesium–free ATP nor by free Mg^{+2} levels.[28] Hexokinase PII is not inhibited by high Mg–ATP levels if magnesium–free ATP is kept at low levels (0.01 mM) in the assay mixture; concentrations of free ATP of 0.1 mM or greater led to maximal inhibition of glucose–phosphorylation activity (activities 30% of maximum value).[29] This second binding site for ATP in hexokinase PII may explain the difference in ATP inhibition between the hexokinases.[13] ADP was an inhibitor for all the kinases;[9,22] Mg–ADP levels of 0.2–0.5 mM at pH values between 6.5–7 inhibited hexokinase PII by 70%, less so for hexokinase PI.[9]

The pH optima for the kinases are between 7.5 and 9.5 pH units.[11] At pH 6.4, the hexokinases are only 10% as active in glucose–phosphorylation activity as at their pH optima, whereas, glucokinase is 40% as active.[11] Glucose–6–phosphate is a weak inhibitor of all the kinases.[11] Levels of 3–phosphoglycerate at 1 mM or higher may activate glucokinase.[11]

MATERIALS AND METHODS

Yeast Strains

Saccharomyces cerevisiae DFY437 and plasmids pBW111, pBW112, and pBW113 were kindly provided by Dan Fraenkel.[12] The host strain *S. cerevisiae* DFY437 (*α lys1 leu2 hxk1 hxk2 glk*) is unable to phosphorylate glucose or fructose. The plasmids were constructed from the YEp13 shuttle vector, and the structural genes *HXK1*, *HXK2*, and *GLK* were cloned by complementation into the plasmids pBW111, pBW112, and pBW113, respectively.[12] The approximate insert sizes were 5.3, 4.8, and 3.8 kilobases, respectively.[12] The plasmids will subsequently be named pHXK1, pHXK2, and pGLK, respectively. *HXK1* encodes for the gene for hexokinase PI, *HXK2* for hexokinase PII, and *GLK* for glucokinase. The host strain cannot grow on glucose. The host strain transformed with any one of these three plasmids will grow on glucose.

Culture Conditions

The strains were grown aerobically in a rotary shaker at 30°C in 1 L flasks containing 400 mL of the following medium: 1% Difco Bacto-Yeast Extract, 2% Difco Bacto-Peptone, and 2% glucose, adjusted to pH 4.5 with citrate buffer (50 mM final buffer concentration). The flasks were inoculated to a final volume percent of 1% with early stationary phase cell cultures grown in the same medium.

Glucose, Ethanol, and Cell Density Assays

Glucose was determined with Sigma Kit 510. Ethanol was measured by gas chromotography, using a Shimadzu GC–9/CR–3A chromatograph (dual FID) / integrator system. The 2 m glass column (3 mm ID) was packed with Chromosorb 101 (80/100) mesh, the helium carrier gas flow rate was 50 mL/min, the detector temperature was 200°C, and the oven temperature was 140°C. Culture optical density was measured at 590 nm, using a Spectronic 21, and cell dry weight was determined from a previously established calibration curve.

Assays of Kinase Activity

Enzyme assays were performed as in Bisson and Fraenkel.[29] Cells were harvested during exponential phase (1 g cell dry weight (CDW)/L). Crude extracts for the determination of total glucose and fructose-phosphorylation activity were prepared using glass beads.[19,29,30] The extract buffer was 2 mM benzamidine hydrochloride, 50 mM K_2HPO_4, 2 mM EDTA, and 3 mM 2-mercaptoethanol, pH 7.4.[29,30] Cells were resuspended in extract buffer with an equal volume of glass beads (0.5 mm diameter) and vortexed 5 min. in the cold. The membrane debris was not removed from the extract by centrifugation.[29] Extracts were placed on ice and assays were performed on the same day. Assays were performed for all three strains at the same time.

The spectrophotometric assay was based upon the coupling of glucokinase or hexokinase activity to glucose-6-phosphate dehydrogenase and phosphoglucose isomerase (for fructose).[19] The assay solution composition was 50 mM imidazole, 0.1 M KCl, 10 mM $MgCl_2$, 2 mM EDTA, 0.4 mM $NADP^+$, 1 mM glucose (10 mM fructose), 1 mM ATP, 4μg of glucose-6-P dehydrogenase and 2μg of phosphoglucose isomerase, pH 7.0.[29] 100 μL of extract was added to assay solution to give a total volume of 1.0 mL. Assays were performed on a Shimadzu UV-260 at 340 nm at 25°C. Total protein was measured, using the Bio-Rad assay with bovine

albumin as standard. All chemicals except the Bio-Rad assay kit were obtained from Sigma and BMB. Spectrophotometric assays were performed in triplicate (for the same culture). Protein assays were performed in duplicate.

NMR Preparation

For NMR experiments, cells were harvested during the exponential phase of growth as described previously.[16] Exponential phase cells (1 g cell dry weight (CDW)/L; 30% of initial glucose consumed) were chilled in an ice bath to 5°C under continuous shaking, then harvested by low speed centrifugation. The cells were then washed twice in an ice-cold, sterile, buffered salt solution: 0.85 g/L KH_2PO_4, 0.15 g/L K_2HPO_4, 0.5 g/L $MgSO_4$, and 0.1 g/L NaCl in 50 mM MES buffer, pH adjusted to 6.

The cells were resuspended in wash medium supplemented with an additional 15 mM P_i at a 1:1 ratio of cell pellet volume to resuspension volume. Cell suspensions (2 mL) were placed in 10 mm o.d. NMR sample tubes, tightly capped, and kept on ice until used, always less than 2 hrs. before an experiment. A "dummy" sample for each experiment was prepared in an identical fashion except that each "dummy" sample contained 20 v/v % D_2O (final sample volume 2.1 mL).

^{13}C NMR Spectroscopy

^{13}C NMR spectra were obtained in the Fourier-transform mode at 125.76 MHz on a Bruker AM-500 NMR spectrometer at 20°C. The "dummy" sample was used for shimming. Free induction decays (FID's) were accumulated in consecutive 1 min. blocks (24 scans, 16K files) using 45° pulses, 2.33 sec. repetition time, and a spectral width of 25000 Hz. Inverse-gated composite-pulse decoupling of protons was employed, at a power of 3 W. Decoupler heating of the sample did not occur. Samples were run unlocked and spinning was not used.

For the cellular samples, [1-^{13}C]glucose (Sigma, 99% isotopic purity) was

added to a total concentration of 80 mM in the sample; then a sequence of spectra were collected during subsequent 1 min. intervals. The C-2 carbon of ethanol was used as an internal reference: it resonates 17.6 ppm downfield from tetramethylsilane, which is assigned to zero ppm. Cell density (CDW/L) was determined for each sample at the end of the experiment.

Calibration experiments for estimation of concentrations were performed by alternating fully relaxed spectra (60 sec. relaxation delay) with spectra as taken previously, using a sample of extracellular medium from the cellular samples after glucose was fully converted. Labelled glucose was added to this solution. Thus, calibration factors were determined for the signals of labeled substrate and all products. Initial glucose concentrations were determined in the cellular samples by extrapolation of combined $C_{1\alpha}$ and $C_{1\beta}$ glucose signals to zero time.

^{31}P NMR Spectroscopy

^{31}P NMR spectra were obtained in the Fourier-transform mode at 202.46 MHz on a Bruker AM-500 NMR spectrometer at 20°C.[16] Free induction decays (FID's) were accumulated in consecutive 1 min. blocks (120 scans, 8K files), using 70° pulses, 0.5 s acquisition time, and a spectral width of 8000 Hz.

For the cellular samples, an initial spectrum was taken; then 75 μL of a 40 wt % glucose solution was added and a sequence of spectra were collected during subsequent 1 min. intervals. Phosphate buffer was added at the end of each experiment for calibration purposes. Endogenous GPC was the chemical shift reference. GPC resonates 0.49 ppm downfield from 85% phosphoric acid, which is assigned to zero ppm. Cell density (CDW/L) was determined for each sample at the end of the experiment.

Calibration experiments for estimation of intracellular concentrations were performed as described previously.[16] Relative concentrations can be determined within $\pm$ 5% for the more intense peaks, $\pm$ 10% for the less intense peaks. For

estimation of intracellular concentrations, 1.67 g wet weight/mL intracellular volume and 0.2 g dry weight/g wet weight were assumed.[31] For estimation of extracellular concentrations, the density of wet yeast was assumed to be 1.0 g wet weight/mL total yeast volume. Intracellular volume was the basis for vacuolar concentrations. Vacuolar concentrations are expressed in units of mol/total intracellular volume, since the intracellular volume fraction comprised of vacuoles is not precisely known. For rough estimates of actual concentrations in the vacuole (mol/volume vacuole), the yeast vacuolar volume is approximately 25% of the protoplast volume.[32]

Data Processing

The FID files taken by the Bruker Aspect-3000 computer were transferred to a VAX(11/780) computer for analysis, using the LAB ONE (TM) NMR1 Spectroscopic Data Analysis Software System.[33] All subsequent processing was performed by the software system on the VAX computer. The FID's were exponentially multiplied by a line broadening of 15 Hz (^{31}P) or 3 Hz (^{13}C), Fourier transformed, phased, and baseline flattened (4^{th} degree polynomial).

pH Determination

As described previously, the cytoplasmic pH was determined by the chemical shift position of P_i^{cyt} using a separately determined *in vitro* relationship between pH and P_i chemical shift at 120 mM ionic strength.[9,34] Absolute values for the cytoplasmic pH can be determined within ± 0.1 pH units.

For estimates of vacuolar pH, the P_i^{vac} resonance was the indicator. The *in vitro* relationship of pH and P_i chemical shift was determined with a solution containing 20 mM Mg^{2+}.[16] Assignments of the cytoplasmic and vacuolar resonances were confirmed by a method described previously.[35]

The P_i^{ex} resonance was the indicator for estimating the extracellular pH. The *in vitro* relationship of pH and P_i chemical shift was determined as described

previously,[16] except that the solution was the same resuspension buffer as used in the *in vivo* experiments. The range of pH values that could be determined from this *in vitro* relationship of pH and P_i is between 4.5 and 8.5 pH units. The accuracy of pH determination around the pKa is ± 0.1 pH units and around the endpoints ± 0.2 pH units.

Estimation of Sugar Phosphate Concentrations

Estimates of the concentrations of the sugar phosphates were determined by a systematic procedure based upon ^{31}P NMR measurements.[16] Two 1-minute FID's were summed and processed in order to provide a better signal-to-noise ratio. The sugar phosphate region of the ^{31}P NMR spectrum was first decomposed by computer analysis (NMR1 software), and the decomposition consistency and identification of individual sugar phosphate resonances were established based on *in vitro* chemical shift calibrations.[16]

IN VITRO ACTIVITIES AND BATCH FERMENTATION BEHAVIOR

The *in vitro* enzyme activities of glucose and fructose phosphorylation for the three recombinant strains (harvested in exponential growth) are compared in Table 1. Differences in the values from Bisson and Fraenkel[36] are due to the relative time at which the cells were harvested for growth, the different prior growth conditions, and difference in the length of time for cell disruption by the glass beads in the extract procedure. (A difference in length of time of bead disruption from 5 to 10 min will decrease the activities by an order of magnitude, for example.) The enzyme assays were repeated for this study in order to ensure that the strains had not mutated in storage.

Strain DFY437:pHXK2 has a glucose–phosphorylation activity from 3–10 times more than that of DFY437:pHXK1 and 5 times more than that of DFY437: pGLK. The recombinant strains with hexokinase PI and glucokinase have roughly

the same glucose–phosphorylation activity. For constitutive expression of the individual kinases in strains carrying single enzymes of glucose phosphorylation, the order of *in vitro* glucose–phosphorylation activity from highest to lowest was *HXK1, HXK2*, then *GLK*.[11]

From a metabolic engineering viewpoint, the strain with increased glucose–phosphorylation activity hopefully would give the highest ethanol yield. Table 2 indicates how the differences in *in vitro* activities between the recombinant strains are manifested under growth in complex medium in shake flasks at 30°C. DFY437:pHXK2, which had the highest glucose–phosphorylation activity, has the slowest growth rate and the lowest biomass yield. DFY437:pGLK has an intermediate growth rate but highest biomass yield. These two strains have the same ethanol yield. DFY437:pHXK1 has the fastest growth rate and the highest ethanol yield (15% greater), and provides an intermediate biomass yield. The strain with the highest glucose–phosphorylation activity *in vitro* did not translate to the highest ethanol yield under growth conditions.

The presence of multicopy plasmids may have some effect on the observed differences in growth behavior. In haploid mutant strains, the order of growth rate from highest to lowest were the *GLK* strain, the *HXK2* strain, then the *HXK1* strain.[11] The increased level of gene expression may have deleterious effects on growth rates as shown in studies of plasmid–host interactions in *S. cerevisiae*.[37]

The strains may not be using the same percentage of kinase activity *in vivo* as compared with *in vitro*. Consequently, the amount of carbon processed may cause differences in the growth behavior. The behavior of these strains under nongrowth conditions will be studied by NMR spectroscopy as described in the following sections. The NMR measurements will provide a type of "assay" of the cells not coupled will growth.

NMR SPECTRA FOR *S. cerevisiae*

A 125.76 MHz ^{13}C NMR spectrum of *S. cerevisiae* DFY437:pHXK2 after feeding of [1–^{13}C] labelled glucose is shown in Figure 2. Inverse–gated ^{1}H decoupling was applied in order to simplify the spectrum. The peaks are assigned from previous work in the literature.[15,38] The signal for glycogen will appear at approximately 103 ppm; in this spectrum, glycogen is not detected above noise levels. The resonances for β and α anomers of glucose appear at 96.7 and 92.9 ppm, respectively. The resonance at 93.9 ppm is from trehalose. The resonances for the fermentation products glycerol, acetate, and ethanol are at 63.3, 24.4, and 17.6 ppm, respectively. Resonances for sugar phosphates such as glucose 6–phosphate, fructose 1,6–diphosphate, and fructose 6–phosphate would appear in the region between 67 and 63 ppm.[15,39] High levels of glycerol obscure the resonance for the C–1 carbon of fructose 1,6–diphosphate and fructose 6–phosphate and the C–6 carbons of all three sugar phosphates. Shorter time periods between scans would increase the signal–to–noise ratio of the spectrum. However, quantification of intracellular metabolites by ^{13}C is difficult, since a large relaxation delay is required between scans in order to unsaturate the resonances.

The concentrations of glucose and extracellular products that contribute major peaks in Figure 2 can be followed with time easily with ^{13}C NMR. Figure 3 shows the levels with time for *S. cerevisiae* DFY437:pHXK2. Concentrations given are based upon intracellular volume so that rates per cell volume can be observed from the slope. [1–^{13}C] labelled glucose is added at time zero. Within five minutes, the quasi–steady–state period is attained in which the fluxes of glucose, ethanol, and glycerol are constant. The levels of trehalose accumulate rapidly in the transition to quasi–steady state and then remain constant. The fermentation ends at the time glucose is exhausted.

The levels of the metabolites as determined from ^{31}P NMR spectra can be obtained in a similar manner. 202.46 MHz ^{31}P NMR spectra of *S. cerevisiae*

during the quasi-steady-state period after glucose feeding are shown in Figure 4. The spectra in Figure 4(A), 4(B), and 4(C) are for strains, DFY437:pHXK1, DFY437:pHXK2, and DFY437:pGLK, respectively.

The assignments of the resonances in Figure 4 are based upon the literature.[35,40–43] The resonances from 5 ppm to 3 ppm are in the sugar phosphate (SP) region. Cytoplasmic inorganic phosphate (P_i^{cyt}), vacuolar inorganic phosphate (P_i^{vac}), and extracellular inorganic phosphate (P_i^{ex}) are the next clearly observable resonances; pH values in these compartments can be determined from the P_i chemical shift resonance. Phosphomannan (PM) in the cell wall is assigned to the resonance at -1.34 ppm. The nucleotide resonances at -5.39 ppm, -10.05 ppm, and -18.90 ppm were assigned to $ATP_\gamma + ADP_\beta$, $ATP_\alpha + ADP_\alpha$, and ATP_β, respectively. The ADP resonances are included for completeness, even though they probably contribute less than 10% of the overall signal.[41] Also, the areas of the ATP_β resonance and the other two nucleotide resonances do not differ within experimental error ($\pm$10%). PP_1 is the sum of several phosphate resonances from pyrophosphate and the terminal phosphates of polyphosphate; the chemical shift of this resonance is pH dependent and also gives an estimate of vacuolar pH. PP_3 are penultimate phosphates from polyphosphate chains, and PP_4 is the inner phosphate from longer polyphosphate. NAD(H) includes both NAD^+ and NADH.[42] Finally, UDPG and similar compounds resonate in the region of -12 ppm.

The spectra in Figure 4 are scaled so that the relative levels from a given resonance can be compared among the strains. The downfield shift in chemical shifts of the sugar phosphates and P_i^{cyt} resonances indicates that cytoplasmic pH is highest in DFY437:pHXK2. DFY437:pGLK has higher phosphomannan, NAD(H), and polyphosphate levels than the other two strains. During the quasi–steady state, levels of the sugar phosphates, intracellular inorganic phosphate, and ATP are constant or fairly constant.[40,41] Cytoplasmic and vacuolar pH values are slowly decreasing in this time period.[35,40] These differences are quantified and

discussed below.

ANALYSIS OF NMR MEASUREMENTS

^{13}C NMR Measurements of Rates and Yields

The rates of glucose consumption, rates of product formation, and final yields from the ^{13}C NMR measurements are given in Table 3. Strain DFY437:pHXK1 has the highest rate of glucose consumption, ethanol production, and ethanol yield and the lowest rates of glycerol production and glycerol yield. Strains DFY437:pHXK2 and DFY437:pGLK have the same ethanol yield and ratio of glucose consumption to ethanol production; however, the rates of ethanol production and glucose consumption are higher in DFY437:pHXK2. DFY437:pHXK2 accumulates more glycerol than the other two strains.

The trends in ethanol yields observed among the strains under growth conditions are the same under the nongrowth conditions in the NMR experiments. Relative differences in ethanol yield between DFY437:pHXK1 and the other two strains were of 15% and 13% under growth and NMR conditions, respectively. The NMR buffer did not contain a nitrogen source or amino acids; consequently, protein synthesis is negligible on the time scale of the NMR experiments. Growth apparently does not alter the regulation and kinetics of the catabolic pathways functioning in the NMR experiment, at least in a relative sense.

The glucose consumption rate and ethanol production rate for DFY437:pHXK1 are 100% greater than the values observed for a healthy diploid strain of *S. cerevisiae* 18790 (all kinases present, growth rate of 0.51 hr^{-1} on YPD) observed under similar NMR conditions.[5] An enhancement of ethanol production rate has also been observed for immobilized versus suspended *S. cerevisiae* 18790.[5,6] The glucose uptake or hexokinase step was suggested to be altered by immobilized cells.[5] Thus, genetic and environmental manipulations have both increased ETOH production.

DFY437:pHXK1 has twice the rate of glucose consumption as DFY437:pGLK, even though the same order of *in vitro* glucose–phosphorylation activity was observed in these strains. In a previous study, a *GLK* strain had a higher ratio of *in vivo* glucose consumption rate to *in vitro* enzyme activity than a *HXK1* strain.[11] The parameter β is defined as the glucose consumption rate divided by the *in vitro* glucose–phosphorylation activity. β is an indication of the utilized enzyme capacity for glucose phosphorylation. In Table 4, the values of β are given for the three recombinant strains in this study. In comparison to the other two strains, DFY437:pHXK2 is underutilizing its potential enzyme activity by an order of magnitude.

Maximal glucose–phosphorylation activity *in vitro* did not correspond to the highest glucose consumption rate and ethanol production rate *in vivo*. The *in vitro* measurements of enzyme activity used in the calculations in Table 4 were performed on cells harvested at the same cell density and prior growth conditions as in the NMR experiments. *In vivo* conditions may be different with respect to factors that significantly affect the rates of reactions catalyzed by the glycolytic enzymes. The results from ^{31}P NMR experiments can indicate differences in the intracellular environment and are discussed next.

Sugar Phosphate Levels

Intracellular concentrations and pH values as determined by ^{31}P and ^{13}C NMR spectroscopy are given in Tables 5, 6, and 7. The quasi–steady–state values determined by ^{31}P NMR are averages of data taken from 6 spectra (6 minutes) in the middle of the time period in which the total sugar phosphate levels are constant. The quasi–steady–state period has been shown in previous studies.[40,41] These times correspond to the time period in which constant fluxes were observed from ^{13}C NMR measurements as shown in Figure 3.

The quasi–steady–state concentrations of the individual sugar phosphates are

given in Table 5. These concentrations were obtained from an analysis method of the SP region in the ^{31}P NMR spectrum.[16] A change in the relative distributions of the sugar phosphates would indicate differences in the rate limiting step in glycolysis, as in previous studies.[7,40] Inspection of the sugar phosphate levels do not reveal many differences between the strains. The total sugar phosphate levels (two resonances are detected for fructose 1,6 diphosphate) are the same for strains DFY437:pHXK1 and DFY437:pHXK2; DFY437:pGLK has 10 mM more sugar phosphate. The individual sugar phosphate levels are similar for the hexokinase strains. Glucose–6–phosphate, fructose–6–phosphate, fructose 1,6–diphosphate, and 3–phosphoglycerate levels for DFY437:pGLK are higher than the corresponding levels of the other two strains by 1–3 mM. Accumulation of sugar phosphates before a block in glycolysis has been observed in many glycolysis mutants of *S. cerevisiae*.[42,44] However, a slower glucose consumption rate does not correspond to higher total sugar phosphate levels for all the strains in this study.

The 1 mM difference in the 3–phosphoglycerate level is a tenfold increase for this metabolite in DFY437:pGLK over the other strains. In this mM level, 3PGA may be an activator of glucokinase.[11] An identical relationship for the three kinase enzymes between glucose 6– phosphate level and inhibition of the kinase enzymes is not evident, since glucose–6–phosphate levels in Table 5 are not correlated with the glucose consumption rates in Table 3.

"NMR Invisible" ADP

The quasi–steady–state nucleotide levels and pH values are given in Table 6. The nucleotide levels as determined by ^{31}P NMR are discussed, since these compounds affect the regulation of many glycolytic enzymes. The sum of ATP + ADP levels are indicated in Table 6; however, this sum is mostly ATP, since a difference was not noted in the ATP_β resonance area and the areas of the two ATP + ADP resonances. The low level of ADP signals in cell extracts of yeast

has been noted.[41] From the adenylate kinase reaction

$$AMP + ATP \rightleftharpoons 2ADP \quad (1)$$

that is assumed to be in equilibrium with an equilibrium constant equal to unity,[43] from the ATP + ADP levels given by the values in Table 6, and from the assumption that the sum of ATP + ADP + AMP is equal to 5 or 6 mM, the range of values of ADP is 0.7 to 2 mM, and the range of values of AMP is 0.1 to 2 mM. Thus, by these calculations, ADP and AMP should be detected in the ^{31}P NMR spectra. However, NMR detects only phosphorus signals from mobile components. This suggests that ADP must be bound tightly to macromolecules in the cell. ADP may be sequestered to mitochondria in such a way that ADP does not generate a detectable signal. Interaction of ADP with catalytic sites of enzymes is not significant enough to make ADP "NMR invisible."[45] The same holds for ATP and most likely for AMP.[44] "Invisible" ADP is a common occurrence for ^{31}P NMR of mammalian tissues and cells.[45] The signal for AMP resonates in the sugar phosphate region and thus, in low levels, would be obscured by the sugar phosphate resonances.

The ^{31}P NMR spectra suggest that levels of mobile ADP and AMP are lower than indicated by assuming equilibrium for the adenylate kinase reaction. However, even if 10% of the ATP + ADP values in Table 6 is ADP, this would make ADP as a potential inhibitor of all of the kinases at the cytoplasmic pH values for the strains (6.5 to 6.8).[9,22] As discussed previously, hexokinase PII could have up to a 70% inhibition in its glucose–phosphorylation activity.[9]

Magnesium Binding to ATP

Since the positions of the ^{31}P resonances of ATP depend on its state of complexation with Mg^{2+}, the ^{31}P NMR spectrum allows a direct determination of the fraction of total ATP that exists as the Mg^{2+} complex.[18,46] ATP and Mg^{2+}

must be in fast exchange compared to the NMR time scale. The fraction of total ATP not complexed to magnesium is given by the following equation:

$$\frac{[ATP]_f}{[ATP]_T} = \frac{\delta_{\gamma\beta}^{cell} - \delta_{\gamma\beta}^{MgATP}}{\delta_{\gamma\beta}^{ATP} - \delta_{\gamma\beta}^{MgATP}}, \tag{2}$$

where $[ATP]_f$ is the amount of magnesium–free ATP, $[ATP]_T$ is the total amount of ATP, $\delta_{\gamma\beta}^{cell}$ is the chemical shift difference between the γ and β resonances for ATP in the spectrum of the cell, and $\delta_{\gamma\beta}^{ATP}$ and $\delta_{\gamma\beta}^{MgATP}$ are the corresponding chemical shift differences for ATP and MgATP controls under simulated intracellular ionic conditions and pH.[46] Chemical shift differences are used in order to eliminate any errors that might result from use of a chemical shift reference.

The ATP_β and ATP_γ chemical shifts as a function of cytoplasmic pH are given in Figure 5 for the three different *S. cerevisiae* strains studied. The dashed–dot lines are from ^{31}P NMR measurements of a 5 mM ATP (no Mg^{2+}) solution with 120 mM ionic strength;[34] the solid line is from ^{31}P NMR data for a solution of 5 mM ATP, 10 mM $MgCl_2$, and 0.18 M KCl.[34] These are solutions of free ATP and ATP 99% complexed with Mg^{2+}, respectively. The dissociation constant for MgATP is 50 ± 10 μM in various solutions of ATP and Mg^{+2} at 25°C and pH 7.2.[18] The ATP_β and ATP_γ chemical shifts from the *in vivo* spectra of all of the strains overlap each other completely, indicating that the fraction of $[ATP]_f$ to $[ATP]_T$ is similar in all of the strains. Furthermore, the difference $\delta_{\gamma\beta}^{cell} - \delta_{\gamma\beta}^{MgATP}$ is zero over all of the pH values in the experiment. The greatest chemical shift measured for this difference was 0.05 ppm, which is within the error of chemical shift determination. Matching the cellular $[ATP]_f$ level to the *in vitro* $[ATP]_f$ level, a value of 0.05 mM $[ATP]_f$ or less for 5 mM $[ATP]_T$ is obtained.

The previous workers, who determined that free ATP at a concentration of 0.10 mM inhibited the glucose–phosphorylation activity for hexokinase PII by 70%, used a dissociation constant of 100 μM to estimate the free ATP concentration.[28] The corresponding free ATP concentration is 0.10 mM for 5 mM total ATP in

the *in vitro* solution of complexed ATP used in Figure 5. For a concentration of total ATP of 4.2 mM as given in Table 6 for DFY437:pHXK2, the concentrations of free ATP are 0.042 mM and 0.084 mM for dissociation constants of 50 μM and 100μM, respectively. As related to a previous study,[28] these levels would inhibit hexokinase PII activity by at least 50%. Thus, magnesium-free ATP might have an inhibitory effect on the hexokinase PII enzyme activity *in vivo* and could explain in part the low value of β observed for strain DFY437:pHXK2 relative to the other strains.

pH Values

The cytoplasmic and vacuolar pH values differed among the strains during the quasi–steady state. The difference between strains DFY437:pHXK2 and the strains DFY437:pHXK1 and DFY437:pGLK is beyond the experimental error in pH determination. The difference in DFY437:pHXK1 compared to DFY437:pGLK may not be significant. These strains all had cytoplasmic pH values within 0.08 pH units of each other at time zero, before glucose addition (data not shown). The slope of a plot of *in vitro* glucose–phosphorylation activity versus pH for the kinases is positive and steep for the range of cytoplasmic pH values observed in this study; maximal activities occur for pH values between 7.5 and 9.5.[11] The differences in cytoplasmic pH observed between the strains is not related to the changes between DFY437:pHXK1 and DFY437:pGLK in the values of β in Table 4. At pH 6.4, glucokinase was 40% as active and the hexokinases were 10% as active compared to maximal *in vitro* glucose–phosphorylation activity.[11] Since the strain with glucokinase operates at a similar cytoplasmic pH as the strain with hexokinase PI and since the strain with glucokinase as a value of β 50% that for the strain with hexokinase PI, pH is removed as a possible explanation for the difference in β values observed between these two strains. The pH differences observed between DFY437:pHXK2 and DFY437:pHXK1 would suggest that the value of β should be higher for DFY437:pHXK2 compared to DFY437:pHXK1,

based upon the previous discussion. However, the value of β is much lower for DFY437:pHXK2, thus eliminating pH differences as an explanation for the value of β for this strain. All the strains operate at an intracellular pH at which glucose phosphorylation activity is not maximized with respect to pH.

Phosphate and Storage Elements

The levels of phosphate in the various compartments, carbon storage polymers, phosphomannan, and the phosphate–polymer polyphosphate are given in Table 7. The strains had the same intracellular P_i levels. In addition, intracellular P_i levels were not depleted at any time during the NMR experiments. Depletion of intracellular P_i has been observed previously for a mutant strain of *S. cerevisiae* in NMR experiments and correlated with the slower rate of glycolysis in this strain.[40]

The extracellular P_i levels remained constant throughout the experiments at the values given in Table 7. This is in contrast to other *S. cerevisiae* strains under similar conditions that used extracellular P_i as a reserve during glycolysis.[40,41] Polyphosphate levels remained constant throughout the experiments except for an initial consumption of 10 mM polyphosphate by the hexokinase strains and 30 mM polyphosphate by the glucokinase strain. Phosphomannan levels are higher for DFY437:pGLK than for the other two strains, which indicates a difference in cell wall morphology.

Strain DFY437:pHXK2 shunted some of its carbon to trehalose and also distributed more of its carbon to glycerol, as shown in Tables 3 and 7. A cofactor in synthesis of trehalose, UDPG, is present at approximately the same intracellular concentrations for all strains, as shown in Table 5. "Excess" ATP levels are proposed to shut off the carbon flow to ETOH and instead shuttle carbon to glycerol through the aldolase triangle.[44] Since DFY437:pHXK2 does not have the highest ATP levels among the strains, this explanation is not clear, unless the free

ATP inhibition on hexokinase PII is communicated as "excess ATP" and does change the carbon flow.

SUMMARY

Differences in growth behavior, glucose consumption, ethanol production, and glycerol production were observed between three recombinant yeast strains, which had been altered in glucose phosphorylation activity. The yield of ethanol was greatest for the strain with hexokinase PI. This strain had the fastest growth rate, the fastest glucose consumption rate and *in vivo* used more of its glucose phosphorylation activity. The hexokinase PII strain has 3–10 times more *in vitro* enzyme activity than the hexokinase PI strain but used an order of magnitude less of its potential activity. The strain with glucokinase used half of its potential activity compared to the strain with hexokinase PI.

The differences observed in cytoplasmic pH was ruled out as an explanation for the activity differences. Levels of ATP and magnesium–free ATP may explain the greatly reduced *in vivo* glucose–phosphorylating activity in the hexokinase PII strain. This strain also had greater levels of trehalose and glycerol. The differences of pH and ATP observed among the strains may not have been predicted *a priori.*

Fermentations under growth and nongrowth (NMR) conditions gave the same trends in ethanol yields for the three strains. NMR spectroscopy provided comprehensive data for assessment of the differences observed among the three strains. The combined use of noninvasive techniques such as NMR spectroscopy with the more traditional *in vitro* measurements will assist in the evaluation of manipulations performed by metabolic engineers. *In vitro* enzyme activities for glucose–phosphorylation did not correlate with *in vivo* glucose consumption rates and hence, ethanol production rates. This result is important for metabolic engineering principles and contrasts the rule–of–thumb of increased enzyme activity (by *in vitro* measurement) for increased production. Understanding the regulation of

manipulated steps is imperative.

Acknowledgement:

This research was supported by the Energy Conversion and Utilization Technology (ECUT) program of the U.S. Department of Energy. The nuclear magnetic resonance experiments reported here were made possible by the facilities of the Southern California Regional Nuclear Magnetic Center (NSF Grant No. CHE-84-40137) and software for NMR spectral analysis was provided by the NIH Resource Laboratory at Syracuse University (Grant No. RR-01317).

REFERENCES

1. J.E. Bailey, D.D. Axe, J.L. Galazzo, K.F. Reardon, A. Seressiotis and J.V. Shanks, *Biochem. Engr. V* (Ann. N.Y. Acad. Sci.), **506**, 1 (1987).

2. B.D. Ensley, B.J. Ratzkin, T.D. Osslund, M.J. Simon, L.P. Wackett, and D.T. Gibson, *Science*, **222**, 167 (1983).

3. S. Anderson, C.B. Marks, R. Lazarus, J. Miller, K. Stafford, J. Seymour, D. Light, W. Rastetter, and D.E. Stell, *Science*, **230**, 144 (1985).

4. J.D. Windass, M.J. Worsey, E.M. Pioli, D. Pioli, P.T.Barth, K.T. Atherton, E.C. Dart, D. Bryom, K. Powell, and P.J. Senior, *Nature*, **287**, 396 (1980).

5. J.L. Galazzo and J.E. Bailey, "*In Vivo* Nuclear Magnetic Resonance Analysis of Immobilization Effects on Glucose Metabolism of Yeast *Saccharomyces cerevisiae*," in preparation.

6. P.M. Doran and J.E. Bailey, *Biotechnol. Bioeng.*, **28**, 73 (1986).

7. J.L. Galazzo and J.E. Bailey, "Fermentation Pathway Kinetics and Metabolic Flux Control in Suspended and Immobilized *Saccharomyces cerevisiae*," in preparation.

8. D. Reibstein, J.A. den Hollander, S.J. Pilkis, and R.G. Shulman, *Biochemistry*, **25**, 219 (1986).

9. S.P. Colowick, "The Hexokinases" in *The Enzymes*, (P.D. Boyer, ed.), vol. 9, Part B, 3rd ed., p. 1-48, Academic Press, New York, (1973).

10. P.K. Maitra, *J. Biol. Chem.*, **245**, 2423 (1970).

11. Z. Lobo and P.K. Maitra, *Arch. Bioc. Biop.*, **182**, 639 (1977).

12. R.B. Walsh, G. Kawasaki, and D.G. Fraenkel, *J. Bacteriol.*, **154**, 1002 (1983).

13. E. Kopetzki, and K.D. Entian, *Eur. J. Biochem.*, **146**, 657 (1985).

14. Y. Fukuda, S. Yamaguchi, H. Hashimoto, M. Shimosaka, and A. Kimura, *Agric. Biol. Chem.*, **48**, 2877 (1984).

15. J.A. Den Hollander, T.R. Brown, K. Ugurbil, and R.G. Shulman, *Proc. Natl. Acad. Sci.*, **76**, 6096 (1979).

16. J.V. Shanks and J.E. Bailey, *Biotechnol. Bioeng.*, in press.

17. J.K.M. Roberts and O. Jardetzky, *Biochem. Biophys. Acta*, **639**, 53 (1981).

18. R.K. Gupta, P. Gupta, and R.D. Moore, *Ann. Rev. Biophys. Bioeng.*, **13**, 221 (1984).

19. J. -M. Gancedo, D. Clifton, and D.G. Fraenkel, *J. Biol. Chem.*, **252**, 4443 (1977).

20. K. -U. Frohlich, K.D. Entian, and D. Mecke, *Gene*, **36**, 105 (1985).

21. E. Kopetzki, K.D. Entian, and D. Mecke, *Gene*, **39**, 95 (1985).

22. P.K. Maitra and Z. Lobo, *Mol. Cell. Biochem.*, **18**, 21 (1977).

23. K.D. Entian, and K. -U. Frohlich, *J. Bacteriol.*, **158**, 29 (1984).

24. L.F. Bisson and D.G. Fraenkel, *Proc. Natl. Acad. Sci.*, **80**, 1730 (1983).

25. L.F. Bisson and D.G. Fraenkel, *J. Bacteriol.*, **159**, 1013 (1984).

26. T.A. Steitz, W.F. Anderson, R.J. Fletteick, and C.M. Anderson, *J. Biol. Chem.*, **252**, 4492 (1977).

27. R.C. McDonald, T.A. Steitz, and D.M. Engelman, *Biochemistry*, **18**, 338 (1979).

28. F. Moreno, T. Fernandez, R. Fernandez, and P. Herrero, *Eur. J. Biochem.*, **161**, 565 (1986).

29. L.F. Bisson and D.G. Fraenkel, *J. Bacteriol.*, **154**, 1002 (1983).

30. G. Kawasaki and D.G. Fraenkel, *Biochem. Biophys. Res. Comm.*, **108**, 1107 (1982).

31. J.M. Gancedo and C. Gancedo, *Biochimie*, **55**, 205 (1973).

32. L.A. Okorokov, L.P. Lichko, and I.S. Kubev, *J. Bacteriol.*, **144**, 661 (1980).

33. LABONE(TM) NMR1 Spectroscopic Data Analysis Software System, Revsion 2.70, (Syracuse University, New Methods Research Inc., 1985).

34. D.G. Gadian, G.K. Radda, R.E. Richards, and P.J. Seeley, "^{31}P NMR in Living Tissue: The Road from a Promising to an Important Tool in Biology," *Biological Applications of Magnetic Resonances*, (Academic Press, New York, 1979).

35. J.V. Shanks and J.E. Bailey, "Elucidation of the Cytoplasmic and Vacuolar Components in the Inorganic Phosphate Region in the ^{31}P NMR Spectrum of Yeast," submitted.

36. L.F. Bisson and D.G. Fraenkel, *J. Bacteriol.*, **155**, 995 (1983).

37. N.A. DaSilva, Ph.D. Dissertation, California Institute of Technology (1988).

38. J.A. den Hollander and R.G. Shulman, *Tetrahedron*, **39**, 3529 (1983).

39. K. Ugurbil, T.R. Brown, J.A. den Hollander, P. Glynn, and R.G. Shulman, *Proc. Natl. Acad. Sci.*, **75**, 3742 (1978).

40. J.V. Shanks and J.E. Bailey, "Comparison of Wild–Type and *REG1* Mutant *Saccharomyces cerevisiae* Metabolic Levels During Glucose and Galactose Metabolism Using ^{31}P NMR," submitted.

41. J.A. den Hollander, K. Ugurbil, T.R. Brown, and R.G. Shulman, *Biochemistry*, **20**, 5871 (1981).

42. G. Navon, R.G. Shulman, T. Yamane, T.R. Eccleshall, K. -B. Lam, J.J. Baronofsky, and J. Marmur, *Biochemistry*, **18**, 21 (1979).

43. R.A. Gage, W. Van Wijngaarden, A.P.R. Theuvenet, G.W.F.H. Borst–Pauwels, and C.A.G. Haasnoot, *Biochim. Biophys. Acta*, **804**, 341 (1984).

44. M. Ciriacy and I. Breitenbach, *J. Bacteriol.*, **139**, 152 (1979).

45. D.G. Gadian, "Nuclear Magnetic Resonance and Its Application to Living Systems," (Oxford University Press, Oxford, 1982).

46. R.K. Gupta and R.D. Moore, *J. Biol. Chem.*, **255**, 3987 (1980).

TABLE 1: *In vitro* Activities of Glucose and Fructose Phosphorylation

	DFY437: pHXK1	DFY437: pHXK2	DFY437: pGLK
GLUCOSE PHOSPHORYLATION (U/mg of protein)	0.5 (2.5)	5.1 (7.2)	0.5 (1.1)
FRUCTOSE PHOSPHORYLATION (U/mg of protein)	2.2 (8.9)	6.3 (7.2)	0.1 (0.2)

values in ( ) from L.F. Bisson and D.G. Fraenkel, *J. Bact.*, **155**, 995 (1983).

TABLE 2: Batch Fermentations on YPD Medium at 30°C

	DFY437: pHXK1	DFY437: pHXK2	DFY437: pGLK
SPECIFIC GROWTH RATE (hr^{-1})	0.41	0.29	0.33
ETHANOL YIELD FROM GLUCOSE (mol/mol)	1.47	1.33	1.30
BIOMASS YIELD FROM GLUCOSE (g cell dry wt./mol)	32	22	39

TABLE 3: Substrate Consumption, Rates of Producion, and Final Product Yields

	DFY437: pHXK1	DFY437: pHXK2	DFY437: pGLK
GLUCOSE CONSUMP. [V_G] (mM/min)	33.1	21.6	17.0
ETHANOL PROD. [V_E] (mM/min)	49.4	26.5	20.5
GLYCEROL PROD. [V_{GLY}] (mM/min)	1.2	4.8	1.5
ACETATE PROD. (mM/min)	+	n.d	n.d.
V_E/V_G	1.5	1.2	1.2
V_{GLY}/V_E	0.04	0.2	0.09
FINAL ETHANOL YIELD (mol ethanol/mol glucose)	1.80	1.61	1.61
FINAL GLYCEROL YIELD (mol glycerol/mol glucose)	0.07	0.2	0.1

+ - detected but too low to quantify
n.d. - not detected

TABLE 4: Fraction used *In Vivo* of Potential Enzyme Activity

	DFY437: pHXK1	DFY437: pHXK2	DFY437: pGLK
UTILIZATION OF ENZYME CAPACITY, β	0.4	0.03	0.2

$\beta = V_G/V_{max}$ where V_G is defined as in Table 3 and
V_{max} = maximal activity of enzyme for glucose phosphorylation.
U/mg of enzyme activity in Table 1 were converted to mM/min.
1.67 g wet weight = 1 mL intracellular volume = 0.167 g protein = 0.334 g dry weight[27]
Unit=μmol/min.

TABLE 5: Quasi–Steady–State Sugar Phosphate Concentrations

	DFY437: pHXK1	DFY437: pHXK2	DFY437: pGLK
GLUCOSE–6–PHOSPHATE (mM)	4	3	6
FRUCTOSE–6–PHOSPHATE (mM)	2	3	4
FRUCTOSE–1,6–DIPHOSPHATE (mM)	11	10	13
3–PHOSPHOGLYCERATE (mM)	0.1	0.1	1

TABLE 6: Quasi–Steady–State Nucleotide Concentrations and pH

	DFY437: pHXK1	DFY437: pHXK2	DFY437: pGLK
ATP+ADP (mM)	3.7	4.2	4.9
NAD(H) (mM)	3.7	4.8	6.1
UDPG (mM)	1.1	1.3	1.2
pH^{cyt}	6.6	6.8	6.5
pH^{vac}	5.9	6.0	5.8
pH^{ex}	≤ 4.5	≤ 4.5	≤ 4.5

TABLE 7: Quasi–Steady–State Phosphate and Storage Metabolite Concentrations

	DFY437: pHXK1	DFY437: pHXK2	DFY437: pGLK
P_i^{cyt} (mM)	18	16	18
P_i^{vac} (mM)	13	12	13
P_i^{ex} (mM)	16	22	11
TREHALOSE	≈1/10 +	+	≈1/10 +
PHOSPHOMANNAN (mM phosphate)	11	12	21
POLYPHOSPHATE (mM phosphate)	160	150	140

+ - estimated at 5 mM, see Figure 3 and text.

FIGURE CAPTIONS

Figure 1: The yeast cell as viewed by ^{31}P and ^{13}C NMR spectroscopy. The boldface components can be measured *in vivo* by NMR. The boxed components can be measured by ^{13}C NMR; the others, by ^{31}P. The compounds marked by an asterick can be measured with an analysis method of the sugar phosphate region in the ^{31}P NMR spectrum.[12] Abbreviations: P_i : inorganic phosphate; ATP : adenosine triphosphate; NAD(H) : nicotinamide adenine dinucleotide.

Figure 2: ^{13}C NMR spectrum at 125.76 MHz of *S. cerevisiae* DFY437:pHXK2 at 20°C during glycolysis. [1-^{13}C] labelled glucose was added to a final concentration of 80 mM to 50 % w/v suspensions of cells. Cells had been grown to mid-log phase on YPD, then harvested and resuspended in MES buffer for the NMR experiment. In this spectrum, glycogen and acetate are not detectable above noise levels. Spectrum represents a 1 min. time accumulation and was recorded using 45° pulses, 2.33 repetition time (0.33 sec. acquisition time, 2.0 sec. relaxation delay); inverse-gated CPD decoupling of protons with a power of 3 Watts was applied. Abbreviations: GLYCOGEN-C1: C1 carbon of glycogen; βG-C1: C1 carbon of the beta anomer of glucose; αG-C1: C1 carbon of the alpha anomer of glucose; TRE-C1: C1 carbon of trehalose; GLYCEROL-C1: C1 carbon of glycerol; ACE-C2 : C2 carbon of acetate; ETOH-C2: C2 carbon of ethanol.

Figure 3: Concentrations with time for glucose fermentation of *S. cerevisiae* DFY437: pHXK2 Concentrations were determined from ^{13}C NMR measurements as shown in Figure 2. Labelled glucose was added at 0^+ sec. The quasi-steady-state period runs from approximately 5 to 15 min., or when the rates of glucose consumption, and ethanol and glycerol production are constant. Concentrations are based upon intracellular volume for rate estimations as given in Table 3. 2 mols of ethanol and glycerol per mol of labelled ethanol and glycerol, respectively, was assumed. Trehalose concentration was estimated assuming its resonance was not saturated in the ^{13}C NMR spectrum.

Figure 4: ^{31}P NMR spectra at 202.46 MHz of anaerobic *S.cerevisiae* suspensions at 20°C during 'steady-state' glycolysis. (A) *S. cerevisiae* DFY437:pHXK1. (B) *S. cerevisiae* DFY437:pHXK2. (C) *S. cerevisiae* DFY437:pGLK. Cell samples were prepared as in Figure 2, except that 80 mM unlabelled glucose was added for the NMR experiment. Metabolism was monitored with time by taking a sequence of spectra. Spectra represent 1 min. time accumulations and were recorded using 70° pulses, 0.5 sec. acquisition time. Spectra are scaled so that peak areas can be compared for a given intracellular resonance between spectra. Comparisons within a spectrum cannot be made between any two

resonances except for polyphosphates. Abbreviations: SP : sugar phosphate; P_i^{cyt} : cytoplasmic inorganic phosphate; P_i^{vac} : vacuolar inorganic phosphate; P_i^{ex} : extracellular inorganic phosphate; PM : phosphomannan; ADP : adenosine diphosphate; PP_1 : pyrophosphate and terminal phosphates of polyphosphate; UDPG : uridine diphosphoglucose; PP_3 : penultimate phosphates of polyphosphate; and PP_4 : middle phosphates of polyphosphate; others as in Figure 1.

Figure 5: Chemical shifts of ATP_β and ATP_γ versus pH. Symbols are chemical shift values from *in vivo* ^{31}P NMR spectra of the strains at the various cytoplasmic pH values that are determined in the cell from the P_i^{cyt} resonance. The dashed–dot line is from a 120 mM ionic strength solution of 5 mM ATP. The solid line is from a solution of 5 mM ATP, 10 mM $MgCl_2$, and 0.18 M KCl; 99% of the ATP in this solution is complexed to magnesium. The free ATP to total ATP ratio is a fraction of the chemical shift differences between the β and γ resonances of ATP of the cell and *in vitro* solutions. Symbols: (□) DFY437:pHXK1; (△) DFY437:pHXK2; (○) DFY437:pGLK.

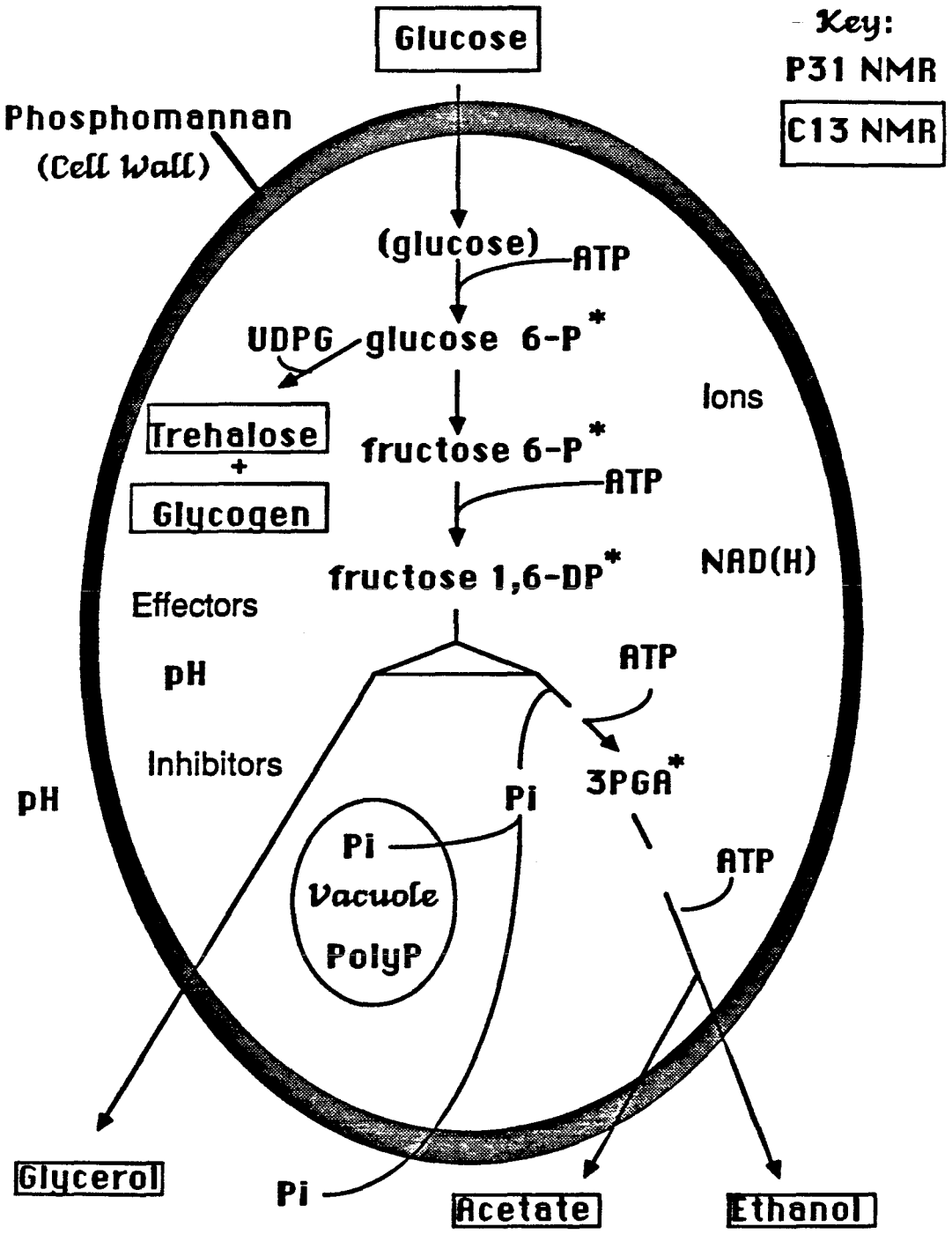
Glucose
Key:
P31 NMR
C13 NMR
Phosphomannan
(Cell Wall)
(glucose)
ATP
UDPG
glucose 6-P*
Ions
Trehalose
+
Glycogen
fructose 6-P*
ATP
fructose 1,6-DP*
NAD(H)
Effectors
pH
ATP
Inhibitors
pH
Pi
3PGA*
Pi
Vacuole
PolyP
ATP
Glycerol
Pi
Acetate
Ethanol

Figure 1

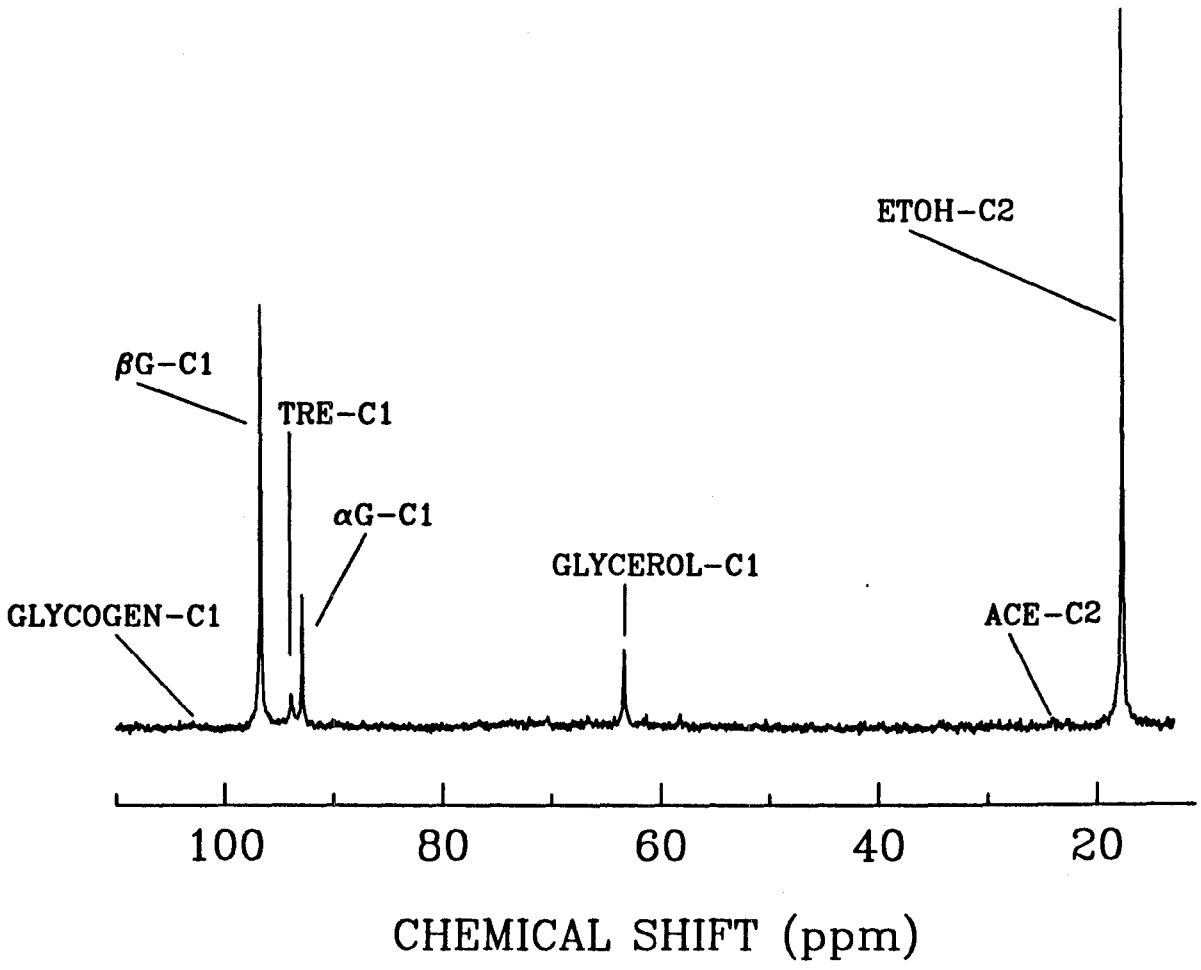
ETOH-C2
βG-C1
TRE-C1
αG-C1
GLYCEROL-C1
GLYCOGEN-C1
ACE-C2
100
80
60
40
20
CHEMICAL SHIFT (ppm)

Figure 2

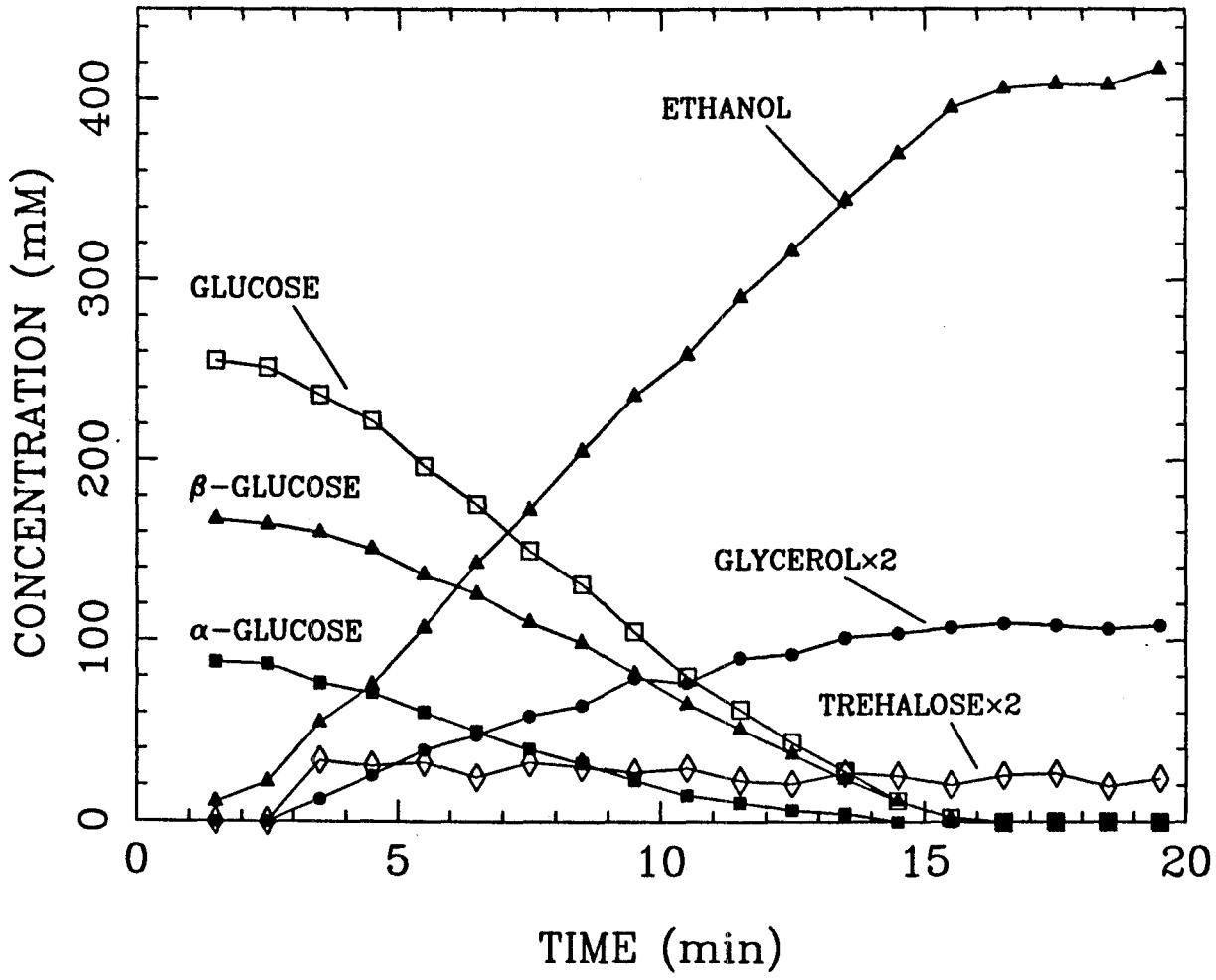
ETHANOL
GLUCOSE
β-GLUCOSE
GLYCEROL×2
α-GLUCOSE
TREHALOSE×2
CONCENTRATION (mM)
0
100
200
300
400
0
5
10
15
20
TIME (min)

Figure 3

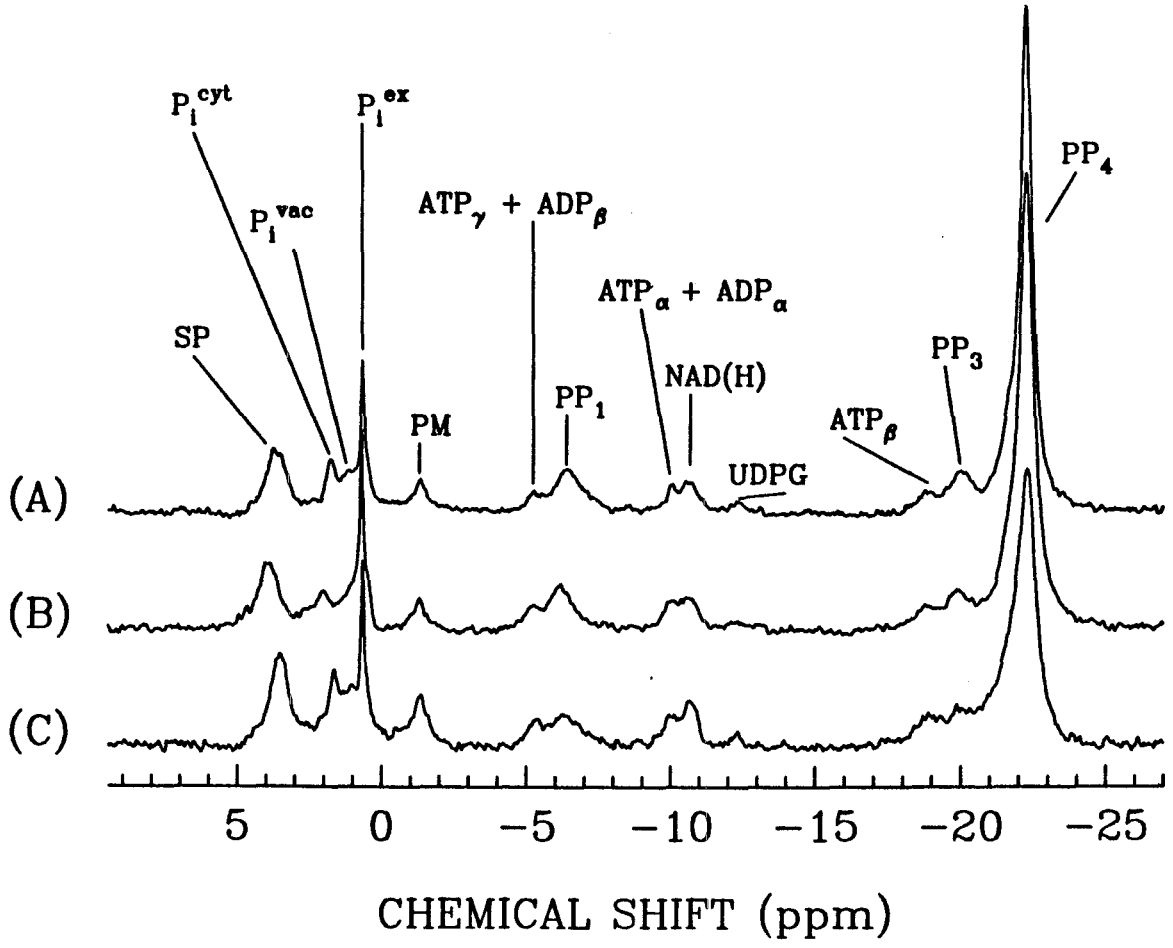
P_i^{cyt}
P_i^{ex}
P_i^{vac}
$ATP_\gamma + ADP_\beta$
$ATP_\alpha + ADP_\alpha$
PP_4
SP
PP_3
NAD(H)
PP_1
PM
ATP_β
UDPG
(A)
(B)
(C)
5
0
−5
−10
−15
−20
−25
CHEMICAL SHIFT (ppm)

Figure 4

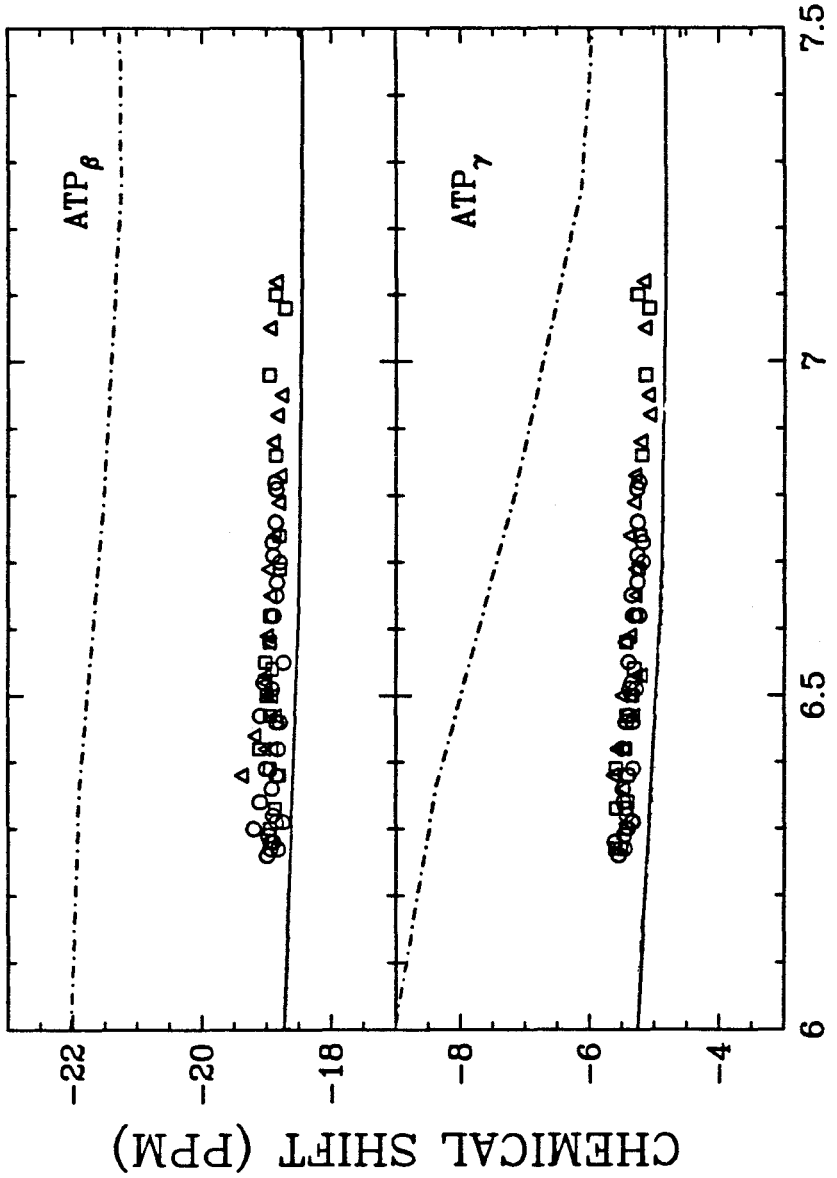

Figure 5

CHAPTER 6

CONCLUSIONS

Data from *in vivo* nuclear magnetic resonance spectroscopy measurements of genetically manipulated *Saccharomyces cerevisiae* have illustrated the usefulness of NMR in metabolic engineering applications. These measurements assessed the consequences of these manipulations by monitoring changes in cellular pH and levels of phosphorylated metabolites as well as substrate and fermentation products for resting cells that had been triggered in metabolism by the addition of a carbon source. Methods developed in this work allowed for more detailed quantitative analysis of the sugar phosphate region and the phosphomonoester region in ^{31}P NMR spectra. The influence of the *reg1* mutation on carbon catabolism appears to happen early in the regulatory circuit of the glycolytic pathway. Alteration of the glucose phosphorylation step was studied with recombinant strains and the consequences on ethanol production, glucose consumption, and the intracellular state was noted. Specific conclusions from the analysis methods and metabolic systems are given at the end of the corresponding chapter.

Some general observations and conclusions can be derived from the work in the preceding four chapters. Published methods on the detailed analysis of *in vivo* NMR spectra are valuable since NMR experiments are now being performed and interpreted by a diverse group of scientists, physicians, and engineers. Observations about a given cellular system appear to be characteristic of that organism. For example, polyphosphate levels are observed commonly in spectra of yeast, but not in *Escherichia coli.*

The phenomena of "NMR–invisible" ADP and magnesium binding of ATP for *S. cerevisiae* as discussed in Chapter 5 will be important in the modeling of cellular processes. The modeler will have a choice of the total ADP level, the "free" ADP, or the sequestered "NMR invisible" ADP as to which one influences the kinetic and regulatory properties of an enzyme. Models that more closely simulate the *in vivo* situation will result from these types of measurements.

An enhancement in ethanol productivity was observed for the recombinant

strain of *S. cerevisiae* that has the hexokinase PI enzyme for glucose phosphorylation. The reasons why this strain worked "the best" was not apparent from the NMR observations. A more precise study should be performed in which the *in vitro* glucose-phosphorylating enzyme activity of hexokinase PI is systematically increased by elevating plasmid number in the cell or by using various strength promoters. NMR experiments of several engineered strains with the only difference being in the *in vitro* enzyme activity could be performed and differences assessed more precisely.

The NMR experiments described in this work were of cells under nongrowth conditions. These experiments allowed the assessment of differences between strains undergoing catabolism of substrate; hence, these measurements were snapshots of the cell as a complex chemical reactor without capabilities for synthesis of biomass. In the future, noninvasive methods of the growing cell will be important in predicting the cells' response in a fermentor. As wide-bore magnets and spectrometer time become increasingly available, on-line NMR will become feasible. The additional factor of biomass synthesis can be taken into account experimentally for the eventual goals sought in metabolic engineering.

APPENDIX A

IN VIVO CHEMICAL SHIFT COORDINATES OF THE SUGAR PHOSPHATES AND CYTOPLASMIC INORGANIC PHOSPHATE

TABLE A1: *In Vivo* Chemical Shift Coordinates as Shown in Chapter 2

P_i^{cyt}	3PGA	α–FDP	α–G6P	β–FDP 1-P	β–FDP 6-P + F6P
2.15	3.78	4.83	4.47	4.13	3.94
2.17	–	4.88	4.44	4.14	3.88
1.98	–	4.71	4.33	3.99	3.75
2.03	–	4.74	4.32	4.04	3.78
1.85	3.44	4.60	4.26	3.90	3.65
1.91	3.51	4.68	4.19	3.92	3.69
1.75	–	4.50	4.20	3.78	3.51
1.73	3.29	4.52	4.02	3.77	3.49
1.67	–	4.44	4.06	3.70	3.42
1.68	3.19	4.42	3.90	3.69	3.42
1.58	3.01	4.30	3.85	3.60	3.30
1.53	–	4.23	3.66	3.50	3.23
1.53	–	4.26	3.82	3.56	3.24
1.51	3.11	4.24	3.78	3.52	3.28
1.52	3.01	4.21	3.70	3.49	3.24
1.56	–	4.32	3.90	3.55	3.29
1.59	–	4.39	–	3.59	3.33
1.46	2.93	4.16	3.70	3.46	3.16
1.56	2.95	4.25	3.69	3.47	3.24
2.39	–	4.94	4.72	4.26	4.09
1.88	3.45	4.63	4.13	3.91	3.65
1.81	3.41	4.55	4.11	3.84	3.58
1.62	3.03	4.28	3.86	3.63	3.25
1.47	2.96	4.10	3.75	3.48	3.16
1.87	3.45	–	–	–	–
1.32	2.62	–	–	–	–
1.67	3.15	–	–	–	–
1.35	2.71	–	–	–	–
1.31	2.65	–	–	–	–
1.33	2.63	–	–	–	–
1.30	2.68	–	–	–	–
1.31	2.68	–	–	–	–
1.31	2.60	–	–	–	–
1.45	2.90	–	–	–	–
1.41	2.77	–	–	–	–
1.73	3.25	–	–	–	–
1.51	2.99	–	–	–	–

– not determined.

APPENDIX B

COMPARISON OF THE SUGAR PHOSPHATE REGION IN SPECTRA OF INTACT YEAST AND PERCHLORIC CELL EXTRACTS OF YEAST

^{31}P NMR experiments were performed for cell suspensions and cell extracts of *Saccharomyces cerevisiae* 18790 and *S. cerevisiae* D603. The ^{31}P NMR assay was performed by monitoring the metabolism of the cell suspension using ^{31}P NMR, stopping the metabolism of the cell suspension while glucose was still being catabolized by freezing the cells with liquid nitrogen and perchloric acid, preparing the cell extract, then using ^{31}P NMR to determine the compounds in the cell extract. In this way, *in vivo* and *in vitro* spectra were taken at the same time in catabolism of glucose.

The ratio of sugar phosphate compounds in the *in vivo* spectrum as determined by the method of analysis in Chapter 2 agreed with the *in vitro* determination.

This work was done in collaboration with Jorge Galazzo.

MATERIALS AND METHODS

Yeast Strains

Saccharomyces cerevisiae ATCC 18790 and *S. cerevisiae* D603 were the yeast strains used, as in Chapter 2. *S. cerevisiae* 18790 is a standard diploid strain and has no known mutations. *S. cerevisiae* D603 is the homozygous diploid version of YM603 (*ade2-101*, *ura3-52*, *his3*, *met*, *lys2-801*, *reg1-501*). The *reg1* mutation inhibits catabolic repression by glucose.

Culture and NMR Preparation

Culture conditions and NMR preparation procedures have been described previously in Chapter 2. The strains were grown aerobically to mid-exponential phase in liquid medium containing 1% yeast extract, 2% bacto-peptone, and 2% glucose, at pH 4.5. The cultures were chilled on ice, then harvested by low speed centrifugation at 4°. The cells were washed twice in an ice-cold sterile buffered

salt solution: 0.85 g/L KH_2PO_4, 0.15 g/L K_2HPO_4, 0.5 g/L $MgSO_4$, and 0.1 g/L NaCl in 50 mM MES buffer, pH adjusted to 6. The cells were resuspended in wash medium supplemented with an additional 15 mM P_i at a 1:1 ratio of cell pellet volume to resuspension volume. Cell suspensions (2 mL) in the NMR tubes were tightly capped, and kept on ice until used for the NMR experiment.

^{31}P NMR Assay

^{31}P NMR spectra of the cellular suspensions were obtained in the Fourier-transform mode at 202.46 MHz on a Bruker AM-500 NMR spectrometer at 20°C as described in Chapter 5. The pulse interval and angle were 0.5 s and 70°, respectively. Free induction decays (FID's) were accumulated in consecutive 2 min. blocks (240 scans, 8K files). Sample spinning and ^{1}H decoupling were not employed.

The yeast suspension was warmed to 20°C in the magnet. An initial spectrum was taken of the cellular suspension, then 75 μL of a 40 wt % glucose solution was added to the cells and a sequence of spectra was collected during subsequent 2 min. intervals. The spectra were monitored at the console while the experiments were in progress; the *in vivo* experiment was stopped when the levels of metabolites in the *in vivo* spectrum indicated that the cells were near the quasi–steady–state period, between 10–20 min after addition of glucose. The yeast suspension was immediately poured into a mortar that had been precooled and filled with liquid nitrogen. 1 mL of concentrated perchloric acid was added to the frozen yeast suspension. The mixture was ground to a powder with a pestle; liquid nitrogen was added to the frozen yeast pellet so that the pellet was immersed while grinding.

The powder sample was then transferred to a Nalgene test tube that had been precooled in dry ice/ ethanol. The test tube was placed in a dry ice/ ethanol bath for 30 min, then thawed in an ice bath ($\approx$5 min). This cycle was repeated two more times, with the freeze period and thaw period about 5 minutes each. The sample

was centrifuged for 15 min at 8500 rpm at 4°C. The supernatant was transferred to another precooled test tube. The supernatant was neutralized with 2 M $KHCO_3$; precipitation of $KClO_4$ stops when the samples reaches neutrality. The pH was checked with Litmus paper. The step of adding $KHCO_3$ was performed in a cold room (8°C). The sample (with precipitate) was set in an ice bath for 10 min, then centrifugation was performed as before to remove the precipitate. The supernatant was passed through a Chelex 100, 200–400 mesh, Biorad Poly–Prep column using H_2O as the solvent; this step removes paramagnetic cations. The sample was then lyophilized overnight in a freeze–dryer. Freeze–dried samples were stored in a -20°C freezer until NMR spectroscopy was applied.

For NMR spectroscopy of extracts, the lyophilized sample was redissolved in double distilled H_2O (plus 20 mM EDTA) equal in volume to the original sample, and placed in 10 mm dia. NMR tubes. D_2O was added to 10% final volume. The sample was kept on ice until used for the NMR experiment. ^{31}P NMR spectra of cell extracts were obtained at 8°C, using a pulse interval of 5 sec and pulse angle of 90°. FID's (8K files) were accumulated for 1000 scans. Inverse–gated pulse decoupling with a power of 2 W and sample spinning of 14 Hz were employed.

Identification of compounds in the sugar phosphate region was determined by adding the individual sugar phosphate compounds and taking an additional spectrum.

Data Processing

The 8K FID files taken by the Bruker Aspect-3000 computer were transferred to a VAX(11/780) computer for analysis using LAB ONE (TM) NMR1 Spectroscopic Data Analysis Software System. All subsequent processing was performed by the software system on the VAX computer. The FID's were multiplied by an exponential apodization function corresponding to a line broadening of 20 Hz for the cellular spectra and 5 Hz for the extract spectra, Fourier transformed, phased,

and baseline flattened (4^{th} degree polynomial).

Estimation of Sugar Phosphate Concentrations

Estimates of the levels of the sugar phosphates were determined by a systematic procedure based upon ^{31}P NMR measurements, as described in Chapter 2. The sugar phosphate region of the ^{31}P NMR spectrum was first decomposed by computer analysis (NMR1 software), and the decomposition consistency and identification of individual sugar phosphate resonances were established based on *in vitro* chemical shift calibrations determined in separate experiments.

TABLE B1: Comparison of Cell Extract vs. *In Vivo* Determinations

	F6P/G6P	3–PGA/FdP	G6P/FdP	α–FdP/β–FdP
18790 *in vivo*	0.42	0.21	0.18	0.10
cell extract	0.46	0.23	0.17	0.08
D603–a *in vivo*	0.30	0.12	0.59	0.08
cell extract	0.34	0.08	0.63	0.11
D603–b *in vivo*	0.45	0.26	0.84	0.10
cell extract	0.51	0.31	0.80	0.15

FIGURE CAPTIONS

Figure 1: ^{31}P NMR spectra of suspension of *S.cerevisiae* 18790 (top frame) and of perchloric acid extracts of the same suspension (bottom frame) 18 min after addition of glucose.

Figure 2: Downfield region of spectra shown in Figure 1. Abbreviations: as in Chapter 2.

Figure 3: Downfield region of spectra as shown in Figure 2 but for *S. cerevisiae* D603. Abbreviations: as in Chapter 2.

Figure 4: *In vivo* vs. *in vitro* relative levels of various sugar phosphate compounds. *In vivo* levels were determined from the spectra of cell suspensions by the deconvolution method described in Chapter 2. *In vitro* sugar phosphate levels were determined by deconvolution and/or integration of the peaks in the sugar phosphate region of spectra of cell extracts. The data for *S. cerevisiae* D603 is from the spectra in Figure 3 and the data for *S. cerevisiae* 18790 is from the spectra in Figure 2.

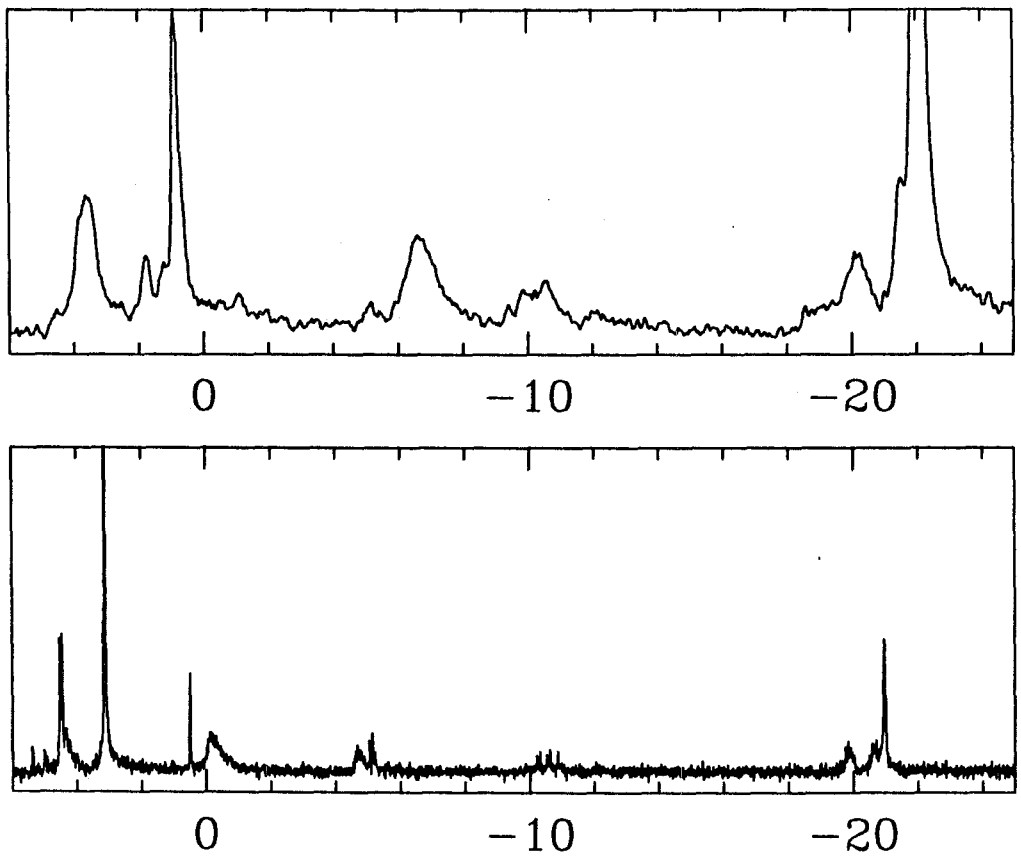

Figure B1

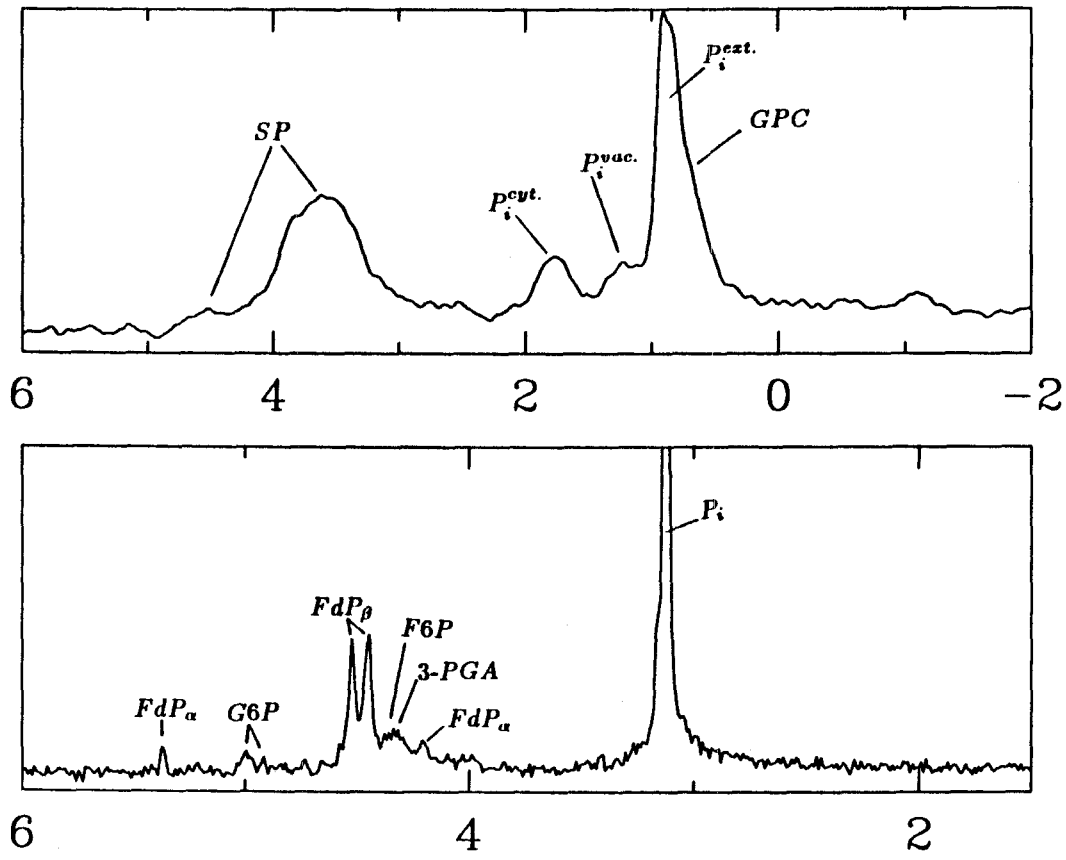
SP
$P_i^{cyt.}$
$P_i^{vac.}$
$P_i^{ext.}$
GPC
6
4
2
0
−2
FdP_α
G6P
FdP_β
F6P
3-PGA
FdP_α
P_i
6
4
2
CHEMICAL SHIFT (PPM)

Figure B2

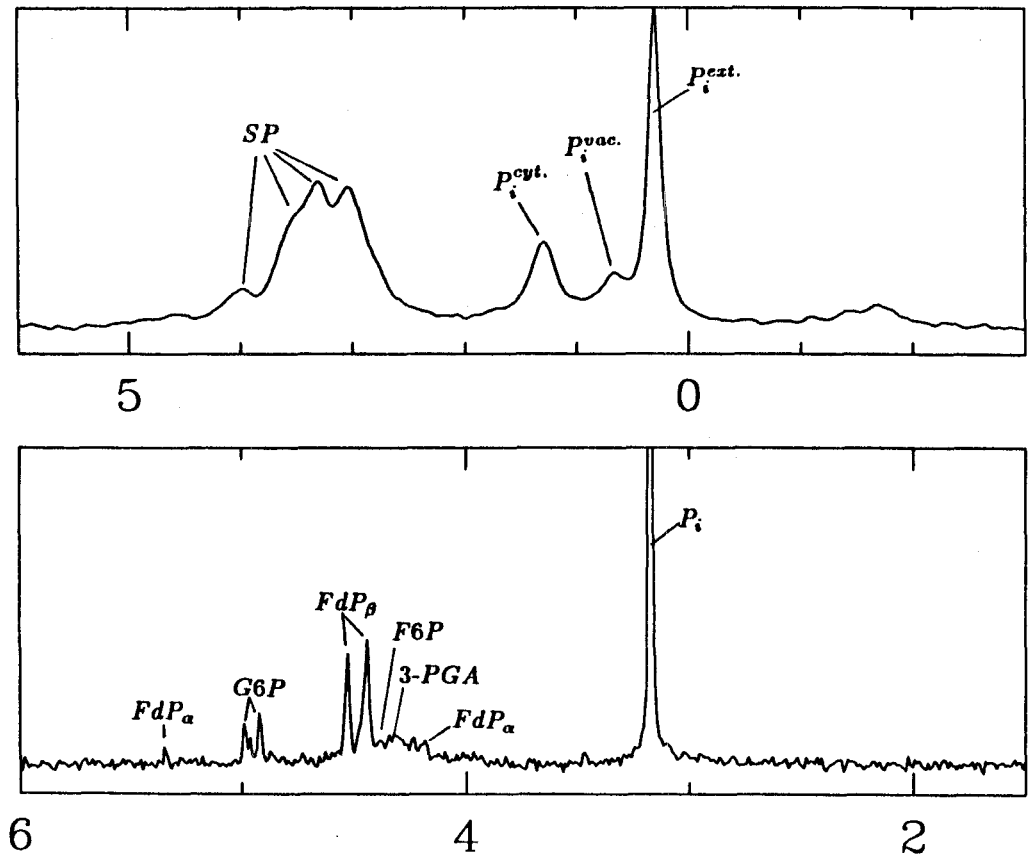
SP
$P_i^{cyt.}$
$P_i^{vac.}$
$P_i^{ext.}$
5
0
P_i
FdP_β
F6P
3-PGA
G6P
FdP_α
FdP_α
6
4
2
CHEMICAL SHIFT (PPM)

Figure B3

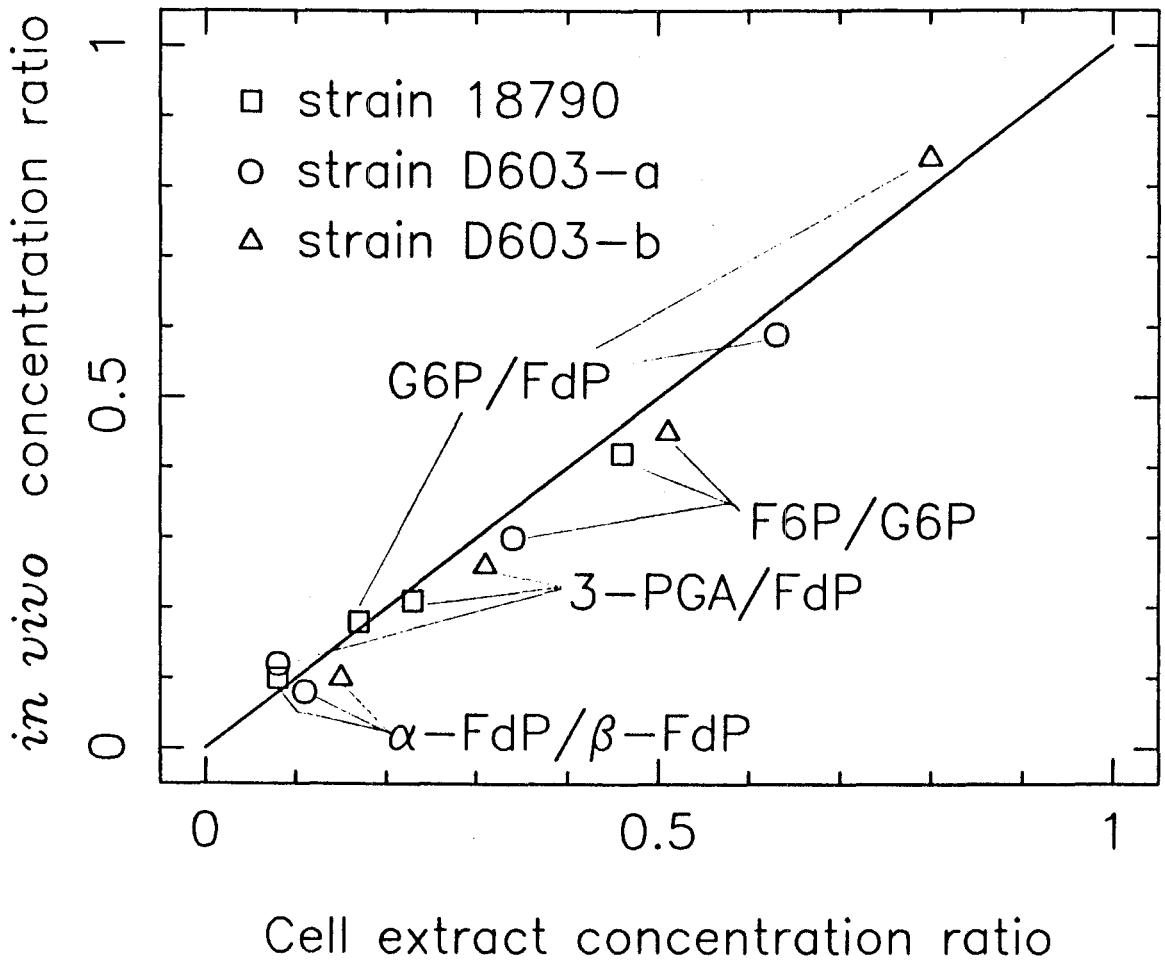
in vivo concentration ratio
0
0.5
1
strain 18790
strain D603−a
strain D603−b
G6P/FdP
F6P/G6P
3−PGA/FdP
α−FdP/β−FdP
0
0.5
1
Cell extract concentration ratio

Figure B4